ISSN: 2153-1196 Volume 9, Number 11, September 2018

Scientific Research Publishing

Journal of Modern Physics

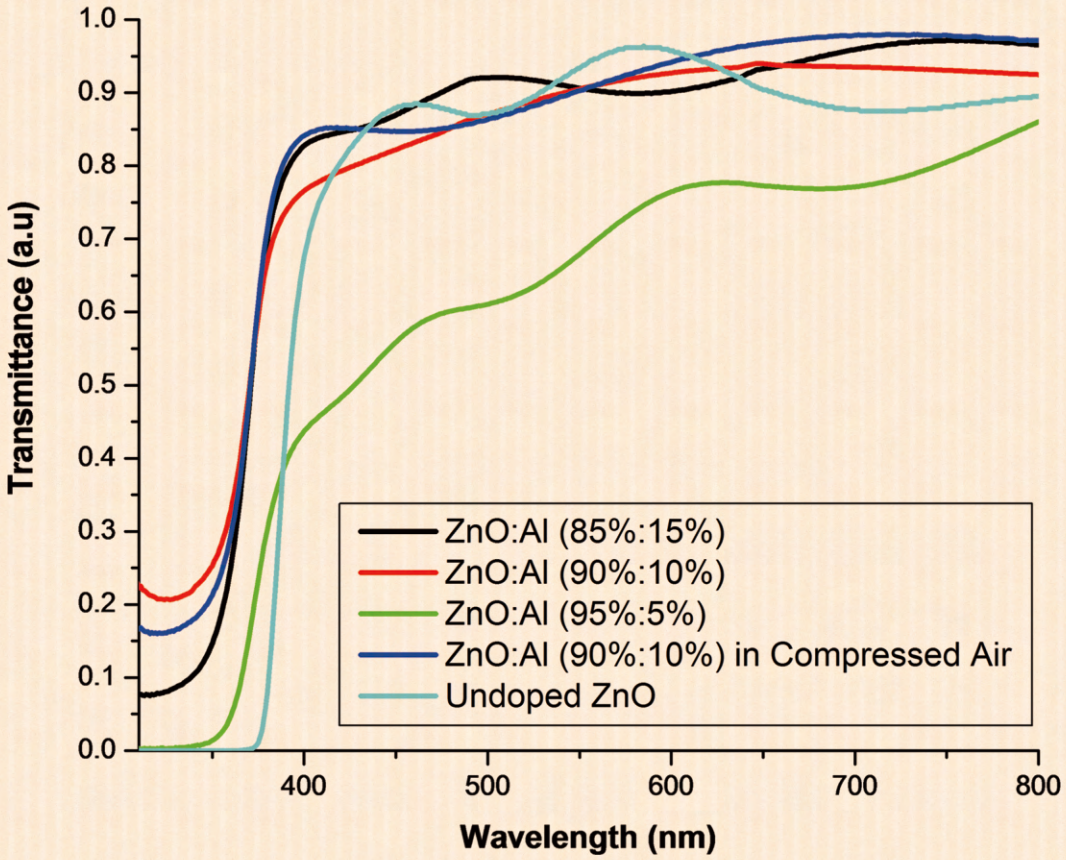

ISSN: 2153-1196
9 772153 119007 11

www.scirp.org/journal/jmp

Journal Editorial Board

ISSN: 2153-1196 (Print) ISSN: 2153-120X (Online)
http://www.scirp.org/journal/jmp

Journal of Modern Physics, 2018, 9, 2021-2099
http://www.scirp.org/journal/jmp
ISSN Online: 2153-120X
ISSN Print: 2153-1196

Table of Contents

Volume 9 Number 11 September 2018

The figure on the front cover is from the article published in Journal of Modern Physics, 2018, Vol. 9, No. 11, pp. 2073-2089 by Olumide Oluwole Akinwunmi, *et al.*

Journal of Modern Physics (JMP)
Journal Information

SUBSCRIPTIONS

The *Journal of Modern Physics* (Online at Scientific Research Publishing, www.SciRP.org) is published monthly by Scientific Research Publishing, Inc., USA.

Subscription rates:
Print: $89 per issue.
To subscribe, please contact Journals Subscriptions Department, E-mail: sub@scirp.org

SERVICES

Advertisements
Advertisement Sales Department, E-mail: service@scirp.org

Reprints (minimum quantity 100 copies)
Reprints Co-ordinator, Scientific Research Publishing, Inc., USA.
E-mail: sub@scirp.org

COPYRIGHT

PRODUCTION INFORMATION

For manuscripts that have been accepted for publication, please contact:
E-mail: jmp@scirp.org

Journal of Modern Physics, 2018, 9, 2021-2034
http://www.scirp.org/journal/jmp
ISSN Online: 2153-120X
ISSN Print: 2153-1196

The Foldy-Wouthuysen Transformation of the Dirac Equation in Noncommutative Phase-Space

Ilyas Haouam, Lyazid Chetouani

Département de Physique, Faculté des sciences exactes, Université des Frères Mentouri, Constantine, Algeria
Email: ilyashaouam@live.fr

How to cite this paper: Haouam, I. and Chetouani, L. (2018) The Foldy-Wouthuysen Transformation of the Dirac Equation in Noncommutative Phase-Space. *Journal of Modern Physics*, **9**, 2021-2034.
https://doi.org/10.4236/jmp.2018.911127

Received: November 9, 2015
Accepted: September 11, 2018
Published: September 14, 2018

Abstract

A method of Foldy-Wouthuysen transformation for relativistic spin-1/2 particles in external fields is proposed; in the present work the basic properties of the Dirac hamiltonian in the FW representation in the noncommutative phase-space are investigated and the Schrödinger-Pauli equation is found, knowing that the used methods for extracting the full phase-space noncommutative Dirac equation are, the Bopp-shift linear translation method, and the Moyal-Weyl product (*-product).

Keywords

Foldy-Wouthuysen Transformation, Nonrelativistic Limit, Noncommutative Schrödinger-Pauli Equation, Phase-Space Noncommutativity, Noncommutative Dirac Equation, Moyal Product, Bopp-Shift Translation

1. Introduction

The Foldy-Wouthuysen transformation (FW) [1] is one of several methods used to investigate the low-energy limit of the relativistic Dirac equation (low-speed); due to a series of sequential unitary transformations [2], it has proven to be the favorite method to meaningfully obtain the nonrelativistic limit of the Dirac equation in which it gives the Schrödinger-Pauli equation [3] [4] [5]; in the FW representation for relativistic particles in external fields, the operators have the same form as in the nonrelativistic quantum theory, this is mainly because of the fact of the hamiltonian and all operators in this representation are block-diagonal, furthermore the basic characteristics of the FW representation are obviously described in [6] [7] [8] [9].

In the present work, the basic properties of the Dirac hamiltonian in the FW representation in the noncommutative phase-space are investigated and the Schrödinger-Pauli equation is found, where the common methods for extracting the full phase-space noncommutative Dirac equation are both of the linear translation method, which known as Bopp-Shift translation in which it matches between the commutative quantum mechanics and the noncommutative quantum mechanics (NCQM) [10], and the Moyal-Weyl product (*-product) [11] [12] [13] [14].

2. Phase-Space Noncommutativity

In the two-dimensional commutative phase-space, the coordinates x_i and the kinetic momentum p_i satisfy the usual canonical commutation relations

$$\left[x_i, x_j\right]=0, \left[p_i, p_j\right]=0, \left[x_i, p_j\right]=i\delta_{ij}\left(i, j=1,2\right). \tag{1}$$

In the recent study results on the phase-space noncommutativity (PSNC) is shown that at very tiny scales (string scales) the space may not commute anymore, let us consider the operators of coordinates and kinetic momentum in a two-dimensional noncommutative phase-space $\hat{x}_i$ and $\hat{p}_i$ respectively, where the noncommutative phase-space operators satisfy the commutation relations

$$\left[\hat{x}_i, \hat{x}_j\right]=i\Theta_{ij}, \left[\hat{p}_i, \hat{p}_j\right]=i\eta_{ij}, \left[\hat{x}_i, \hat{p}_j\right]=i\hbar^{eff}\delta_{ij}\left(i, j=1,2\right), \tag{2}$$

with the effective Plank constant being

$$\hbar^{eff}=\hbar\left(1+\frac{\Theta\cdot\eta}{4\hbar^2}\right), \tag{3}$$

where

$$\Theta_{ij}=\epsilon_{ijk}\Theta_k, \Theta_k=\left(0,0,\Theta\right), \eta_{ij}=\epsilon_{ijk}\eta_k, \eta_k=\left(0,0,\eta\right),$$

Θ, η are noncommutative parameters, they are real-valued and antisymmetric constant matrices with dimension of (length)^2 and (momentum)^2, respectively.

The noncommutativity in phase-space can be realized in terms of Moyal-Weyl product (*-product) [15] [16] [17] which means that the noncommutativity information is encoded in the Moyal product, defined as

$$\begin{aligned}\left(f\star g\right)\left(\hat{x}\right)&=\exp\left[\frac{i}{2}\Theta_{ab}\partial_{x_a}\partial_{x_b}\right]f\left(x_a\right)g\left(x_b\right)\\&=f\left(x\right)g\left(x\right)+\sum\nolimits_{a=1}\left(\frac{1}{n!}\right)\left(\frac{i}{2}\right)^2\Theta^{a_1b_1}\cdots\Theta^{a_nb_n}\partial_{a_1}\cdots\partial_{a_k}f\left(x\right)\partial_{b_1}\ldots\partial_{b_k}g\left(x\right).\end{aligned} \tag{4}$$

The noncommutative phase-space operators are related to the commutative phase-space one, due to the so-called Bopp-shift linear transformation [18] [19] [20], knowing that the latter induced from the *-product, and it is given by

$$\begin{aligned}\hat{x}&=x-\frac{1}{2\hbar}\Theta p_y \qquad \hat{y}=y+\frac{1}{2\hbar}\Theta p_x\\ \hat{p}_x&=p_x+\frac{1}{2\hbar}\eta y \qquad \hat{p}_y=p_y-\frac{1}{2\hbar}\eta x\end{aligned} \tag{5}$$

If $\Theta = \eta = 0$ the noncommutative phase-space algebra reduces to the commutative one.

3. Nonrelativistic Limit of the Dirac Equation in Noncommutative Phase-Space

3.1. The Dirac Equation in Noncommutative Phase-Space

As it known by the use of the *-product, we obtain the Dirac equation for the noncommutative quantum mechanics [21] [22]

$$H(\hat{x},\hat{p})\star\psi(\hat{x}) = E\psi, \tag{6}$$

knowing that the Dirac equation in interaction with the electromagnetic four-potential A_μ in commutative phase-space is

$$\left[c\alpha_i\left(p_i - \frac{e}{c}A_i(x)\right) + eA_0(x) + \beta mc^2\right]\psi = E\psi(x), \tag{7}$$

where $\psi(x,t) = \mathrm{e}^{\frac{-iEt}{\hbar}}\begin{pmatrix}\phi(x)\\ \chi(x)\end{pmatrix}$ is the wave function (bi-spinor) in the Dirac representation.

At first we achieve the noncommutativity in space, by the mapping between the noncommutative coordinates $\hat{x}$ and the commutative coordinates x using the *-product, with the help of Equation (4) we find

$$H(\hat{x},\hat{p})\star\psi(\hat{x}) = \left[c\alpha_i\left(\hat{p}_i - \frac{e}{c}A_i(\hat{x})\right) + eA_0(\hat{x}) + \beta mc^2\right]\star\psi(\hat{x}). \tag{8}$$

Consider the electromagnetic potential $(x) = hx$, where h is a constant, the derivations in the Equation (4) roughly turned off in the first order, then Equation (8) can be written as follows

$$\begin{aligned} H(\hat{x},\hat{p})\star\psi(\hat{x}) = {} & H(x,\hat{p})\psi(x) + \frac{i}{2}\Theta_{ab}\partial_a\left[c\alpha_i\left(\hat{p}_i - \frac{e}{c}A_i(x)\right)\right. \\ & \left. + eA_0(\hat{x}) + \beta mc^2\right]\partial_b\psi(x) + \mathrm{O}(\Theta^2) \\ = {} & E\psi(x), \end{aligned} \tag{9}$$

with $\partial_a\left(c\alpha_i\hat{p}_i\right) = \partial_a\left(\beta mc^2\right) = 0$, Equation (9) reduced to

$$H(x,\hat{p})\psi(x) - \frac{ie}{2}\theta_{ab}\partial_a\left[\hat{\alpha}_i\left(A_i(x)\right) - A_0(\hat{x})\right]\partial_b\psi(x) = E\psi(x). \tag{10}$$

Anew we achieve the noncommutativity in phase by the mapping between the noncommutative kinetic momentum $\hat{p}$ and the commutative one p, using Equation (5) to get the following full noncommutative phase-space Dirac equation

$$\begin{aligned} H(\hat{x},\hat{p})\star\psi(\hat{x}) = {} & \left[c\alpha_i\left(p_i + \frac{1}{2\hbar}\eta_{ij}x_j - \frac{e}{c}A_i(x)\right) + eA_0(x) + \beta mc^2\right. \\ & \left. - \frac{ie}{2}\Theta_{ab}\partial_a\left(\alpha_i\left(A_i(x)\right) - A_0(x)\partial_b\right)\right]\psi(x) \\ = {} & E\psi(x), \end{aligned} \tag{11}$$

rewrite the Equation (11) in a more compact form (see **Appendix A** for the simplification):

$$\begin{aligned}\hat{H}\star\psi_{(NC)} &= \left[c\vec{\alpha}\left(\vec{p}-\frac{e}{c}\vec{A}\right)+eA_0+\beta mc^2+\frac{c}{\hbar}(\vec{\alpha}\times\vec{x})\cdot\vec{\eta}\right.\\ &\left.+\frac{e}{\hbar}\left(\vec{\nabla}\left(\vec{\alpha}\vec{A}-A_0\right)\times\vec{p}\right)\cdot\vec{\Theta}\right]\psi_{(NC)}\\ &= E\psi_{(NC)},\end{aligned} \tag{12}$$

where $\psi_{(NC)}=\exp\left[\frac{-i\left(E+\frac{c}{\hbar}(\vec{\alpha}\times\vec{x})\cdot\vec{\eta}\right)t}{\hbar}\right]\begin{pmatrix}\phi(\hat{x})\\ \chi(\hat{x})\end{pmatrix}$ is the wave function in noncommutative phase-space.

3.2. Foldy-Wouthuysen Transformation in Noncommutative Phase-Space

Deriving the Schrödinger-Pauli equation in noncommutative phase-space, which is the nonrelativistic limit of the Dirac equation in a simple way using the Foldy-Wouthuysen transformation, this one achieved by a series of successive unitary transformations performed on the phase-space noncommutative Dirac hamiltonian in Equation (12), knowing that it is only applicable to weak fields.

The Dirac hamiltonian in PSNC is given by

$$\hat{H}=c\vec{\alpha}\left(\vec{p}-\frac{e}{c}\vec{A}\right)+eA_0+\beta mc^2+\frac{c}{\hbar}(\vec{\alpha}\times\vec{x})\cdot\vec{\eta}+\frac{e}{\hbar}\left(\vec{\nabla}\left(\vec{\alpha}\vec{A}-A_0\right)\times\vec{p}\right)\cdot\vec{\Theta}, \tag{13}$$

in order to perform the FW transformation, we have to rewrite the Dirac hamiltonian Equation (13) to the form:

$$\hat{H}=\hat{\theta}+\hat{\epsilon}+\beta mc^2, \tag{14}$$

where the Dirac hamiltonian is divided into block diagonal and off diagonal parts denoted even operator $\hat{\epsilon}$ and odd operator $\hat{\theta}$ respectively[1].

$$\begin{aligned}\hat{\epsilon} &= eA_0-\frac{e}{\hbar}\left(\vec{\nabla}(A_0)\times\vec{p}\right)\cdot\vec{\Theta}\\ \hat{\theta} &= c\vec{\alpha}\left(\vec{p}-\frac{e}{c}\vec{A}\right)+\frac{c}{\hbar}(\vec{\alpha}\times\vec{x})\cdot\vec{\eta}+\frac{e}{\hbar}\left(\vec{\nabla}\left(\vec{\alpha}\vec{A}\right)\times\vec{p}\right)\cdot\vec{\Theta},\end{aligned} \tag{15}$$

these are defined to satisfy

$$\beta\hat{\theta}=-\hat{\theta}\beta \quad \text{and} \quad \beta\hat{\epsilon}=\hat{\epsilon}\beta\,. \tag{16}$$

Because of the presence of the odd operators (of $\vec{\alpha}$ matrices), the Dirac hamiltonian is not block diagonalized, so that we try to eliminate odd operators from the Dirac hamiltonian, by applying *FW* transformation

$$\begin{aligned}\psi'_{(NC)} &= \mathrm{e}^{i\hat{S}}\psi_{(NC)}\\ \hat{H}' &= \mathrm{e}^{i\hat{S}}\hat{H}\mathrm{e}^{-i\hat{S}},\end{aligned} \tag{17}$$

[1]Odd operators (off diagonal in Pauli-Dirac basis): $\alpha_i,\gamma_i,\cdots$ even operators (diagonal in Pauli-Dirac basis): $\beta,\Sigma,1,\cdots$ suffice at the 4rd order of $\hat{S}$.

with $\hat{s}$ is Hermitian and it is of the form

$$\hat{s} = \frac{-i}{2mc^2}\beta\hat{\theta}. \tag{18}$$

Using the Maclaurin series expansion of $e^{i\hat{s}}$ defined as $e^{i\hat{s}} = 1 + \frac{i\hat{s}}{1!} + \frac{(i\hat{s})^2}{2!} + \cdots$ in the Equation (17) yields a transformed Dirac hamiltonian (*Campbell-Baker-Hausdorff expansion*) [23] [24]

$$\begin{aligned}\hat{H}' = \hat{H} + i\left[\hat{s},\hat{H}\right]_- + \frac{i^2}{2!}\left[\hat{s},\left[\hat{s},\hat{H}\right]_-\right]_- + \frac{i^3}{3!}\left[\hat{s},\left[\hat{s},\left[\hat{s},\hat{H}\right]_-\right]_-\right]_- + \cdots \\ + \frac{i^n}{n!}\left[\hat{s},\left[\hat{s},\cdots\left[\hat{s},\hat{H}\right]_-\cdots\right]_-\right]_- + \cdots\end{aligned} \tag{19}$$

Writing our hamiltonian, restricting ourselves to terms up to order $1/\left(mc^2\right)^3$, thus we suffice at the 4[rd] order of $\hat{S}$,

$$\begin{aligned}\hat{H}' = \hat{H} + i\left[\hat{s},\hat{H}\right]_- - \frac{1}{2}\left[\hat{s},\left[\hat{s},\hat{H}\right]_-\right]_- - \frac{i}{6}\left[\hat{s},\left[\hat{s},\left[\hat{s},\hat{H}\right]_-\right]_-\right]_- \\ - \frac{1}{24}\left[\hat{s},\left[\hat{s},\left[\hat{s},\left[\hat{s},\beta mc^2\right]_-\right]_-\right]_-\right]_- + \cdots\end{aligned} \tag{20}$$

Using the properties mentioned in Equation (16) and with Equation (14) and Equation (18), knowing that

$$\beta\left[\hat{\theta},\hat{\epsilon}\right]_- = -\left[\hat{\theta},\hat{\epsilon}\right]_-\beta, \tag{21}$$

we calculate the various commutators of $\hat{s}$ and $\hat{H}$

$$i\left[\hat{s},\hat{H}\right]_- = -\hat{\theta} + \frac{1}{mc^2}\hat{\beta}\hat{\theta}^2 + \frac{\hat{\beta}}{2mc^2}\left[\hat{\theta},\hat{\epsilon}\right]_- \tag{22}$$

$$\frac{i^2}{2!}\left[\hat{s},\left[\hat{s},\hat{H}\right]_-\right]_- = -\frac{1}{2mc^2}\hat{\beta}\hat{\theta}^2 - \frac{1}{2m^2c^4}\hat{\theta}^3 + \frac{1}{8m^2c^4}\left[\hat{\theta},\left[\hat{\theta},\hat{\epsilon}\right]_-\right]_-, \tag{23}$$

$$-\frac{i}{6}\left[\hat{s},\left[\hat{s},\left[\hat{s},\hat{H}\right]_-\right]_-\right]_- = \frac{1}{6m^2c^4}\hat{\theta}^3 - \frac{1}{6m^3c^6}\hat{\beta}\hat{\theta}^4 + \frac{1}{48m^3c^6}\hat{\beta}\left[\hat{\theta},\left[\hat{\theta},\left[\hat{\theta},\hat{\epsilon}\right]_-\right]_-\right]_-, \tag{24}$$

with the same manner we continue, with taking into account only terms of the order $1/\left(m_0c^2\right)^3$, we get

$$-\frac{1}{24}\left[\hat{S},\left[\hat{S},\left[\hat{S},\left[\hat{S},\hat{\beta}mc^2\right]_-\right]_-\right]_-\right]_- \approx \frac{1}{24m^3c^6}\hat{\beta}\hat{\theta}^4, \tag{25}$$

by collecting the terms of $\hat{H}'$ Equations ((22), (25)), we find

$$\begin{aligned}\hat{H}' = \hat{H} - \hat{\theta} + \frac{1}{mc^2}\hat{\beta}\hat{\theta}^2 + \frac{\hat{\beta}}{2mc^2}\left[\hat{\theta},\hat{\epsilon}\right]_- - \frac{1}{2mc^2}\hat{\beta}\hat{\theta}^2 - \frac{1}{2m^2c^4}\hat{\theta}^3 \\ - \frac{1}{8m^2c^4}\left[\hat{\theta},\left[\hat{\theta},\hat{\epsilon}\right]_-\right]_- + \frac{1}{6m^2c^4}\hat{\theta}^3 - \frac{1}{6m^3c^6}\hat{\beta}\hat{\theta}^4 \\ - \frac{1}{48m^3c^6}\hat{\beta}\left[\hat{\theta},\left[\hat{\theta},\left[\hat{\theta},\hat{\epsilon}\right]_-\right]_-\right]_- + \frac{1}{24m^3c^6}\hat{\beta}\hat{\theta}^4,\end{aligned} \tag{26}$$

$$= \hat{\epsilon} + \hat{\beta}\left\{mc^2 + \frac{1}{2mc^2}\hat{\theta}^2 - \frac{1}{8m^3c^6}\hat{\theta}^4\right\} + \frac{\hat{\beta}}{2mc^2}\left[\hat{\theta},\hat{\epsilon}\right]_- - \frac{1}{3m^2c^4}\hat{\theta}^3 - \frac{1}{8m^2c^4}\left[\hat{\theta},\left[\hat{\theta},\hat{\epsilon}\right]_-\right]_- - \frac{1}{48m^3c^6}\hat{\beta}\left[\hat{\theta},\left[\hat{\theta},\left[\hat{\theta},\hat{\epsilon}\right]_-\right]_-\right]_-, \quad (27)$$

as it shown in the Equation (27) the new hamiltonian is not free of the odd operator, the odd part not omit, so By further FW transformation we reduce the odd part of the transformed hamiltonian, so we perform a second transformation, remembering that the product of two even or odd operators is an even operator.

To reduce the odd part of the transformed hamiltonian, thus we chose

$$\hat{s}' = \frac{-i}{2mc^2}\beta\hat{\theta}', \quad (28)$$

in where

$$\hat{H}' = \hat{H} + \hat{\theta}' + \hat{\epsilon}' + \hat{\beta}mc^2, \quad (29)$$

with

$$\hat{\theta}' = \frac{\hat{\beta}}{2mc^2}\left[\hat{\theta},\hat{\epsilon}\right]_- - \frac{1}{3m^2c^4}\hat{\theta}^3 - \frac{1}{48m^3c^6}\hat{\beta}\left[\hat{\theta},\left[\hat{\theta},\left[\hat{\theta},\hat{\epsilon}\right]_-\right]_-\right]_-, \quad (30)$$

$$\hat{\epsilon}' = \hat{\epsilon} + \frac{1}{mc^2}\hat{\beta}\hat{\theta}^2 - \frac{1}{8m^3c^6}\hat{\beta}\hat{\theta}^4 - \frac{1}{8m^2c^4}\left[\hat{\theta},\left[\hat{\theta},\hat{\epsilon}\right]_-\right]_-, \quad (31)$$

$$\hat{H}'' = \mathrm{e}^{i\hat{s}'}\hat{H}'\mathrm{e}^{-i\hat{s}'}, \quad (32)$$

$$\hat{H}'' = \hat{H}' + i\left[\hat{s}',\hat{H}'\right]_- - \frac{1}{2}\left[\hat{s}',\left[\hat{s}',\hat{H}'\right]_-\right]_- - \frac{i}{6}\left[\hat{s}',\left[\hat{s}',\left[\hat{s}',\hat{H}'\right]_-\right]_-\right]_- - \frac{1}{24}\left[\hat{s}',\left[\hat{s}',\left[\hat{s}',\left[\hat{s}',\beta mc^2\right]_-\right]_-\right]_-\right]_- + \cdots \quad (33)$$

We restrict ourselves to terms up to order $1/\left(mc^2\right)^3$, as in the first FW transformation (knowing that $\hat{\theta}' \sim \frac{1}{mc^2}$), so that the new hamiltonian is

$$\hat{H}'' = \hat{\beta}mc^2 + \hat{\epsilon}' + \frac{\hat{\beta}}{2mc^2}\left[\hat{\theta}',\hat{\epsilon}'\right]_- + \frac{1}{2mc^2}\hat{\beta}\hat{\theta}'^2 - \frac{1}{2m^2c^4}\hat{\theta}'^3 - \frac{1}{8m^2c^4}\left[\hat{\theta}',\left[\hat{\theta}',\hat{\epsilon}'\right]_-\right]_-. \quad (34)$$

The terms proportional to $\hat{\theta}'^3$ and $\hat{\theta}'^2$ contain large powers of $1/mc^2$, therefore they can be neglected, more precisely we take into account only terms of order that we restrict ourselves in the expansion, and thus Equation (34) is given by

$$\hat{H}'' \simeq \hat{\beta}mc^2 + \hat{\epsilon}' + \frac{\hat{\beta}}{2mc^2}\left[\hat{\theta}',\hat{\epsilon}'\right]_- = \hat{\beta}mc^2 + \hat{\epsilon}' + \hat{\theta}'', \quad (35)$$

$\hat{H}''$ is not yet free of the odd operators, we apply a third FW transformation to eliminate $\hat{\theta}''$,

$$\hat{H}''' = \mathrm{e}^{i\hat{s}''}\hat{H}''\mathrm{e}^{-i\hat{s}''}, \quad (36)$$

with

$$\hat{s}'' = \frac{-i}{2mc^2}\beta\hat{\theta}'', \quad (37)$$

so that

$$\hat{H}''' \simeq \hat{\beta}mc^2 + \hat{\epsilon}' = \hat{\beta}mc^2 + \hat{\epsilon} + \frac{1}{mc^2}\hat{\beta}\hat{\theta}^2 - \frac{1}{8m^3c^6}\hat{\beta}\hat{\theta}^4 - \frac{1}{8m^2c^4}\left[\hat{\theta},\left[\hat{\theta},\hat{\epsilon}\right]_-\right]_- . \quad (38)$$

Finally the transformed hamiltonian is completely free of odd operators, next we calculate the various terms of the Equation (38), according to Equation (15), we make use of the following known relations for three arbitrary vectors $\vec{A}$, $\vec{B}$ and $\vec{C}$:

$$\vec{A}\cdot\left(\vec{B}\times\vec{C}\right) = \vec{B}\cdot\left(\vec{C}\times\vec{A}\right) = \vec{C}\cdot\left(\vec{A}\times\vec{B}\right), \left(\vec{A}\times\vec{B}\right)\cdot\vec{C} = \left(\vec{B}\times\vec{C}\right)\cdot\vec{A} = \left(\vec{C}\times\vec{A}\right)\cdot\vec{B}, \quad (39)$$

the Equation (15) becomes

$$\hat{\theta} = c\vec{\alpha}\left(\vec{p} - \frac{e}{c}\vec{A}\right) + \frac{c}{\hbar}\vec{\alpha}\left(\left(\vec{x}\times\vec{\eta}\right) + \frac{e}{c}\vec{\nabla}\vec{A}\left(\vec{p}\times\vec{\Theta}\right)\right) = c\vec{\alpha}\left(\vec{p} - \frac{e}{c}\vec{A}\right) + \frac{c}{\hbar}\vec{\alpha}\vec{\Omega}, \quad (40)$$

with

$$\vec{\Omega} = \vec{x}\times\vec{\eta} + \frac{e}{c}\vec{\nabla}\vec{A}\left(\vec{p}\times\vec{\Theta}\right), \quad (41)$$

yields

$$\hat{\theta}^2 = c^2\left(\vec{\alpha}\left(\vec{p} - \frac{e}{c}\vec{A}\right)\right)^2 + \frac{2c}{\hbar}\vec{\alpha}\left(\vec{p} - \frac{e}{c}\vec{A}\right)\vec{\alpha}\vec{\Omega} + \frac{c^2}{\hbar^2}\left(\vec{\alpha}\vec{\Omega}\right)^2, \quad (42)$$

using the following relation[2]

$$\left(\vec{\alpha}\vec{A}\right)\left(\vec{\alpha}\vec{B}\right) = \vec{A}\vec{B} + i\vec{\Sigma}\cdot\left(\vec{A}\times\vec{B}\right), \quad (43)$$

we obtain

$$\begin{aligned}\hat{\theta}^2 = {} & c^2\left(\vec{\alpha}\left(\vec{p} - \frac{e}{c}\vec{A}\right)\right)^2 + \frac{2c}{\hbar}\left(\vec{p} - \frac{e}{c}\vec{A}\right)\vec{\Omega} + \frac{c^2}{\hbar^2}\vec{\Omega}^2 \\ & + ic^2\vec{\Sigma}\cdot\left[\frac{i\hbar e}{c}\vec{B} + \frac{2}{\hbar}\left(\vec{p} - \frac{e}{c}\vec{A}\right)\times\vec{\Omega} + \frac{1}{\hbar}\vec{\Omega}\times\vec{\Omega}\right],\end{aligned} \quad (44)$$

and

$$\begin{aligned}\frac{1}{8m^2c^4}\left[\hat{\theta},\hat{\epsilon}\right]_- = {} & -\frac{i\hbar}{8m^2c^4}c\vec{\alpha}\vec{\nabla}A_0 \\ & + \frac{1}{8m^2c^4}\left\{\left[\frac{e}{\hbar}\left(\vec{\nabla}\left(A_0\right)\times\vec{p}\right)\cdot\vec{\Theta}, c\vec{\alpha}\left(\vec{p} - \frac{e}{c}\vec{A}\right) + \frac{c}{\hbar}\vec{\alpha}\vec{\Omega}\right]_- + \left[\frac{c}{\hbar}\vec{\alpha}\vec{\Omega}, eA_0\right]_-\right\},\end{aligned} \quad (45)$$

for $A_0 = V$ we have $\vec{\nabla}V = -\vec{E}$ and using Equation (45) we have

$$\begin{aligned}\left[\hat{\theta},\left[\hat{\theta},\hat{\epsilon}\right]_-\right]_- = {} & \frac{e\hbar^2c^2}{8m^2c^4}\vec{\nabla}\vec{E} + \frac{ie\hbar^2c^2}{8m^2c^4}\vec{\Sigma}\cdot\vec{\nabla}\times\vec{E} \\ & + \frac{e\hbar}{4m^2c^4}\vec{\Sigma}\cdot\vec{E}\times\vec{p} + \left[\frac{c}{\hbar}\vec{\alpha}\vec{\Omega}, \frac{i\hbar}{8m^2c^4}c\vec{\alpha}\vec{E}\right]_- \\ & + \left[\hat{\theta}, \frac{1}{8m^2c^4}\left\{\left[c\vec{\alpha}\left(\vec{p} - \frac{e}{c}\vec{A}\right) - \frac{c}{\hbar}\vec{\alpha}\vec{\Omega}, \frac{e}{\hbar}\left(\vec{\nabla}\left(A_0\right)\times\vec{p}\right)\cdot\vec{\Theta}\right]_- + \left[\frac{c}{\hbar}\vec{\alpha}\vec{\Omega}, eA_0\right]_-\right\}\right]_-,\end{aligned} \quad (46)$$

[2] $\alpha^i\alpha^j = \alpha^i\beta^2\alpha^j = -\beta\alpha^i\beta\alpha^j = \gamma^i\gamma^j = -\frac{1}{2}\left(\left\{\gamma^i,\gamma^j\right\} + \left[\gamma^i,\gamma^j\right]\right) = -g^{ij} + i\epsilon^{ijk}\Sigma^k = \delta^{ij} + i\epsilon^{ijk}\Sigma^k$

using Equation (43) we simplify Equation (46) (see **Appendix B**), to have

$$\begin{aligned}\left[\hat{\theta},\left[\hat{\theta},\hat{\epsilon}\right]_-\right]_- &= \frac{e\hbar^2c^2}{8m^2c^4}\vec{\nabla}\vec{E}+\frac{ie\hbar^2c^2}{8m^2c^4}\vec{\Sigma}\cdot\vec{\nabla}\times\vec{E}+\frac{e\hbar}{4m^2c^4}\vec{\Sigma}\cdot\vec{E}\times\vec{p}\\ &+\frac{ic^2}{8m^2c^4}\left(\left[\vec{\Omega},\vec{E}\right]_-+2i\vec{\Sigma}\left(\vec{\Omega}\times\vec{E}\right)\right)+\frac{1}{8m^2c^4}\frac{e}{\hbar}\left[\left(c\left(\vec{p}-\frac{e}{c}\vec{A}\right)+\frac{c}{\hbar}\vec{\Omega}\right),\right.\\ &\left.\left[\left(c\left(\vec{p}-\frac{e}{c}\vec{A}\right)-\frac{c}{\hbar}\vec{\Omega}\right),\left(\vec{E}\times\vec{p}\right)\cdot\vec{\Theta}\right]_- -c\left[\vec{\Omega},V\right]_-\right]_-\\ &+\frac{1}{8m^2c^4}\frac{e}{\hbar}i\vec{\Sigma}\left\{-2\left(\vec{E}\times\vec{p}\right)\cdot\vec{\Theta}\cdot\left(c\left(\vec{p}-\frac{e}{c}\vec{A}\right)-\frac{c}{\hbar}\vec{\Omega}\right)\right.\\ &\times\left(c\left(\vec{p}-\frac{e}{c}\vec{A}\right)+\frac{c}{\hbar}\vec{\Omega}\right)+2c\left[\vec{\Omega},V\right]_-\times\left(c\left(\vec{p}-\frac{e}{c}\vec{A}\right)+\frac{c}{\hbar}\vec{\Omega}\right)\\ &\left.+\left[\left(c\left(\vec{p}-\frac{e}{c}\vec{A}\right)+\frac{c}{\hbar}\vec{\Omega}\right)\times\left(c\left(\vec{p}-\frac{e}{c}\vec{A}\right)-\frac{c}{\hbar}\vec{\Omega}\right),\left(\vec{E}\times\vec{p}\right)\cdot\vec{\Theta}\right]_-\right\}.\end{aligned} \tag{47}$$

Adding the various contributions Equations ((44), (47)), in Equation (38), with assuming $\frac{1}{8m^3c^6}\hat{\theta}^4\sim\frac{1}{8m^3c^6}\vec{p}^4$, and For $\psi_{FW}=\begin{pmatrix}\varphi\\0\end{pmatrix}$ the Schrödinger-Pauli equation is

$$\begin{aligned}i\hbar\frac{\partial}{\partial t}\varphi &= \left\{\hat{\beta}\left(mc^2+\frac{1}{2m}\left(\vec{p}-\frac{e}{c}\vec{A}\right)^2-\frac{1}{8m^3c^6}\vec{p}^4+\frac{1}{m\hbar}\left(\vec{p}-\frac{e}{c}\vec{A}\right)\vec{\Omega}+\frac{1}{2m\hbar^2}\vec{\Omega}^2\right.\right.\\ &\left.\left.+\frac{i}{2m}\vec{\Sigma}\left(\frac{2}{\hbar}\left(\vec{p}-\frac{e}{c}\vec{A}\right)\times\vec{\Omega}+\frac{1}{\hbar^2}\vec{\Omega}\times\vec{\Omega}\right)\right)+eV-\frac{e\hbar}{2mc}\hat{\beta}\vec{\Sigma}\vec{B}-\frac{ie\hbar^2c^2}{8m^2c^4}\vec{\Sigma}\cdot\vec{\nabla}\times\vec{E}\right.\\ &-\frac{e\hbar}{4m^2c^4}\vec{\Sigma}\cdot\vec{E}\times\vec{p}+\frac{e}{\hbar}\left(\vec{E}\times\vec{p}\right)\cdot\vec{\Theta}-\frac{e\hbar^2c^2}{8m^2c^4}\vec{\nabla}\vec{E}-\frac{ic^2}{8m^2c^4}\left(\left[\vec{\Omega},\vec{E}\right]_-+2i\vec{\Sigma}\left(\vec{\Omega}\times\vec{E}\right)\right)\\ &-\frac{1}{8m^2c^4}\frac{e}{\hbar}\left\{\left[\left(c\left(\vec{p}-\frac{e}{c}\vec{A}\right)+\frac{c}{\hbar}\vec{\Omega}\right)\times\left(c\left(\vec{p}-\frac{e}{c}\vec{A}\right)-\frac{c}{\hbar}\vec{\Omega}\right),\left(\vec{E}\times\vec{p}\right)\cdot\vec{\Theta}\right]_-\right.\\ &+2c\left[\vec{\Omega},V\right]_-\times\left(c\left(\vec{p}-\frac{e}{c}\vec{A}\right)+\frac{c}{\hbar}\vec{\Omega}\right)-2\left(\vec{E}\times\vec{p}\right)\cdot\vec{\Theta}\left(c\left(\vec{p}-\frac{e}{c}\vec{A}\right)-\frac{c}{\hbar}\vec{\Omega}\right)\\ &\left.\left.\times\left(c\left(\vec{p}-\frac{e}{c}\vec{A}\right)+\frac{c}{\hbar}\vec{\Omega}\right)\right\}\right\}.\end{aligned} \tag{48}$$

The reason of the explicit noncommutative terms entangled in the obtained Schrödinger-Pauli Equation (48), (in FW representation) is that the effect of the noncommutativity in the Dirac equation appears as a kind of potential which depends on noncommutativity parameters (η, and Θ), then after applying the nonrelativistic limit that potential is the responsible on generating a new terms and a modified known terms, which contain the noncommutative parameters (reduced in $\vec{\Omega}$), in Equation (48), where terms in the first parenthesis describe the NC nonrelativistic kinetic energy, and its first NC nonrelativistic correction (at least to the order of approximation we have considered), this is manifested as a terms contain phase-space NC parameters added to the known terms, then

successive two terms describe the electrostatic energy and the magnetic dipole energy, thereafter $-\frac{e\hbar}{4m^2c^4}\vec{\Sigma}\cdot\vec{E}\times\vec{p}+\frac{e}{\hbar}\left(\vec{E}\times\vec{p}\right)\cdot\vec{\Theta}$, represents the Θ-modified spin-orbit interaction term, in a spherically symmetric potential, with $\vec{\nabla}\times\vec{E}=0, \vec{E}=-\vec{\nabla}V\left(r\right)=-\frac{1}{r}\frac{\partial V}{\partial r}\vec{r}$, and $\vec{r}\times\vec{p}=\vec{L}$,

$$\Theta\text{-modified spin-orbit term}=\frac{e\hbar}{4m^2c^4}\frac{1}{r}\frac{\partial V}{\partial r}\vec{\Sigma}\cdot\vec{L}-\frac{e}{\hbar}\frac{1}{r}\frac{\partial V}{\partial r}\vec{L}\cdot\vec{\Theta}. \tag{49}$$

Next term in Equation (48), $-\frac{e\hbar^2c^2}{8m^2c^4}\vec{\nabla}\vec{E}-\frac{ic^2}{8m^2c^4}\left(\left[\vec{\Omega},\vec{E}\right]_-+2i\vec{\Sigma}\left(\vec{\Omega}\times\vec{E}\right)\right)$, represents the $\Theta\eta$-modified Darwin term (attributed to the Zitterbewegung [25] [26] [27]), with $\vec{E}=-\vec{\nabla}V\left(r\right)$ and $\vec{A}=0$, $\vec{\Omega}=\vec{x}\times\vec{\eta}$,

$$\begin{aligned}&\Theta\eta\text{-modified Darwin term}\\&=-\frac{e\hbar^2c^2}{8m^2c^4}\vec{\nabla}V-\frac{ic^2}{8m^2c^4}\left(\left[\vec{x}\times\vec{\eta},\vec{\nabla}V\right]_-+2i\vec{\Sigma}\left(\vec{x}\times\vec{\eta}\times\vec{\nabla}V\right)\right).\end{aligned} \tag{50}$$

The other terms in the Equation (48) represent the NC Schrödinger-Pauli equation corrections.

Essentially the intriguing part of our result is the fact that noncommutative effects grant a $\Theta\eta$-modified terms entangled in the obtained NC Schrödinger-Pauli equation.

Under the condition that space-space and momentum-momentum are all commutative (namely, $\eta=0$, $\Theta=0$) the results return to that of usual quantum mechanics.

4. Conclusions

In conclusion, the phase-space noncommutativity effect is introduced in the Dirac equation and subsequently the Foldy-Wouthuysen transformation is exploited to reduce the system in presence of electromagnetic field to a nonrelativistic regime, which gives the Schrödinger-Pauli equation.

Knowing that the phase-space noncommutativity effect is introduced by applying both of the Bopp-shift linear translation method, and the Moyal-Weyl product.

The usage of the FW representation in most cases allows one to reduce the problem of finding a classical limit of relativistic quantum mechanical equations to the replacement of operators in the hamiltonian of the quantum mechanical equations of motion by the respective classical quantities, even with noncommutativity in phase and space, and the effects of the latter are manifested in the various terms of the obtained hamiltonian.

Conflicts of Interest

The authors declare no conflicts of interest regarding the publication of this paper.

References

[1] Foldy, L.L. and Wouthuysen, S.A. (1950) *Physical Review*, **78**, 29. https://doi.org/10.1103/PhysRev.78.29

[2] Greiner, W. (2000) Quantum Mechanics an Introduction, 4th Edition, Vol. I, Springer, Berlin.

[3] Greiner, W. (1994) Quantum Mechanics. 3rd Edition, Springer, Berlin, Heidelberg.

[4] Davydov, A.S. (1965) Quantum Mechanics. 2nd Edition, Pergamon, Oxford.

[5] Messiah, A. (1968) Quantum Mechanics, Vol. II. Wiley, New York.

[6] Costello, J.P. and McKellar, B.H.J. (1995) *American Journal of Physics*, **63**, 1119-1121. https://doi.org/10.1119/1.18017

[7] Silenko, A.J. (2003) *Journal of Mathematical Physics*, **44**, 2952. https://doi.org/10.1063/1.1579991

[8] Silenko, A.J. (2008) *Physical Review A*, **77**, Article ID: 012116. https://doi.org/10.1103/PhysRevA.77.012116

[9] Nikitin, A.G. (1998) *Journal of Physics A*: *Mathematical and General*, **31**, 3297-3300. https://doi.org/10.1088/0305-4470/31/14/015

[10] Delduc, F., Duret, Q., Gieres, F. and Lefrancois, M. (2008) *Journal of Physics Conference Series*, **103**, Article ID: 012020. https://doi.org/10.1088/1742-6596/103/1/012020

[11] Douglas, M.R. and Nekrasov, N.A. (2001) *Reviews of Modern Physics*, **73**, 977-1029. https://doi.org/10.1103/RevModPhys.73.977

[12] Connes, A., Douglas, M.R. and Schwarz, A. (1998) *JHEP*, **9802**, 003. https://doi.org/10.1088/1126-6708/1998/02/003

[13] Seiberg, N. and Witten, E. (1999) *JHEP*, **9909**, 032. https://doi.org/10.1088/1126-6708/1999/09/032

[14] Chaichian, M., Demichev, A. and Presnajder, P. (2000) *Nuclear Physics B*, **567**, 360. https://doi.org/10.1016/S0550-3213(99)00664-1

[15] Mirza, B. and Mohadesi, M. (2014) *Communications in Theoretical Physics*, **42**, 664-668. http://iopscience.iop.org/0253-6102/42/5/664

[16] Bastos, C., Bertolami, O., Dias, N.C. and Prata, J.N. (2008) *Journal of Mathematical Physics*, **49**, Article ID: 072101. https://doi.org/10.1063/1.2944996

[17] Eftekharzadeh, A. and Hu, B.L. (2005) *Brazilian Journal of Physics*, **35**, 333-342. https://doi.org/10.1590/S0103-97332005000200019

[18] Li, K., Wang, J. and Chen, C. (2005) *Modern Physics Letters A*, **20**, 2165-2174. https://doi.org/10.1142/S0217732305017421

[19] Jiang, X., Long, C. and Qin, S. (2013) *Journal of Modern Physics*, **4**, 940-944. https://www.doi.org/10.4236/jmp.2013.47126

[20] Hassanabadi, H., Molaee, Z. and Zarrinkamar, S. (2014) *Advances in High Energy Physics*, **2014**, Article ID: 459345. http://dx.doi.org/10.1155/2014/459345

[21] Adorno, T.C., Baldiotti, M.C., Chaichian, M., Gitman, D.M. and Tureanu, A. (2009) *Physics Letters B*, **682**, 235-239. https://doi.org/10.1016/j.physletb.2009.11.003

[22] Bertolami, O. and Queiroz, R. (2011) *Physics Letters A*, **375**, 4116-4119. https://doi.org/10.1016/j.physleta.2011.09.053

[23] Schwabl, F. (1995) Quantum Mechanics. Springer, Berlin.

[24] Kurlin, V. (2007) *Journal of Lie Theory*, **17**, 525-538. arXiv:math/0606330.

[25] Hestenes, D. (1990) *Foundations of Physics*, **20**, 1213-1232. https://doi.org/10.1007/BF01889466

[26] Huang, K. (1952) *American Journal of Physics*, **20**, 479. https://doi.org/10.1119/1.1933296

[27] Barut, A.O. and Bracken, A.J. (1981) *Physical Review D*, **23**, 2454. https://doi.org/10.1103/PhysRevD.23.2454

Appendix A: Moving from Equation (11) to Equation (12)

The simplification to move from Equation (11) to Equation (12):

Using $\eta_{ij}=\eta\epsilon_{ij}$ and $\eta_k=\frac{1}{2}\epsilon_{kij}\eta_{ij}$, we find:

$$\begin{aligned}\alpha_i\frac{c}{2\hbar}\eta_{ij}X_j&=\frac{c}{2\hbar}\left(2\eta_k\epsilon_{kij}^{-1}\right)\alpha_iX_j\\&=\frac{c}{\hbar}\eta_k\epsilon_{kij}\alpha_iX_j,\end{aligned}\tag{51}$$

where $\epsilon_{kij}=\epsilon_{ijk}$, knowing that $\left(U\times V\right)_\mu=\epsilon_{\mu\nu\lambda}U_\nu V_\lambda$,

$$\begin{aligned}\frac{c}{\hbar}\eta_k\epsilon_{kij}\alpha_iX_j&=\frac{c}{\hbar}\left(\vec{\alpha}\times\vec{X}\right)_k\eta_k\\&=\frac{c}{\hbar}\left(\vec{\alpha}\times\vec{X}\right)\vec{\eta},\end{aligned}\tag{52}$$

with the same manner we prove that

$$\begin{aligned}&-ie\Theta_k\epsilon_{abk}\partial_a\left(\vec{\alpha}\vec{A}-A_0\right)\partial_b\\&=-ie\frac{\hbar}{\hbar}\Theta_k\epsilon_{abk}\partial_a\left(\vec{\alpha}\vec{A}-A_0\right)\partial_b\\&=\frac{e}{\hbar}\left(\vec{\nabla}\cdot\left(\vec{\alpha}\vec{A}-A_0\right)\times\vec{p}\right)\cdot\vec{\Theta}.\end{aligned}\tag{53}$$

Appendix B: The Elimination of $\vec{\alpha}$ from the Two Last Terms in Equation (46)

Using The Equation (43) we find

$$\begin{aligned}\left[\frac{c}{\hbar}\vec{\alpha}\vec{\Omega},\frac{i\hbar}{8m^2c^4}c\vec{\alpha}\vec{E}\right]_-&=\frac{c}{\hbar}\vec{\alpha}\vec{\Omega}\frac{i\hbar}{8m^2c^4}c\vec{\alpha}\vec{E}-\frac{i\hbar}{8m^2c^4}c\vec{\alpha}\vec{E}\frac{c}{\hbar}\vec{\alpha}\vec{\Omega}\\&=\frac{c^2}{\hbar}\frac{i\hbar}{8m^2c^4}\left\{\vec{\alpha}\vec{\Omega}\vec{\alpha}\vec{E}-\vec{\alpha}\vec{E}\vec{\alpha}\vec{\Omega}\right\}\\&=\frac{ic^2}{8m^2c^4}\left\{\vec{\Omega}\vec{E}+i\vec{\Sigma}\left(\vec{\Omega}\times\vec{E}\right)-\vec{E}\vec{\Omega}-i\vec{\Sigma}\left(\vec{E}\times\vec{\Omega}\right)\right\}\\&=\frac{ic^2}{8m^2c^4}\left\{\left[\vec{\Omega},\vec{E}\right]_-+i2\vec{\Sigma}\left(\vec{\Omega}\times\vec{E}\right)\right\}.\end{aligned}\tag{54}$$

And for the second term

$$\begin{aligned}&\left[c\vec{\alpha}\left(\vec{p}-\frac{e}{c}\vec{A}\right)+\frac{c}{\hbar}\vec{\alpha}\vec{\Omega},\frac{-1}{8m^2c^4}\left[\left(c\vec{\alpha}\left(\vec{p}-\frac{e}{c}\vec{A}\right)-\frac{c}{\hbar}\vec{\alpha}\vec{\Omega}\right),\frac{e}{\hbar}\left(-\vec{E}\times\vec{p}\right)\cdot\vec{\Theta}\right]_-\right.\\&\left.-\frac{1}{8m^2c^4}\left[\frac{c}{\hbar}\vec{\alpha}\vec{\Omega},eV\right]_-\right]_-\\&=\left[c\vec{\alpha}\left(\vec{p}-\frac{e}{c}\vec{A}\right)+\frac{c}{\hbar}\vec{\alpha}\vec{\Omega},\frac{-1}{8m^2c^4}\frac{c}{\hbar}e\vec{\alpha}\left[\vec{\Omega},V\right]_-\right]_-\\&+\left[c\vec{\alpha}\left(\vec{p}-\frac{e}{c}\vec{A}\right)+\frac{c}{\hbar}\vec{\alpha}\vec{\Omega},\frac{-1}{8m^2c^4}\left[\left(c\vec{\alpha}\left(\vec{p}-\frac{e}{c}\vec{A}\right)-\frac{c}{\hbar}\vec{\alpha}\vec{\Omega}\right),\frac{e}{\hbar}\left(\vec{\nabla}\left(A_0\right)\times\vec{p}\right)\cdot\vec{\Theta}\right]_-\right]_-,\end{aligned}\tag{55}$$

we start with the 1st term of the above Equation (55)

$$
\begin{aligned}
&\left[c\vec{\alpha}\left(\vec{p}-\frac{e}{c}\vec{A}\right)+\frac{c}{\hbar}\vec{\alpha}\vec{\Omega},\frac{-1}{8m^2c^4}\frac{c}{\hbar}e\vec{\alpha}\left[\vec{\Omega},V\right]_-\right]_- \\
&=-\vec{\alpha}\left(c\left(\vec{p}-\frac{e}{c}\vec{A}\right)+\frac{c}{\hbar}\vec{\Omega}\right)\left(\frac{1}{8m^2c^4}\frac{c}{\hbar}e\vec{\alpha}\left[\vec{\Omega},V\right]_-\right) \\
&\quad+\left(\frac{1}{8m^2c^4}\frac{c}{\hbar}e\vec{\alpha}\left[\vec{\Omega},V\right]_-\right)\vec{\alpha}\left(c\left(\vec{p}-\frac{e}{c}\vec{A}\right)+\frac{c}{\hbar}\vec{\Omega}\right) \\
&=\left[\frac{1}{8m^2c^4}\frac{c}{\hbar}e\vec{\alpha}\left[\vec{\Omega},V\right]_-,\left(c\left(\vec{p}-\frac{e}{c}\vec{A}\right)+\frac{c}{\hbar}\vec{\Omega}\right)\right]_- \\
&\quad+2i\frac{1}{8m^2c^4}\frac{c}{\hbar}e\vec{\Sigma}\left(\left[\vec{\Omega},V\right]_-\right)\times\left(c\left(\vec{p}-\frac{e}{c}\vec{A}\right)+\frac{c}{\hbar}\vec{\Omega}\right),
\end{aligned}
\tag{56}
$$

using Equation (39), we continue with the 2nd term,

$$
\begin{aligned}
&\left[c\vec{\alpha}\left(\vec{p}-\frac{e}{c}\vec{A}\right)+\frac{c}{\hbar}\vec{\alpha}\vec{\Omega},\frac{1}{8m^2c^4}\left[\left(c\vec{\alpha}\left(\vec{p}-\frac{e}{c}\vec{A}\right)-\frac{c}{\hbar}\vec{\alpha}\vec{\Omega}\right),\frac{e}{\hbar}\left(\vec{E}\times\vec{p}\right)\cdot\vec{\Theta}\right]_-\right]_- \\
&=\frac{1}{8m^2c^4}\frac{e}{\hbar}\left\{\left(c\left(\vec{p}-\frac{e}{c}\vec{A}\right)+\frac{c}{\hbar}\vec{\Omega}\right)\left\{\left(c\left(\vec{p}-\frac{e}{c}\vec{A}\right)-\frac{c}{\hbar}\vec{\Omega}\right)\left(\vec{E}\times\vec{p}\right)\cdot\vec{\Theta}\right.\right. \\
&\quad\left.-\left(\vec{E}\times\vec{p}\right)\cdot\vec{\Theta}\left(c\left(\vec{p}-\frac{e}{c}\vec{A}\right)-\frac{c}{\hbar}\vec{\Omega}\right)\right\}-\left\{\left(c\left(\vec{p}-\frac{e}{c}\vec{A}\right)-\frac{c}{\hbar}\vec{\Omega}\right)\left(\vec{E}\times\vec{p}\right)\cdot\vec{\Theta}\right. \\
&\quad\left.\left.-\left(\vec{E}\times\vec{p}\right)\cdot\vec{\Theta}\left(c\left(\vec{p}-\frac{e}{c}\vec{A}\right)-\frac{c}{\hbar}\vec{\Omega}\right)\right\}\left(c\left(\vec{p}-\frac{e}{c}\vec{A}\right)+\frac{c}{\hbar}\vec{\Omega}\right)\right\} \\
&\quad+\frac{1}{8m^2c^4}\frac{e}{\hbar}i\vec{\Sigma}\left\{\left(c\left(\vec{p}-\frac{e}{c}\vec{A}\right)+\frac{c}{\hbar}\vec{\Omega}\right)\left(c\left(\vec{p}-\frac{e}{c}\vec{A}\right)-\frac{c}{\hbar}\vec{\Omega}\right)\left(\vec{E}\times\vec{p}\right)\cdot\vec{\Theta}\right. \\
&\quad-\left(c\left(\vec{p}-\frac{e}{c}\vec{A}\right)+\frac{c}{\hbar}\vec{\Omega}\right)\left(\vec{E}\times\vec{p}\right)\cdot\vec{\Theta}\left(c\left(\vec{p}-\frac{e}{c}\vec{A}\right)-\frac{c}{\hbar}\vec{\Omega}\right) \\
&\quad-\left(\vec{E}\times\vec{p}\right)\cdot\vec{\Theta}\left(c\left(\vec{p}-\frac{e}{c}\vec{A}\right)-\frac{c}{\hbar}\vec{\Omega}\right)\left(c\left(\vec{p}-\frac{e}{c}\vec{A}\right)+\frac{c}{\hbar}\vec{\Omega}\right) \\
&\quad\left.-\left(\vec{E}\times\vec{p}\right)\cdot\vec{\Theta}\left(c\left(\vec{p}-\frac{e}{c}\vec{A}\right)-\frac{c}{\hbar}\vec{\Omega}\right)\times\left(c\left(\vec{p}-\frac{e}{c}\vec{A}\right)+\frac{c}{\hbar}\vec{\Omega}\right)\right\} \\
&=\frac{1}{8m^2c^4}\frac{e}{\hbar}\left\{\left(c\left(\vec{p}-\frac{e}{c}\vec{A}\right)+\frac{c}{\hbar}\vec{\Omega}\right)\left\{\left[\left(c\left(\vec{p}-\frac{e}{c}\vec{A}\right)-\frac{c}{\hbar}\vec{\Omega}\right),\left(\vec{E}\times\vec{p}\right)\cdot\vec{\Theta}\right]_-\right\}\right. \\
&\quad\left.-\left\{\left[\left(c\left(\vec{p}-\frac{e}{c}\vec{A}\right)-\frac{c}{\hbar}\vec{\Omega}\right),\left(\vec{E}\times\vec{p}\right)\cdot\vec{\Theta}\right]_-\right\}\left(c\left(\vec{p}-\frac{e}{c}\vec{A}\right)+\frac{c}{\hbar}\vec{\Omega}\right)\right\} \\
&\quad+\frac{1}{8m^2c^4}\frac{e}{\hbar}i\vec{\Sigma}\left\{\left(c\left(\vec{p}-\frac{e}{c}\vec{A}\right)+\frac{c}{\hbar}\vec{\Omega}\right)\times\left(c\left(\vec{p}-\frac{e}{c}\vec{A}\right)-\frac{c}{\hbar}\vec{\Omega}\right)\left(\vec{E}\times\vec{p}\right)\cdot\vec{\Theta}\right. \\
&\quad-\left(\vec{E}\times\vec{p}\right)\cdot\vec{\Theta}\left(c\left(\vec{p}-\frac{e}{c}\vec{A}\right)-\frac{c}{\hbar}\vec{\Omega}\right)\times\left(c\left(\vec{p}-\frac{e}{c}\vec{A}\right)+\frac{c}{\hbar}\vec{\Omega}\right) \\
&\quad-\left(\vec{E}\times\vec{p}\right)\cdot\vec{\Theta}\left(c\left(\vec{p}-\frac{e}{c}\vec{A}\right)+\frac{c}{\hbar}\vec{\Omega}\right)\times\left(c\left(\vec{p}-\frac{e}{c}\vec{A}\right)-\frac{c}{\hbar}\vec{\Omega}\right) \\
&\quad\left.-\left(\vec{E}\times\vec{p}\right)\cdot\vec{\Theta}\left(c\left(\vec{p}-\frac{e}{c}\vec{A}\right)-\frac{c}{\hbar}\vec{\Omega}\right)\times\left(c\left(\vec{p}-\frac{e}{c}\vec{A}\right)+\frac{c}{\hbar}\vec{\Omega}\right)\right\},
\end{aligned}
\tag{57}
$$

finally we find

$$\frac{1}{8m^2c^4}\frac{e}{\hbar}\left[\left(c\left(\vec{p}-\frac{e}{c}\vec{A}\right)+\frac{c}{\hbar}\vec{\Omega}\right),\left[\left(c\left(\vec{p}-\frac{e}{c}\vec{A}\right)-\frac{c}{\hbar}\vec{\Omega}\right),\left(\vec{E}\times\vec{p}\right)\cdot\vec{\Theta}\right]_-\right]_-$$
$$+\frac{1}{8m^2c^4}\frac{e}{\hbar}i\vec{\Sigma}\left\{\left[\left(c\left(\vec{p}-\frac{e}{c}\vec{A}\right)+\frac{c}{\hbar}\vec{\Omega}\right)\times\left(c\left(\vec{p}-\frac{e}{c}\vec{A}\right)-\frac{c}{\hbar}\vec{\Omega}\right),\left(\vec{E}\times\vec{p}\right)\cdot\vec{\Theta}\right]_-\right. \quad (58)$$
$$\left.-2\left(\vec{E}\times\vec{p}\right)\cdot\vec{\Theta}\left(c\left(\vec{p}-\frac{e}{c}\vec{A}\right)-\frac{c}{\hbar}\vec{\Omega}\right)\times\left(c\left(\vec{p}-\frac{e}{c}\vec{A}\right)+\frac{c}{\hbar}\vec{\Omega}\right)\right\}.$$

Journal of Modern Physics, 2018, 9, 2035-2044
http://www.scirp.org/journal/jmp
ISSN Online: 2153-120X
ISSN Print: 2153-1196

Critical Limit Principle of Maximum Entropy and Reinterpretation of Scaling Laws

Yougang Feng

College of Physics, Guizhou University, Guiyang, China
Email: ygfeng45@aliyun.com

How to cite this paper: Feng, Y.G. (2018) Critical Limit Principle of Maximum Entropy and Reinterpretation of Scaling Laws. *Journal of Modern Physics*, **9**, 2035-2044.
https://doi.org/10.4236/jmp.2018.911128

Received: August 16, 2018
Accepted: September 11, 2018
Published: September 14, 2018

Abstract

The critical limit principle of maximum entropy is put forward, it's a sufficient condition to obtain accurate critical points, and ensure that the new phase system is still in the maximum entropy state. Two representations for the phase transition of Ising models are found; the universal formula of critical points is explained by thermodynamics. From the point of view of fractal geometry and the correspondence between symmetry and conservation, the scaling laws are reinterpreted. The self consistence equations for the universal class are set up, by which and the scaling laws higher accurate exponents to date are obtained. The temperature where the self similar transformation disappears is calculated.

Keywords

Entropy, Critical-Point, Scaling, Exponent, Self-Consistence

1. Introduction

As a fundamental issue, the critical phenomena theory has pervaded modern physics, the approach to the critical point, the critical fluctuation, and the critical exponents help us understand critical laws deeply. The precise calculation of critical points and critical exponents is the common goal of the researchers. The symmetry analysis that is usually applied in particle physics makes our research to a new state, and has got more quantitative results [1]. There are some important models, among which Ising model is particularly striking. However, the accurate evaluation of the critical points was always an unsolvable problem for 3d models by conventional theory. The main difficulty is that one cannot get the exact value of a block spin because all conventional theories and methods are limited to Euclidean geometry. Euclidean geometry uses simple graphics as a tool

to study certain objects with complexity. On the contrary, fractal geometry gets a simple result when using complicated self similar (SS) transformation. By means of fractal geometry, the accurate critical points for 2d and 3d models are obtained [2]. For an infinite lattice system, it seems that there are two ways to an ordered state: 1) In the fractal geometry sense, the local lattices are correlated to each other to form finite size block spins, and the system is ordered by infinite hierarchical SS transformation, *i.e.*, the block side length can be considered as the lattice correlation length, and it is finite. 2) From the eyes of the Euclidean geometry, all lattices are correlated to one another to construct an ordered system, the correlation length is infinite. The system entropy in the first way is greater than that of the second way, since the ordering degree of the system in the first way is lower than that in the second way. In a word, relative to infinity, the finite correlation length makes the system more chaotic, thus the system entropy is greater.

The focus of both views is the lattice correlation length. Whether the correlation length is infinite or finite, we can respond in only one of the two ways. In fact, the concept of infinite correlation length is merely a theoretical assumption. We can't measure the infinite length; we can only measure the exponent υ that is associated with the length in term of the conventional theory. According to the assumption, the infinite correlation length occurs at the critical temperature T_{cf}, and disappears at the temperature T that is in the vicinity of T_{cf}, and $T < T_{cf}$. The idea that the ordered state is derived from the lattice correlation is reasonable, but the argument that the correlation length disappears suddenly in the vicinity of T_{cf} is hard to convince us. Let a system have N_m lattices in total, a block contain N lattices, the maximum hierarchy number of the SS transformation be r_m, we have

$$r_m = \ln N_m / \ln N \tag{1}$$

where the symbol "ln" represents natural logarithm. If the system is infinite, $N_m \to +\infty$, with the deceasing of temperature the lattice correlation length n increases from n^*, which is the block side length at the critical pint, to infinity, so does N at T_{cs}, where the correlation length becomes infinity and the whole system is a block [1]. Since N is finite at the critical point, no matter what value N takes, r_m will tend to infinity due to the infinite N_m. However, this is an ideal situation that can't occur in nature. The exponent υ is a measurable parameter, and a specimen that can be measured only has limited size and lattices N_m, although it may be approximately considered as infinity. It is the finite N_m that leads to that the maximum hierarchy number r_m can't become infinity: When the temperature decreases after the transition, the correlation length (the block side length n) increases, and r_m is changing smaller and smaller with N is getting bigger and bigger. This proves that the exponent υ describes actually the behavior of the number r_m rather than the correlation length's. For example, for the irreducible lattice system of Ising model [2], r_m behaves as

$$r_m \propto \left|T - T_{cf}\right|^{-\upsilon} \tag{2}$$

For the reducible lattice system [2], we have the similar conclusion.

This paper is formed by the above point of view. In Section 2, we put forward the critical limit principle of maximum entropy. We prove again the uniqueness of the critical point. From the dual relation of J and S^2, we find two representations for the phase transition: spin representation and coupling constant representation. We clarify, in the thermodynamics sense, the meaning of the critical point. From the point of view of the SS transformation, we reinterpret the scaling laws that they are conserved laws corresponding to the symmetry transformation. We set up universal class self consistence constant and the relevant equations for the exponents, and point out that the exponents must satisfy simultaneously the scaling laws and the equations, and the scaling laws are available for the whole renormalization region $T_{cs} < T \le T_{cf}$ rather than in the vicinity of T_{cf}. The structural meaning of the disorder-order phase transition is that the original lattice spin system has become the self-similar block spin system. In Section 3, we calculate T_{cs} and exponents, get a group of exponents, which is the most accurate and self consistent datum to date. Section 4 is conclusion remark. For simplicity, both blocks and sub-blocks are uniformly called blocks in this paper, and the relation between the sub-block's dimension and the block's dimension for the reducible lattice system is given by the formula (6.2) of reference [2].

2. Theory

2.1. Critical Limit Principle of Maximum Entropy

The conventional theory thinks that since lattice spins are correlated over scales up to the correlation length ζ, it may be plausible to regard the spins with regions up to ζ in size as behaving like a single block spin of side length n, and $n \le \zeta$, *i.e.*, the block formation originates from the infinite correlation length. It's said that one can get accurate critical point only if let n take ζ, if $\zeta \to +\infty$. In fact, this is not true [2].

We find that there exist simultaneously two sorts of blocks: n_+-blocks and n_--blocks, only one of them can become ordered, another disordered [1]. So, there are two kinds of correlation lengths: the first refers to the ordered, the second to the disordered. They are different from each other, resulting in that both are finite. Consider a system consisting of infinite subsystems, the values of spins of the i-th subsystem are identical and equal to S_i, the free energy is F_i; the system free energy F is given by

$$F = \sum_{i=1}^{\infty} P_i F_i \tag{3}$$

where P_i is the occurrence probability of the i-th subsystem. The value of P_i can't change the influence of the singularity of F_i on the singularity of F. If P_i is determined by Gaussian distribution, F is also the Gaussian distribution free energy, and represented in the form as the Equation (11) of reference [2]. The

Gaussian distribution makes the system in the maximum entropy state [1]. We then get a principle:

Critical limit principle of maximum entropy: A thermodynamic equilibrium system keeps itself in the maximum entropy state before disorder-order phase transition, and tends to the critical point in this manner.

According to the fractal theory that a system containing a large plenty of lattice spins becomes ordered as the same as a point spin is a kind of spin contraction mapping, which ensures the uniqueness and existence of self similar transformation [3]. This principle pledges the uniqueness of the critical point. It is this principle that helps us get accurate critical points for 2d and 3d models [2]. It's should be emphasized that the Gaussian distribution differs from the Gaussian model, the former determine which subsystem is that we need; the latter allows the system change the value of the block spin at the same temperature, although all block spins have the identical value. The common feature of both systems is they have the same free energy singularity. This means that we can get the critical point by Gaussian model. Using the fixed-point Equation (5) of reference [1], we can prove that the block side length n^* at the critical point is unique and finite. For the triangle lattice system, substituting $N=(n+1)(n+2)/2$, see [2], into the equation:

$$(2-D_{\min})n^2+3(1-D_{\min})n-2D_{\min}=0 \tag{4}$$

Equation (4) has only a positive finite real solution n^* due to $1<D_{\min}<2$. For the tetrahedron lattice system, $N=\left(n^3+6n^2+11n+6\right)/6$, see [2], the equation becomes

$$(3-D_{\min})n^3+(12-6D_{\min})n^2+(11-11D_{\min})n-6D_{\min}=0 \tag{5}$$

This equation has a unique finite real root n^*. As the same reason, there is a unique finite side length n^* at the critical point for any one system, which accords with the result of numerical calculation [2].

2.2. Dual Relation

The energy conservation of transformation produces a dual relation of J and S^2 [2]:

$$ZJS^2=2Djs^2 \tag{6}$$

where the lattice spin $s^2=1$, its coupling constant j, the block fractal dimension is D, its spin square is S^2, coupling constant J, and coordinate number Z. For a given system Z is constant. Let $J=j$, we get spin representation:

$$S^2=(2D/Z)s^2 \tag{7}$$

If let $S^2=s^2$, we have coupling constant representation from Equation (6):

$$J=(2D/Z)j \tag{8}$$

The two representations are equivalent. In the early renormalization group (RG) theory the coupling constant representation is adopted [4]. In the Gaussian

distribution, we use the spin representation [2]. Both relate to the common transformation $(2D/Z)$, and the fractal dimension D takes the minimum $D_{\min}$ at the critical point. The theory that the critical point is a fixed point in the coupling constant representation should be equivalent to that the $D_{\min}$ at the critical point corresponds to the fixed point of the block side length in the spin representation as the two representations describe the same case.

2.3. Universal Formula of Critical Points for Ising Models

The singularity of the free energy gives rise to

$$ZJS_{\min}^2 = k_B T_{cf} \tag{9}$$

This is a universal relation for the critical points of Ising models [2], where T_{cf} is the disorder-order phase transition temperature, k_B Boltzmann constant. At a temperature T, a system has a definite mean energy $\langle E \rangle$, its free energy F and entropy S_e obey thermodynamic condition:

$$F = \langle E \rangle - TS_e \tag{10}$$

Only if the entropy S_e is maximum can the free energy F be minimized when the T is constant. That the block spin takes the minimum when the system reaches to T_{cf} is the best selection to satisfy the condition. We may view $ZJS_{\min}^2$ as an ordering tendency, $k_B T_{cf}$ as a disordering tendency caused by thermal motion. The critical point not only is a balance point for the two tendencies, but also a starting point of the ordering of the system. The fact that the block spin formation is the self-organization behavior and the cooperation phenomena of the lattice spins. Discussing the atomic system, Dirac pointed out that the observed specific heats at ordinary temperatures are given fairly well by a theory that takes into account merely the motion of each atom as a whole and assigns no internal motion to it at all [5]. Likewise, we should only consider the interaction between the block spins, the interaction between the lattice spins exists only inside the block spins. Under the condition of the maximum system entropy, the increasing of the ordering degree is compensated by the decreasing of temperature, and the ordering tendency overwhelms the disordering tendency below T_{cf}:

$$ZJS^2 > k_B T \tag{11}$$

It's the lattice correlation length that determines the size of the block space, *i.e.*, the block side length. The lower the temperature, the longer the correlation length, and the larger the block side length (the block spin) and the higher the ordering degree. By means of boundary condition, Onsager carried the plane square lattice system onto a torus, and obtained a lager critical point than ours [2] [6]: 0.4407 > 0.4387, which means his model has lower critical temperature than the model on the plane. The lower critical temperature originates in the boundary condition, which requires an extra ordering degree, besides the plane systems.

2.4. Reinterpretation of Scaling Laws—Symmetry and Conservation

The T_{cf} is just the critical temperature T_c defined by the conventional phase transition theory. We notice that there is no singularity behavior below T_{cf}, *i.e.*, the block structure exists until T_{cs} and the block spins replace the lattice spins. We call the region $T_{cs} < T \le T_{cf}$ as renormalization region, rather than merely the criticality one.

The scaling laws are based on the scaling hypothesis, which is purely a conjecture. Taking Ising model as an example, we interpret it by Euclidean geometry and fractal geometry. From the point of view of Euclidean geometry, the reason why the GR theory works is that the lattice correlation length becomes infinity in the vicinity of T_{cf}, such that the influence of all finite microscopic characteristic lengths are wiped out, and the correlation length is a unique characteristic quantity. The singularities of thermodynamic parameters are attributed to the correlation length singularity, and any size transformation can't change the form of the free energy function, only changes the parameter scaling. On the other hand, the transformation hierarchy is emphasized in terms of fractal geometry: The formation of blocks with finite side length n begins at T_{cf}, they can go through r-hierarchical SS transformations at the same temperature, and the original lattice spin system is replaced by the block spin system. For any finite value of r, one can find the same form of the free energy function represented by the block spins, no matter what value of r will be. Clearly, both interpretations describe the same phenomena. It's impossible to explain in terms of Euclidean geometry the uniqueness of the block side length n^* at the critical point and the coexistence of n_+-blocks and n_--blocks. In fact, the renormalization transformation is just the self similar one. In a word, the geometrical structure and the physical parameters function forms on the (r + 1)-th hierarchy maintain the original ones on the r-hierarchy. By the forms, we are unable to recognize which belong to the r-hierarchy and what is the actual value of r. The indistinguishability means symmetry [7]. The SS transformation comes essentially from the spacetime homogeneity and is a special type of symmetrical transformation, differing from the conventional operations such as rotation, translation, inversion, etc. The GR is a symmetry group, its corresponding conserved quantity is the scaling, and there exists scaling invariance. The scaling laws do be the conservation laws.

For a universal class of space dimension d and order parameter dimension m, there are two independent conserved constants: p and q, they can be considered as the magnitudes of two orthogonal constant vectors $\boldsymbol{p}$ and $\boldsymbol{q}$, respectively. According to Wilson theory [8], p and q are given by

$$p \propto \ln\left(2D/Z\right)/\ln N, \quad q \propto \ln\left(\sqrt{2D/Z}\right)/\ln N \tag{12}$$

where the elementary excitation of block spins is badly neglected [9]. The actual relation between p and q should be as

$$p = \sigma\left(d,m\right)q \tag{13}$$

where $\sigma\left(d,m\right)$ is a universal class self consistence constant. Three parameters

in this equation, only two of them are independent. p and q control six exponents:

$$\alpha = 2 - 1/p\,,\quad \beta = (1-q)/p\,,\quad \gamma = (2q-1)/p \tag{14}$$

$$\delta = q/(1-q)\,,\quad \eta = d(1-2q)+2\,,\quad \upsilon = 1/pd \tag{15}$$

They determine four scaling laws:

$$\alpha + 2\beta + \gamma = 2\,,\quad \gamma = \beta(\delta - 1) \tag{16}$$

$$\gamma = \upsilon(2-\eta)\,,\quad \upsilon d = 2 - \alpha \tag{17}$$

Using Equations (13)-(17), there should theoretically be 15 self consistence equations for $\sigma(d,m)$ by the combinations of any two different exponents. But, the combinations of α and υ, η and δ have no consequence, 13 equations are actually established:

$$\sigma_1 = 1/(2-\alpha-\beta)\,,\quad \sigma_2 = 1/(\beta+\gamma)\,,\quad \sigma_3 = 2d/\left[(2-\alpha)(2+d-\eta)\right] \tag{18}$$

$$\sigma_4 = (\delta+1)/\delta(2-\alpha)\,,\quad \sigma_5 = 2/(\gamma+2-\alpha)\,, \tag{19}$$

$$\sigma_6 = 1/(\beta\delta)\,,\quad \sigma_7 = 1/(d\upsilon-\beta)\,,\quad \sigma_8 = (\delta-1)/(\delta\gamma)\,,\quad \sigma_9 = 2/(\gamma+d\upsilon) \tag{20}$$

$$\sigma_{10} = (4-2\eta)/\gamma(d+2-\eta)\,,\quad \sigma_{11} = 2d/\left[\upsilon d(d+2-\eta)\right] \tag{21}$$

$$\sigma_{12} = (1+\delta)/(\upsilon d\delta)\,,\quad \sigma_{13} = (d-2+\eta)/\beta(d+2-\eta) \tag{22}$$

The conservation requires that all exponents should not only obey the scaling laws, but also satisfy the self consistence equations, and $\sigma_i = \sigma(d,m)$ for all i, $i = 1,2,\cdots,13$. Our experience indicates that the scaling laws are not sensitive to the errors of the exponents: if the deviation between the exponents values and a law is 0.0001, the difference between the high accurate value of the exponent and its crude value is usually greater than 0.0001. As this reason, the exponents must strictly obey the laws. In most cases, the self consistence equations have higher sensitivity to the exponents values: the exponents that can comply with the laws are not necessarily accord with them. Only those exponents that satisfy both the laws and the self consistence equations have higher accuracy.

The experimental datum illustrate that all order parameters curves are smoothly continuous when the temperature is below T_{cf} [8]. We think that the scaling laws and the self consistence equations are applicable to the renormalization region $T_{cs} < T \le T_{cf}$, and the exponents values are determined by T. The relevant power law can be written as

$$(T_y - T)^{\pm x} \tag{23}$$

where T_y is in the normalization region, $T_y > T$, and T in the vicinity of T_y, $x = \alpha,\beta,\gamma,\delta,\eta,\upsilon$, their positive and negative signs are the same as the ones' at T_{cf-0}, which is in the vicinity of T_{cf}, and $T_{cf-0} < T_{cf}$. For example, by Equations ((1), (2), and (23)), we get

$$\ln N \propto (\ln N_m)(T_y - T)^{\upsilon} \tag{24}$$

N increases with the decreasing of T. Equation (24) verifies that the power law is a characteristic of fractals [10].

3. Discussion

3.1. Calculation of T_{cs}

Whether it is irreducible system or reducible system [2], the blocks disappear at T_{cs}, where the mean energy $\langle E \rangle$ of the elementary excitation of the block spins vanishes. We then get the following consequence [9]

$$\langle E \rangle = \int_0^{x_D} \frac{x^2}{\mathrm{e}^x - 1} \mathrm{d}x = 0 \tag{25}$$

where $x = \hbar\omega / k_B T$, $x_D = \hbar\omega_D / k_B T_{cs}$, $\hbar$ is Plank constant, ω the magnetic phonon frequency, ω_D the Debye frequency. Generally, we may get T_{cs} from the integral equation. If $\mathrm{e}^x \gg 1$, $\mathrm{e}^x - 1 \approx \mathrm{e}^x$. Equation (25) simplifies as

$$\int_0^{x_D} x^2 \mathrm{e}^{-x} \mathrm{d}x = 0 \tag{26}$$

This leads to an algebraic equation

$$x_D^2 \mathrm{e}^{-x_D} + 2x_D \mathrm{e}^{-x_D} + 2\mathrm{e}^{-x_D} - 2 = 0 \tag{27}$$

We'll get T_{cs} from the solution. If $\mathrm{e}^x \approx 1$, Equation (25) becomes

$$\int_0^{x_D} x \mathrm{d}x = 0 \tag{28}$$

$x_D = 0$, the solution is unreasonable.

3.2. Numerical Estimation of Critical Exponents

The elementary excitation of block spins also contributes to the free energy non-singularity [9]. In addition, there is disorder-order state transformation between the n_+-blocks and the n_--blocks [2], all these add the complexity of calculating the exponents. Usually, they are obtained by numerical approximation, in which process it's common practice to introduce appropriate adjustable parameters. The usual methods involve ε-expansion, field theory, Monte Carlo, high-temperature expansion, etc. [11]. A number of expansions are divergent, for example, the ε-expansion. An experienced author can get more exact results from the series by using Borel summation and educated guess. In this regard, Zinn-Justin achieved success [12]. Unfortunately, we examine that his exponents can't satisfy simultaneously the scaling laws and the self consistence equations. The self consistence equations provide us a new key for the numerical simulation. Based on the datum given by him and others [8] [11] [12] [13] [14], we get higher accurate solutions by golden section method and numerical approximation in the scaling laws and the self consistence equations. They are listed in the **Table 1** below, including the exponents of 2d Ising model. Because all exponents are dependent on the constant $\sigma(d,m)$, the repetitive operation may produce an extra additive effect of errors. In order to reduce the superposition, we make the p, q, and the constant $\sigma(d,m)$ accurate to the sixth decimal place, the exponents and

Table 1. Universal class self consistence constant and critical exponents.

d,m	$\sigma(d,m)$	q	p	α	β	γ	δ	η	υ
2.1	8/15	15/16	1/2	0	1/8	7/4	15	1/4	1
3.1	0.638613	0.827204	0.528263	0.1070	0.3271	1.2388	4.7872	0.0368	0.6310
3.2	0.610231	0.817227	0.498697	−0.0052	0.3665	1.2722	4.4713	0.0966	0.6684
3.3	0.583511	0.826243	0.482122	−0.0742	0.3604	1.3534	4.7552	0.0425	0.6914

constant σ_i accurate to the fourth decimal place, so as to let the extra errors lie as behind as possibly the fourth decimal point. In principle, if we want the exponents and the constant σ_i to be accurate to the x-th decimal place, the constant $\sigma(d,m)$, p, and q should be to the (x + 2)-th decimal place. For example, the following exponents and σ_i for the universal class of $d = 3$ and $m = 1$ are accurate to the sixth decimal point, $x = 6$: $\alpha = 0.107063$, $\beta = 0.327093$, $\gamma = 1.238571$, $\delta = 4.787153$, $\eta = 0.036779$, $\upsilon = 0.630979$, $\sigma_i = 0.638633(i = 1,2,\cdots,13)$; and the others to the eighth decimal place: $\sigma(3,1) = 0.63863311$, $p = 0.52827948$, $q = 0.82720347$. This group of exponents is the most accurate and self consistent datum to date. More accurate exponents will be obtained by the same method.

4. Conclusion Remark

The critical limit principle of maximum entropy introduces a correct way to obtain accurate critical points. The reinterpretation of the scaling laws from the correspondence between symmetry and conservation gives us a new understanding of scaling invariance. Based on the experimental and theoretical datum given by other authors, and applying golden section method and numerical approximation in the scaling laws and the self consistence equations, we can get higher accurate exponents.

Conflicts of Interest

The author declares no conflicts of interest regarding the publication of this paper.

References

[1] Feng, Y.G. (2018) *Journal of Modern Physics*, **9**, 241-249. https://doi.org/10.4236/jmp.2018.92016

[2] Feng, Y.G. (2014) *American Journal of Modern Physics*, **3**, 184-194.

[3] Kigami, J. (2001) Analysis on Fractals. Cambridge University Press, Cambridge. https://doi.org/10.1017/CBO9780511470943

[4] Domb, C. and Green, M.S. (1976) Phase Transitions and Critical Phenomena, Vol. 6. Academic Press, London.

[5] Dirac, P.A.M. (1958) The Principles of Quantum Mechanics. 4th Edition, Oxford University Press, Oxford.

[6] Onsager, L. (1944) *Physical Review*, **65**, 117. https://doi.org/10.1103/PhysRev.65.117

[7] Weyl, H. (1952), Symmetry. Princeton University Press, New Jersey. https://doi.org/10.1515/9781400874347

[8] Ma, S.-K. (1976) Modern Theory of Critical Phenomena. W. A. Benjamin, Inc., Massachusetts.

[9] Feng, Y.G. (2014) *American Journal of Physics*, **3**, 211-217.

[10] Bak, P., Tang, C. and Wiesenfeld, K. (1987) *Physical Review Letters*, **59**, 381-383. https://doi.org/10.1103/PhysRevLett.59.381

[11] Binney, J.J., Dowrick, N.J., Fisher, A.J. and Newman, M.J. (1992) The Theory of Critical Phenomena: An Introduction to the Renormalization Group. Oxford University Press, Oxford.

[12] Zinn-Justin, J. (2007) Phase Transitions and Renormalization Group. Oxford University Press, Oxford. https://doi.org/10.1093/acprof:oso/9780199227198.001.0001

[13] Moshe, M. and Zinn-Justin, J. (2003) *Physics Reports*, **385**, 69-228. https://doi.org/10.1016/S0370-1573(03)00263-1

[14] Pelissetto, A. and Vicari, E. (2002) *Physics Reports*, **368**, 549-727. https://doi.org/10.1016/S0370-1573(02)00219-3

Journal of Modern Physics, 2018, 9, 2045-2072
http://www.scirp.org/journal/jmp
ISSN Online: 2153-120X
ISSN Print: 2153-1196

Three Conditions Leading to a Unified (Quasi-Newtonian) Physics

Alfredo Bacchieri

University of Bologna, Bologna, Italy
Email: abacchieri@libero.it

How to cite this paper: Bacchieri, A. (2018) Three Conditions Leading to a Unified (Quasi-Newtonian) Physics. *Journal of Modern Physics*, **9**, 2045-2072.
https://doi.org/10.4236/jmp.2018.911129

Received: June 28, 2018
Accepted: September 11, 2018
Published: September 14, 2018

Abstract

It is shown that the *total* escape speed u (*i.e. from all the masses in space*), which depends on the *total* gravitational potential U through the relation $u = (-2U)^{1/2}$, tends to c; then, under the 1st condition $c = u$, and assuming (as a 2nd condition) the light as composed of longitudinally-extended, elastic (*i.e.* variable length) and massive particles, (photons), emitted at speed u referred to the *initial* location (O) of their source, we show that c referred to O becomes invariant despite any motion of its source from O. We revised the Doppler effect for the light, the gravitational redshift cause, the time dilation, highlighting the differences with respect to the Relativity. In the 2nd part, considering (3rd condition) the electron charge as a point-particle fixed to the electron surface and facing the atom nucleus during the electron orbit, the light-matter interaction becomes a consequence of the *particular* impacts between these photons and the circling electrons: e.g., on H atom, we found 137 circular orbits only, the last one being the ionization orbit, where the electron orbital speed becomes $v_i = c/137^2$. [*Classical* physics, under the assumption that a circling electron should produce (like a macroscopic electric circuit), an electro-magnetic radiation, implies that this *claimed* effect has to cause the electron fall into its nucleus: on Section 2.5, we show that the e.m. radiation of a circling electron only happens *between* two circular orbits].

Keywords

Doppler Effect for the Light, Harvard Tower Experiment, Gravitational Redshift, Time Dilation, Absorption/Emission, Photoelectric and Compton Effects

1. Speed of Light

1.1. Introduction

This paper is based on the following assumptions:

1) Finite mass of the universe.

2) Newton's absolute time and space.

Then, the following two conditions:

- Equality between the speed of light c and the *total* escape speed u.
- Light composed of longitudinal-extended, elastic particles, as defined on Section 1.4.

We obtain, on the 1st Part, these main results:

1) The measured constancy of c is due, first, to the constancy of the *total* gravitational potential U on Earth: indeed, the max variation of U on Earth, occurring between Aphelion and Perihelion, leads to a negligible $\Delta u_{AP} = 0.10\ \text{m}\cdot\text{s}^{-1}$; moreover, the speed of light emitted by a source, either fixed or in motion from its *initial* location O (where the photons emission starts), is invariant with respect to O;

2) Doppler effect equations for the light, slightly different from the relativistic ones;

3) The *compensating velocity*, (to restore the resonance source-absorber on Harvard Tower Experiment), has same value but contrary direction with respect to the one predicted by GR;

4) The variation of U from ground to GPS satellite level, implying a decrease of c and consequently a decrease of the frequency of the photons emitted by atomic clocks at that altitude, give them an increase of their counted time (inducing them to run faster);

5) High gravitational redshifts are due to the increase of c (inducing the increase of the photons length λ) during their path toward the Earth where $|U_o| >> |U_{\to\infty}|$.

On the 2nd part, under the third condition claiming that the electron charge can be considered as a point-particle fixed to the electron surface, and facing the atom nucleus during the electron orbit, we got these results:

On H atom:

6) $n = 1, 2, \cdots, 137$ electron circular progressive orbits, not an infinite number; n also represents the number of admitted photons (of the same ray) absorbed (or emitted) by the electron during two electron orbits: (in fact, the photons total number along each circular double-orbit (in short d-orbit) becomes n^2, as shown on Section 2.4);

7) The electron radius becomes $r_e = \left[(1/137\alpha) - 1\right] r_0$ (instead of its *classical* value $r_e = \alpha^2 r_B$ with $r_B = \alpha/4\pi R_\infty$ the Bohr radius and α the fine structure constant); $r_0 = \alpha/4\pi R_H$ is the orbit of the electron charge, while the orbit of the electron barycenter (electron *effective* orbit) becomes $r_0' = r_0 + r_e = r_0/137\alpha$;

8) The electron charge orbital speed along r_0 becomes $v_0 = \alpha c$, while the electron *effective* orbital speed along the orbit r_0' becomes $v_0' = c/137$;

9) The electron *radial* speed (due to the impacts *photons*-electron) becomes $w_{n^2} = c/137^2$ constant for every circular orbit; along the orbit #137, the electron orbital speed becomes $v_{137} = c/137^2$ and since $w_{n^2} = v_{137}$ there is ionization.

10) On Photoelectric effect the number of *photons* hitting a circling electron varies from n_f related to the specific threshold frequency ν_f ($=W_f/h$) to $(n_f)^{½}$ related to a higher frequency corresponding to the lower frequency occurring for the Compton effect; for instance, it is shown that, as for Caesium (having $W_f \cong 2$ eV), $n_f = 361$;

11) Compton effect (CE) needs one *photon* only; our Doppler effect equations for the light lead to Compton Eq., while, as for the Relativity, the CE is not a Doppler effect.

1.2. Total Escape Speed u and Evidences That $u = c$

As known, considering in space only one mass M, (for simplicity its barycenter), the gravitational potential U in a point O, assuming $U_\infty = 0$, is $U = -MG/s$, with s the distance M-O. The conservation of energy applied to a particle m (of unitary mass) coming from the infinity, gives $E = U + K$, with $K = ½u^2$ its kinetic energy, therefore for $E = 0$, one finds $U = -K$, yielding

$$u = \sqrt{-2U} = \sqrt{2MG/s} \tag{1}$$

which is a scalar, (called *escape speed*), representing the value of the velocity $\mathbf{u}$, (referred to M), a massive particle needs to reach the infinity; hence the relation

$$\mathbf{v}_{Mm} = \mathbf{u} \quad [\text{with} \quad |\mathbf{u}| = u = (-2U)^{½}] \tag{2}$$

represents the condition, as for a point-particle m, to be provided with the *absolute* escape velocity $\mathbf{u}$ (*absolute* means here referred to M) whereas considering a generic point O,

$$\mathbf{v}_{Om} \equiv \mathbf{u}_O \quad [\text{with} \quad |\mathbf{u}_O| = u_O = (-2U_O)^{½}] \tag{3}$$

represents the condition, regarding m, to be provided with the *relative* escape velocity $\mathbf{u}_O$, where *relative* means here referred to a generic point O; (anyhow, our *claimed* variable length of photons, during their emission from a source S gives them an invariant speed referred to any considered point O, in spite of any velocity $\mathbf{v}_{OS}$).

Regarding the possibility to define the escape speed from two or more masses, ***we point out that considering*** M ***as a real mass, the potential*** U, in a considered point, *has to be regarded as the sum of the partial potentials* U_n *due to each partial mass* M_n ***composing the mass*** M; therefore, as for two masses, we have

$$U_{1,2} \equiv U_1 + U_2 = -(M_1 G/s_1) - (M_2 G/s_2) \tag{4}$$

yielding $u_{1,2} \equiv \sqrt{-2U_{1,2}} = \sqrt{-2(U_1 + U_2)}$ thus we can write

$$u_{1,2}^2 = -2U_{1,2} = u_1^2 + u_2^2 \tag{5}$$

while for all the n masses in space we get

$$u \equiv (-2U)^{½} = (-2\Sigma U_n)^{½} = (2\Sigma M_n G/s_n)^{½} = \sqrt{\Sigma u_n^2} \tag{6}$$

representing the *total* escape speed.

For instance, the escape speed from the Earth surface, due to Earth and Sun only, becomes $u_{E,S}^2 = u_E^2 + u_S^2 = (2M_E G/R_E) + (2M_S G/d)$ with R_E the Earth ra-

dius, and d the distance Earth-Sun giving $u_{E,S} \cong 42$ km/s, while the escape speed from our Galaxy can be *roughly* expressed as $u_g \simeq (2M_g G/d_g)^{1/2}$ where $M_g \simeq 10^{42}$ kg is our Galaxy mass and $d_g \simeq 30$ kly $\simeq 3 \times 10^{20}$ m the distance between the Earth and our Galaxy centre, giving $u_g \simeq 8 \times 10^5$ m·s^{-1}.

Now, the mass of universe, by some authors, is estimated [1] [2] [3] to be $M_u \cong 10^{53}$ kg; about the same value is given through the number ($\cong 10^{22}$) of observable stars [4] [5] [6], and since from Earth the distribution of the masses appears to be homogeneous and isotropic, under our assumption $U_\infty = 0$, we may assume their density as decreasing toward the infinity like a function $\rho = \rho_c e^{-as}$ being $\rho_c \cong 9.2 \times 10^{-27}$ kg/m^3 the *critical density*.

Writing the mass of universe as

$$M_u = \int_0^\infty 4\pi s^2 \rho_c e^{-as} ds = 4\pi\rho_c \int_0^\infty s^2 e^{-as} ds = \frac{8\pi\rho_c}{a^3} \cong 10^{53} \text{kg} \tag{7}$$

we find

$$a = \left(8\pi\rho_c / M_u\right)^{\frac{1}{3}} \cong 1.3 \times 10^{-26} \text{m}^{-1} \tag{8}$$

and since, on Earth, the variation of potential due to an increase of the distance ds, can be written dU = −dm G/s with dm = $\rho 4\pi s^2$ds and $\rho = \rho_c e^{-as}$, the potential on Earth becomes

$$\begin{aligned} U_0 &= -\int_0^\infty \left(4\pi s^2 / s\right) G\rho_c e^{-as} ds = -4\pi\rho_c G \int_0^\infty e^{-as} s ds \\ &= -4\pi\rho_c G / a^2 \cong -4.5 \times 10^{16} \text{J} \end{aligned} \tag{9}$$

yielding

$$u_0 = \left(-2U_0\right)^{1/2} \cong \left(9 \times 10^{16}\right)^{1/2} \cong 3 \times 10^8 \text{ m/s}. \tag{10}$$

We can therefore infer that, on Earth, $u_0 = c_0$, giving $c_0^2/2 = -U_0$ and, in general,

$$c = \left(-2U\right)^{1/2} = u. \tag{11}$$

The equality $c = u$, which implies the massiveness of light, means that, along any free path, the speed of light only depends on the value of the potential along that path.

The equality $c = u$ is also supported by a cosmological reason: in fact, if $c > u$ the energy of light will be lost forever and furthermore the *observable* masses, following the always increasing mass of light going toward the infinity, will also tend to the infinity moving away from each other. On the contrary, if $c < u$, all the masses in space, (having speed lower than u), will tend to a gravitational collapse, whereas for $c = u$, the mass of light, tending to the infinity in an unlimited time, appears to be the necessary mass to avoid the two events (collapse or dispersion).

1.3. Annual Variation, on Earth, of the Total Escape Speed

On Earth, a small variation of the total escape speed u_o, from Equation (11) written as $u^2 = -2U$ yielding $2u = -2\text{d}U/\text{d}u$, can be written as

$$\Delta u = -\Delta U / u_0 \tag{12}$$

where ΔU is the variation of the *total* potential on Earth, mainly due to the variable distance Earth-Sun; so, between Aphelion and Perihelion, where $a = (1 + e)d$ and $p = (1 - e)d$ are the respective distances Earth-Sun, with e (=0.0167) the eccentricity of the Earth's orbit and $d \cong 1.5 \times 10^{11}$ m the average distance Earth-Sun, and since $pa \cong d^2$, and $(a - p) = 2ed$, we get

$$\begin{aligned} \Delta u_{AP} &= -\Delta U_{AP}/u_0 = -\left(U_P - U_A\right)/u_0 = \left[\left(M_S G/p\right) - \left(M_S G/a\right)\right]/u_0 \\ &\cong M_S G\left(a-p\right)/d^2 u_0 \cong M_S G 2ed/d^2 u_0 \cong M_S Ge/du_0 \cong +0.10 \text{ m s}^{-1} \end{aligned} \tag{13}$$

with $M_S = 2 \times 10^{30}$ kg the mass of the Sun, and we note that Δu_{AP} is compatible with the accuracy of the value of the speed of light in vacuum (on Earth) c_0 = 299,792,458 m·s^{-1}.

1.4. Definition of Photons and Their Speed

The Galileo's velocity composition law (since different parts of a moving object may have different velocity) is strictly valid for point-particles, and therefore the light cannot be a succession of point-particles (otherwise it should follow this Galileo's law), hence we may infer that the light, to comply both this law and the equality $c = u$, could be composed of particular particles, photons, (whose physical characteristics are then shown on §2.2), as defined:

Longitudinally-extended, elastic (variable length) and massive particles emitted by a source during an *emission time* T at speed $c = u$ moving individually or along rays, (continuous succession of photons where every *tail* corresponds to the *front* of the next one).

Photons speed: the measurement of the speed of a point-particle (or regarding an object, its barycentre), is defined through the ratio $v = d/t$ with d the distance between **two Observers** (O_1 and O_2) and t ($=t_2 - t_1$) the time the particle/barycentre needs to cover such a distance; on the contrary, every photon may have different length with respect to two Observers, (like, for instance, an elastic thread during its stretching), hence to define the speed of *one* photon, we must consider its length λ divided its *transit time* T_t (time the whole particle needs to cross **one Observer**). Therefore the relation

$$c = \lambda / T_t \tag{14}$$

represents the speed of *one* photon referred to a considered Observer, whereas the relation $c = d/t$, written as

$$c = d/t = n\lambda / nT_t = \lambda / T_t \tag{14-a}$$

where n is the number of photons (of one ray) each of them having length λ, and where $t = nT_t$ is the transit time of the n photons, represents the *average* speed of the light along d.

1.5. Invariance of *c* for Observers at Rest with Respect to the Initial Location O of a Source of Light, Despite Any Velocity v_{OS}

Referring to **Figure 1**, let O be the location (with respect to all the masses in

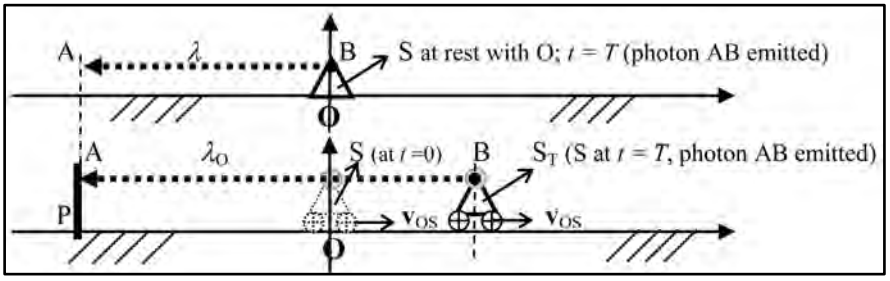

Figure 1. Emission of the photon AB by a source S either at rest or in motion from O.

space) of the source S at the time ($t = 0$) the *front* A is emitted; therefore O represents the location of the *initial* emission of a considered photon.

The Earth's surface, where c_0 is practically constant, has to be intended as the basic reference frame for the parameters of light (λ, ν) while other frames, because of the Doppler effect, would give, for the same source, different values. So, still referring to Figure 1, we intend the frame O as fixed to the Earth's surface. We also intend:

T: emission time of the considered photon AB.

λ: length of the emitting photon if S is fixed to O during T.

λ_O: length of an emitting photon if S during T is in motion with respect to O.

T_t: transit time of one photon (T_O for O, T_P for P, while $T_S = T$).

On Figure 1, if S during T is fixed to O, the speed of the front A (considered as a point-particle), see Equation (3), is $v_{OA} = u_O$, where u_O only depends on the location of O, thus, at $t = T$, the length λ of the photon AB corresponds to the path covered by A, so we have

$$v_{OA}T = u_O T \equiv \quad (= \quad v_{SA}T \quad \text{for S fixed to O during } T). \tag{15}$$

If S has velocity $\mathbf{v}_{OS}$ with respect to O, the velocity of the front A, referred to S, being $\mathbf{v}_{SA} = \mathbf{v}_{SO} + \mathbf{v}_{OA}$ and since from (3), $\mathbf{v}_{OA} = \mathbf{u}_O$, becomes

$$\mathbf{v}_{SA} = \mathbf{v}_{SO} + \mathbf{u}_O \Rightarrow v_{SA} = u_O \pm v_{OS} \tag{16}$$

with the sign + if photon and source have opposite direction; then

$$v_{SA}T\left(\equiv \lambda_O\right) = u_O T \pm v_{OS}T \Rightarrow \lambda_O = \lambda\left(1 \pm \beta\right) \quad [\text{with} \quad \beta = v_{OS}/u_O\,] \tag{17}$$

where λ_O is the length of the emitted photons when S is in motion from O. We point out that the variation of the photons length only depends on $\mathbf{v}_{OS}$.

Now, the *transit time* T_t for the Observer O, can be written

$$T_O = T \pm v_{OS}T/u_O = T\left(1 \pm \beta\right) \quad [\text{with} \quad \beta = v_{OS}/u_O\,] \tag{18}$$

corresponding to the algebraic sum of the time $T\,(=\lambda/u_O)$ the front A needs to cover the path λ, plus the time the tail B (emitted, like every part of the photon, at speed u_O referred to O), needs to cover the path $S_T - O = v_{OS}T$, that is $\Delta T = v_{OS}T/u_O$. (As for the observer P showed on Figure 1, being $\mathbf{v}_{OP} = 0$, then $T_P = T_O$).

Thus, the speed of the photon AB referred to O, since T_O increases/decreases together with λ_O, as per Equation (14), becomes

$$u_O = \frac{\lambda_O}{T_O} = \frac{\lambda(1\pm\beta)}{T(1\pm\beta)} = \frac{\lambda}{T} \equiv c \tag{19}$$

showing that *the speed of a photon referred to an Observer fixed to the source initial location*, (O), *is invariant despite any motion of the source with respect to* O.

The ***frequency*** of the light referred to a generic Observer O, on our bases, has to be defined as $\nu = n/T_t$ with n the number of photons, of the same ray, crossing the Observer during their transit time T_t. Hence, for $T_t = 1$ s, we have $\nu = n$ meaning that the frequency corresponds to the number of photons, same ray, transiting in 1 s, while, for $n = 1$, the frequency becomes

$$\nu = 1/T_t \tag{20}$$

We point out that the photons frequency emitted by a source S, under the condition $v_{OS} = 0$, has to be equal to the one observed by O; this is also valid if O and S belong to different potential, (e.g., the equality of the number of balls falling from the top of a tower with respect to an Observer at the tower base), and therefore the condition $v_{OS} = 0$ always implies $\nu_S = \nu_O$ whatever is the distance source-observer.

[We also point out that, according to the Relativity, (due to the *claimed* constancy of c and because of the Doppler effect), an Observer in relative motion from a source should observe different wavelength as well as different frequency for emitted light; on the contrary, on our results, if the source is fixed to its initial location (the ground on Earth), the length of the *emitted* photons is invariant, while c and ν are varying, as hereafter shown].

Referring now to Figure 2, let P be an observer (represented at different times, by P_A and P_B) moving with velocity $\mathbf{v}_{OP}$ from O along the same direction of the photons while the source S is moving from O with velocity $\mathbf{v}_{OS}$ contrary to them; we assume the photon AB totally emitted at the time the front A reaches P_A (for simplicity as $t = 0$). [In fact, after this emssion, the source may even disappear].

Now, the transit time T_P of the photon AB is given, see Equation (18), by T_O plus the time T_{OP} $(= \pm v_{OP}T/c)$ due to the motion of P from O, and since $\mathbf{v}_{SP} = \mathbf{v}_{SO} + \mathbf{v}_{OP}$, we can write

$$T_p = T \pm \frac{v_{SO}T}{c} \pm \frac{v_{OP}T}{c}\left(= T \pm \frac{v_{SP}T}{c}\right) = T(1\pm\beta\pm\beta_P), \quad \left[\text{with } \beta_p = \pm\frac{v_{OP}}{c}\right] \tag{21}$$

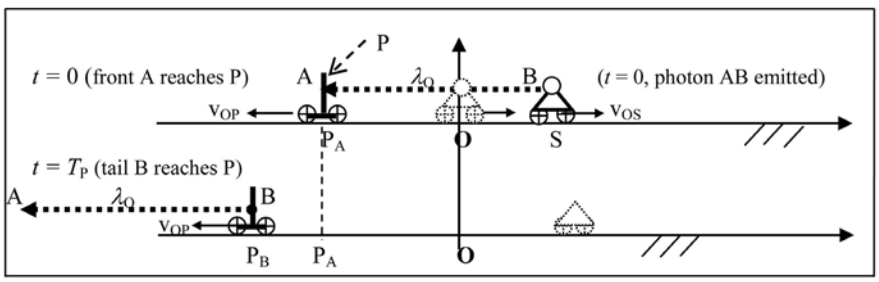

Figure 2. The Observer P moves from P_A to P_B during the transit time T_P of the photon AB while the source is moving from its initial emission location O.

corresponding to the interval between the time the front A reaches P_A (at $t = 0$) and the time the tail B leaves P_B; hence

$$c_p = \lambda_O / T_p = \lambda(1 \pm \beta) / T(1 \pm \beta \pm \beta_p) = c(1 \pm \beta) / (1 \pm \beta \pm \beta_p). \quad (22)$$

[In short, the motion of S (from O) causes a variation of the photon length, while the relative motion observer-source varies the observer transit time and its related frequency].

On next Figure 3, we analyse the parameters c, λ, ν of five configurations regarding a source S, the considered frame O (practically the Earth's surface) and an Observer P.

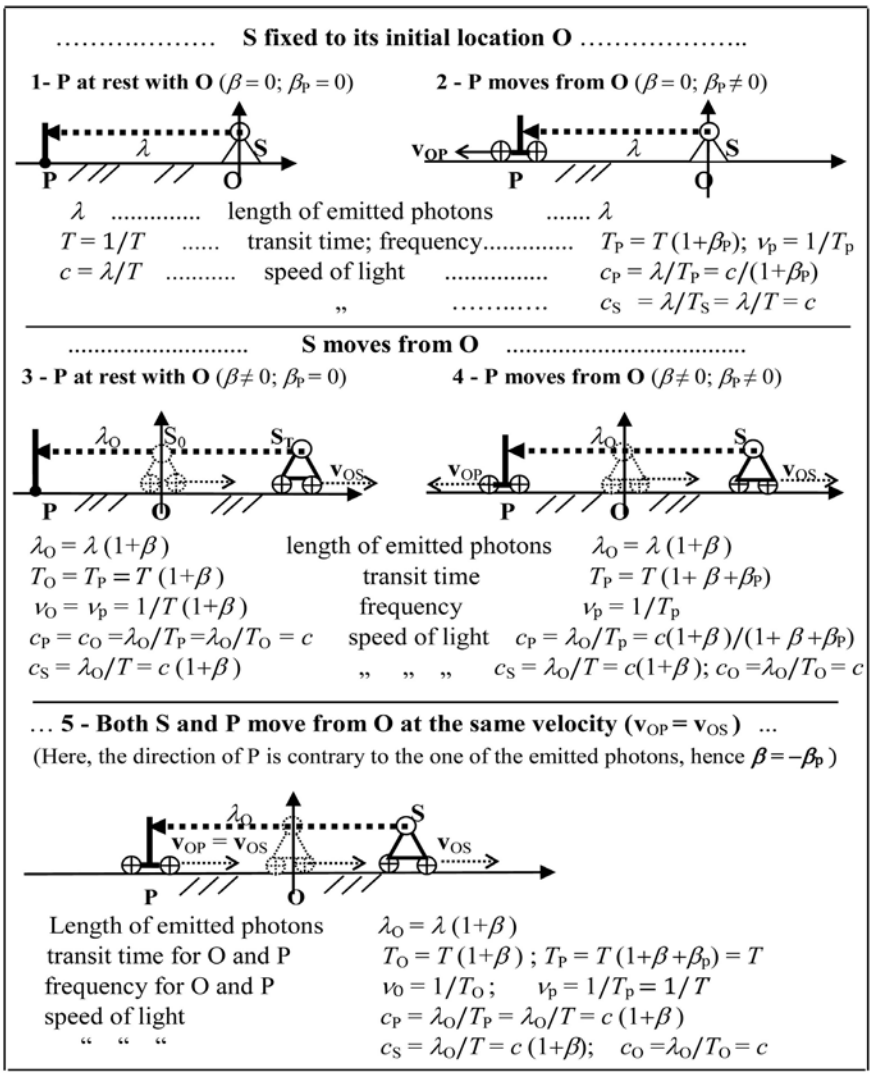

Figure 3. Five configurations regarding a source *S*, *a* frame O and an Observer *P*.

where

$\beta = v_{OS}/c$, relative speed of S with respect to O,

$\beta_p = v_{OP}/c$ relative speed of P,

$c = \lambda/T$ basic speed of light, referred to conf. #1,

$\lambda_O = \lambda(1 \pm \beta)$ length of emitted photon,
$T_S = T$ photon transit time for S, equal to its emission time,
$T_O = T(1 \pm \beta)$; T_t for O; sign + if S and photon have *opposite direction*,
$T_P = T(1 \pm \beta \pm \beta_P)$; T_t for P; $+\beta_P$ if P and photon have *same direction*,
$c_S = \lambda_O / T_S = \lambda_O / T$; speed of light observed by S,
$c_P = \lambda_O / T_P$ speed of light observed by P,
$c_O = \lambda_O / T_O$ speed of light observed by O.

Regarding the measurements of c through the method $c = d/t$ carried out along a double path, the light emitted inside the measurement system (MS), because of the interaction light-matter, has to be absorbed and then re-emitted by the 2nd Observer which, during the re-emission, becomes a new emitting source; therefore the above equations regarding transit time and photon length, are also valid for the re-emitted photons which now have contrary direction, hence $\beta' = -\beta$ and also $\lambda' = -\lambda_O$ giving to c, along a double path, the constant value c.

[Light emitted outside the MS: at the time the light is crossing the MS, this becomes the new emitting source].

1.6. Doppler Effect for the Light, New Equations

The Equation (17) represents our *longitudinal Doppler effect* for the light, while the general case of this effect, assuming $v_{OS} << \lambda$ (hence OP ≅ PB), see **Figure 4(a)**, can be written as

$$\lambda_0 = \lambda \pm v_{OS} T \cos\alpha = \lambda\left(1 \pm \beta \cos\alpha\right) \quad (\text{with} \quad \beta = v_{OS}/c\,) \tag{23}$$

with α the angle between the direction of λ_O and $\mathbf{v}_{OS}$.

As for the *Transverse Doppler effect*, see **Figure 4(b)**, in general, we have

$$\lambda_0 = \sqrt{\lambda^2 \pm \left(v_{OS} T\right)^2} = \lambda\sqrt{1 \pm \beta^2} \tag{24}$$

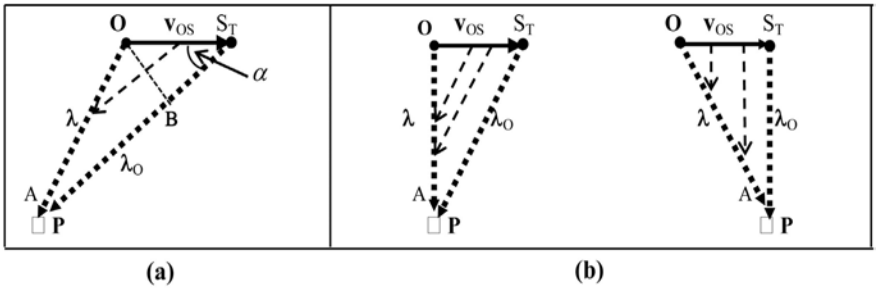

Figure 4. Doppler effect (DE). (a) General case; (b) Transverse DE with S receding/approaching an observer P. Dotted arrows inside the triangles represent the photon λ_O during its emission.

As for *a source circling around an Observer* P, the **Figure 5** shows that the length of the photon λ emitted when its source is fixed to O, becomes λ_O when S is circling with velocity $\mathbf{v}_{OS}$.

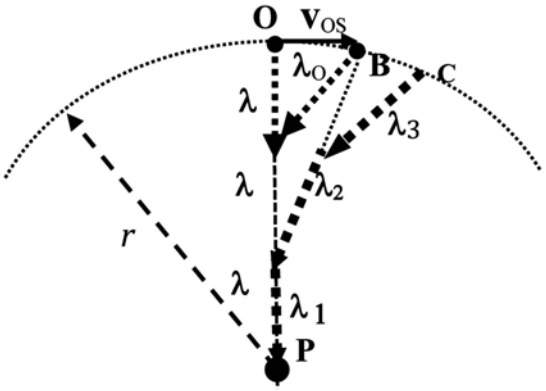

Figure 5. Photons emitted while their source is circling around P.

[The succession of the photons λ represents a ray if S is at rest with P, while the succession $\lambda_1 \to \lambda_3$ represents a ray if S is circling around P, with O, B, C the emission points of the circling source]. Then, assuming $\lambda_O > \lambda$, we have

$$\lambda_O = \sqrt{\lambda^2 + (v_{OS}T)^2} = \lambda\sqrt{1+\beta^2} = \lambda\sqrt{1+\omega^2 r^2/c^2} \tag{25}$$

while the photon transit time, being T the emission time of λ becomes

$$T_O = T\sqrt{1+\beta^2} = T\sqrt{1+\omega^2 r^2/c^2} \tag{26}$$

with r the orbit radius, ω the source angular speed, giving to any photon, speed $c_O = c$.

1.7. Re-Visitation of the Harvard Tower Experiment (HTE), Time Dilation, Gravitational Redshift

General Relativity predicts that the gravitational field of the Earth will cause a photon emitted downwards (towards the Earth) to be blueshifted: scope of HTE experiment was to detect this shift of light. A Mossbauer source S was placed on the top of a tower (height $h \cong 22$ m) emitting photons toward the tower base where an Absorber went out of resonance; the experiment did not clarify if the non-resonance was due to a variation of λ or ν; indeed, because of the claimed constancy of c, both of them should have varied their initial values during the path tower-base.

According to our bases, we have different evaluations of this experiment. Let us first consider S at the base and A at its top, see **Figure 6**.

It is a fact that if S and A are at relative rest at the same level (*e.g.* both on the ground), then A is in resonance and it is also a fact that other experiments effected at this regard, e.g. Blatt, [7], show that ***if S moves toward the absorber***, *not contrarily*, the absorber goes out of resonance: indeed, if S is fixed to the ground, the length of emitted photons (as previously shown) is constant, whereas if S moves with respect to its initial emission location (the ground), the photon length varies, thus we may infer that the resonance is physically related to the constancy of the length of photons.

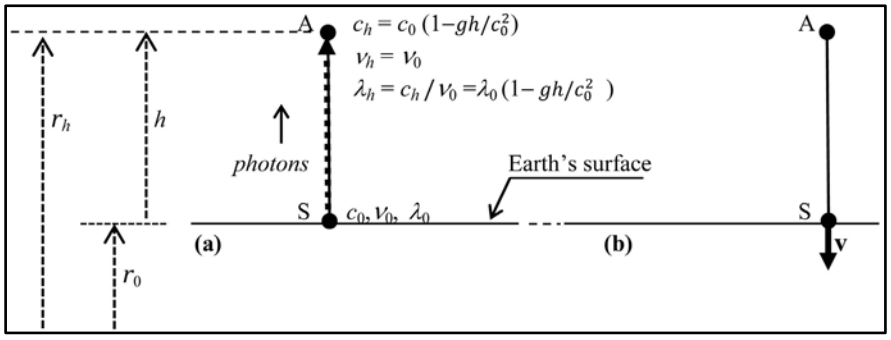

Figure 6. Harvard tower experiment scheme; source at the base, absorber A at the top, our results. (a) S and A at rest, so $\nu_h = \nu_0$; c0, ν_0, λ_0 parameters of photons emitted by S on the ground; c_h, ν_h, λ_h photons arrived to A where $\lambda_h < \lambda_0$ thus a blue shift as for A; (b) Direction of the compensating velocity to balance the blue shift via Doppler effect, so to obtain in altitude c_0, ν_0, λ_0.

Now, referring to Figure 6, if S, on the ground, emits photons reaching A at height h, because of the variation of potential, following our relation $c = (-2U)^{½}$, it will be $c_0 \to c_h$; since S and A are at reciprocal rest, it turns out that, as shown just after the Equation (20), it is always $\nu_h = \nu_0$ (in spite of any variation of potential between S and A) yielding $\lambda_h = c_h/\nu_h$. Therefore, with r_0 the radius of Earth (hence $r_h = r_0 + h$) and M_E the mass of Earth, writing the (11) as $c^2 = -2U$, we get $2c = -2\mathrm{d}U/\mathrm{d}c$ hence from r_0 to r_h and since $\Delta c = -\Delta U/c$ with $\Delta U = U_{Eh} - U_{E0} = -(M_E G/r_h) + M_E G/r_0$, we find

$$\frac{c_h - c_0}{c_0} = -\frac{\Delta U}{c_0^2} = -\frac{M_E G h}{r_h r_0 c_0^2} \cong -gh/c_0^2 \Rightarrow c_h = c_0\left(1 - gh/c_0^2\right) \tag{27}$$

(where $\Delta U = gh$); then for $\nu_h = \nu_0$ we have

$$\begin{aligned} &\lambda_h = c_h/\nu_h = c_0\left(1 - gh/c_0^2\right)/\nu_0 = \lambda_0\left(1 - gh/c_0^2\right) \\ &\Rightarrow \left(\lambda_h - \lambda_0\right)/\lambda_0 = -gh/c_0^2 = \frac{c_h - c_0}{c_0} \end{aligned} \tag{28}$$

and since $\lambda_h < \lambda_0$, *contrary* to Relativity, A observes a blue-shift effect.

Thus, to restore the resonance via Doppler Effect (DE), see Figure 6(b), S has to *recede* from A in order that the *photon* length could increase, see Equation (17), from λ_h to $\lambda_0 = \lambda_h(1+\beta)$ with $\beta = v_{AS}/c \equiv v/c$; therefore, equating the relative variation of the *photon* length due to the DE, that is $(\lambda_h - \lambda_0)/\lambda_0 = -v/c$, to the one due to the altitude, $\Delta\lambda/\lambda_0$, as given by (28), we get

$$v/c = gh/c_0^2 \Rightarrow v = gh/c_0 = 7.5\times10^{-7}\ \mathrm{m/s} \quad (\text{for } h = 22.5\ \mathrm{m}) \tag{29}$$

i.e. the value of the compensating velocity.

This value is also predicted by GR which, implying a decrease of v for the light moving from the base to the top, predicts an opposite direction of the compensating velocity **v** with respect to the one shown on Figure 6(b); at this regard, Pound-Rebka and Pound-Snider, [8] [9] [10], gave no clear indication about the direction of **v**, since S and A, during the experiment, were moved sinusoidally.

Now, see Figure 7, with A on the base, and taking S to the top, the experience

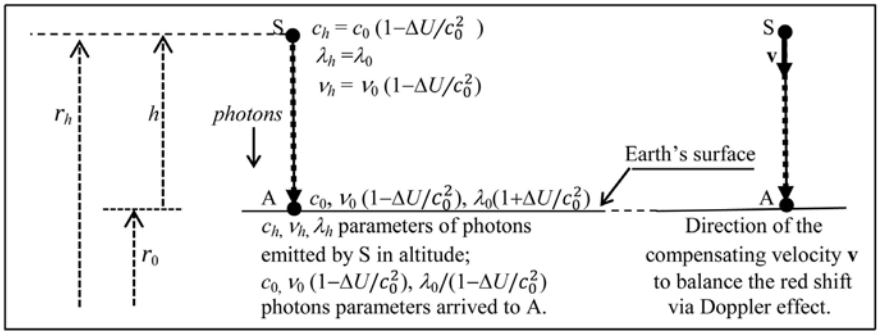

Figure 7. Harvard tower experiment scheme; source on the top, our results.

shows that the absorber goes out of resonance. Indeed, with S on the top, the (27) shows $c_h < c_0$, but what about the initial parameters of the *photons* emitted in altitude, ν_h and λ_h?

Well, it is known that atomic clocks give an increase of their counted time in altitude ($T_h > T_0$, hence $\nu_h < \nu_0$), therefore taking these clocks from ground to h, their frequency ν_h has to follow the same decrease as c_h; this implies $\lambda_h = \lambda_0$ so the frequency of photons emitted in altitude becomes

$$\nu_h = \frac{c_h}{\lambda_h} = \frac{c_0\left(1-\dfrac{gh}{c_0^2}\right)}{\lambda_0} = \nu_0\left(1-\frac{gh}{c_0^2}\right) = \nu_0\left(1-\Delta U/c_0^2\right). \tag{30}$$

Now, with S emitting photons toward the base, since S and A are at rest, their frequency remains constant during their path top-base, meaning that $\nu_{h-0} = \nu_0\left(1-\Delta U/c_0^2\right)$, while the length of photons reaching the base, and considering that now h is negative, becomes

$$\lambda_{h-0} = c_0/\nu_{h-0} = c_0/\nu_0\left(1-\Delta U/c_0^2\right) = \lambda_0\left(1+gh/c_0^2\right) \tag{31}$$

showing an increase of λ from the top to the base. Hence the absorber, on the base, will state, ***contrary to GR***, a red-shift, hence, to compensate it via Doppler shift, see Figure 7, S has now to move toward A; *on the contrary, according to GR, A and S should recede from each other.* We also highlight two points:

- The increase of λ for photons moving from h to the ground, gives a reason to the gravitational red shift related to far sources.
- The decrease of ν during the path h-ground gives a reason to the lower frequency of the light coming from far sources.

Time dilation: Atomic clocks in altitude (h-clocks) are ticking *faster* than identical clocks on the ground (g-clocks): at height h, see (27), we have $\left(c_h - c_0\right)/c_0 = -\Delta U/c_0^2$, while taking a clock to a GPS satellite, see also Figure 7(a), from (30), one finds

$$T_h = T_0\Big/\left(1-\frac{\Delta U}{c_0^2}\right) = T_0/\left(1-\delta\right) \Rightarrow T_h - \delta T_h = T_0 \quad \left[\text{where } \frac{\Delta U}{c_0^2} \equiv \delta\right] \tag{32}$$

with T_h the counted time of one photon emitted by a h-clock, while T_0 by a g-clock. Thus the variation of the counted time between the two clocks, for *every*

emitted photon, due to the altitude, becomes

$$\Delta T_{\text{ph}} = T_h - T_0 = T_h \delta \tag{33}$$

and since the frequency of photons is their number emitted in 1 s along one ray, the term

$$n_{1\text{s}} \equiv \nu_0 t_{1\text{s}} \quad (\text{with} \quad t_{1\text{s}} = 1\,\text{s}) \tag{34}$$

is the number of photons (atomic transition of Cs 137) constituting one-second on the ground; then, since $\nu_h = \nu_0\left(1 - \Delta U/c_0^2\right)$, see (30), the following relation

$$\Delta n_{1\text{s}} = \nu_h \Delta T_{\text{ph}} = \frac{\nu_0\left(1 - \dfrac{\Delta U}{c_0^2}\right)\left(T_0 \dfrac{\Delta U}{c_0^2}\right)}{1 - \dfrac{\Delta U}{c_0^2}} = \nu_0 T_0 \frac{\Delta U}{c_0^2} = \frac{\Delta U}{c_0^2} \tag{35}$$

is the variation of $n_{1\text{s}}$ emitted in 1 s by a *h*-clock; now, see (27), $\Delta U = M_{\text{E}} Gh/r_h r_0$ and since $r_h \cong 26{,}600$ km, $r_0 \cong 6400$ km, with $h \cong 20{,}200$ km, the increase of counted time in one day (ΔT_{1d}) of a *h*-clock, with respect to a g-clock, becomes

$$\Delta T_{1\text{d}} = \Delta n_{1\text{s}} \times 86400\ \text{s} = 86400\,\Delta U/c_0^2 = 45.5\ \mu\text{s} \tag{36}$$

hence this effect is a consequence of the variation of *U*; indeed, as shown later on, the values of the H atom frequencies depend on *c*, thus, on our bases, on *U*.

Now let us find the variation of the counted time, between the two clocks, due to their relative motion; thus, being $v_{\text{S}} = 2$ ($2\pi r_h/86{,}400 = 3870$ m/s the orbital speed of GPS satellites, (corresponding to two orbits/day), it turns out that the counted time variation, between a *h*-clock and an Observer E at the centre of Earth, due to their relative motion, is given by Equation (26) which, in our case, with $\beta_{\text{S}} = v_{\text{S}}/c$ ($\cong 1.3 \times 10^{-5}$) becomes

$$T_{\text{E}} = T_h\sqrt{1+\beta_{\text{S}}^2} \cong T_h\left(1 + \frac{\beta_s^2}{2}\right) \quad (\text{valid for} \quad \beta_{\text{S}}^2 << 1) \tag{37}$$

with T_E the photon counted time for the Observer E; then, with v_0 the Earth's rotational speed ($\cong 460$ m/s at the equator), since $\beta_0^2 = (v_0/c)^2 << \beta_{\text{S}}^2 = (v_{\text{S}}/c)^2$ and calling $T_0 \cong T_h\left(1+\beta_0^2\right)$ the photon counted time of a g-clock with respect to a clock at the Earth's centre E, we can write $T_0 \cong T_E$; thus, the difference between the two transit times T_h and T_0 ($\cong T_E$) due to their relative motion, is

$$\Delta T'_{\text{ph}} = T_h - T_0 \cong T_h - T_{\text{E}} = T_h - T_h\left(1 + \frac{\beta_s^2}{2}\right) = -T_h\beta_{\text{S}}^2/2\,. \tag{38}$$

Then, as above, $\Delta n'_{1\text{s}} \equiv \nu_h \Delta T'_{\text{ph}} = -\nu_h T_h \beta_{\text{S}}^2/2 = -\beta_{\text{S}}^2/2$ is the variation of the number of *photons* emitted by a *h*-clock in 1 s; so the variation of the counted time, in one day, is

$$\Delta T'_{1\text{d}} = -\left(\frac{\beta_{\text{S}}^2}{2}\right)86400\ \text{s} = -7.2\ \mu\text{s} \tag{39}$$

showing a decrease of the counted time for a g-clock due to their relative mo-

tion; hence

$$\Delta T_{\text{tot1d}} = \Delta T_{\text{1d}} + \Delta T'_{\text{1d}} = 38.3\,\mu\text{s/day} \tag{40}$$

which is also predicted, (with different reason), by GR. To prevent this effect, before launching, the daily counted time (T_{1d}) of clocks, has to be decreased by ≅38 μs.

In short, the *time dilation* is a consequence of the variation of U, hence of c: indeed, as show on §2.3, the admitted/emitted frequency on H atom (and of course the one of the other elements) varies together with c.

Gravitational redshift

As for the Relativity, the only way to explain high cosmological redshifts is the Doppler effect, (which implies an *incredible* universe expansion at a speed $v_u \cong c$), whereas, on our results, *disregarding the reciprocal motion between a (far) source and an Observer on Earth*, which implies $\nu = \nu_0$, we get $c/\lambda = c_0/\lambda_0$, where ν_0, c_0 and λ_0 are the values on Earth, hence for $c_0 > c$ one gets $\lambda_0 > \lambda$, that is a red shift observed on Earth; therefore, the shifts here observed can be expressed as

$$z \equiv \frac{\Delta\lambda}{\lambda} = \frac{\Delta c}{c} = \frac{c_0 - c}{c} = \frac{c_0}{c} - 1 = \sqrt{U_0/U} - 1 \tag{41}$$

with U_0 the potential on Earth, U the one on the source. Thus, apart from Doppler effects, z turns out to be the variation of c (as well as λ) during the path of light toward a different potential. In particular, with s the distance Earth-source, for $s <$ ≅45 Mpc, [11], (roughly corresponding to $-0.01 < z < +0.01$) if U (potential on the source) is, in *absolute value*, higher than the potential on Earth U_0, the (41) gives, on Earth, $z < 0$ (blue shift), and vice versa for $|U| < |U_0|$; thus, for $s <$ ≅45 Mpc, these red/blue shifts indicate that the potential, may increase or decrease with respect to $|U_0|$. In the range ≅$0.01 < z <$ ≅0.20, (where z follows the Hubble's law), the (41), written as

$$U = U_0/(1+z)^2 \cong U_0/(1+2z) \cong U_0(1-2z) \quad \text{(valid for } z << 1\text{)} \tag{42}$$

shows that, for $z << 1$, U depends linearly on z, as Hubble's law; then, for $s \to \infty$, $U \to 0$, hence $z \to \infty$, see Table 1.

[For $s >$ ≅45 Mpc, z is always positive, hence we may infer that our galaxy is practically near/close to the middle of the masses of universe (where $|U|$ has the max value)].

Table 1. Calculated values of U and c related to the observed shifts on earth.

blue/redshift	z	s (Mpc)	$U/U_0 = 1/(z+1)^2$	$U/U_0 \cong 1-2z$ valid for z << 1	$c/c_0 \cong 1/(z+1)$
blue/red shift	−0.01 → 0.01	<≅45	0.98-1.02	0.98-1.02	0.99 - 1.01
red shift	≅0.01	≅45	0.98	0.98	0.99
red shift	0.20	900	0.69	0.60	0.83
red shift	1		0.25		0.50
red shift	→∞	→∞	→0		→0

2. Interaction Light-Matter

2.1. Electron Structure and Photon-Electron Impact Point

On our basis, (light composed of *our* photons), the interaction light-matter requires that to move a circling electron toward outer orbits, the impact photon-electron has to occur, see **Figure 8(a)**, in a *radial way*, (giving origin to the radial velocity **w**), otherwise, other impacts could cause the electron fall into the nucleus, due, for instance, to an impact where the velocity of photons and electron have contrary direction.

To be radial, the impact must occur in a specific point, fixed to the electron surface, we call it *Impact Point*, which, *during the electron*, *orbit*, has to face its nucleus, (up to its removal), giving to the electron one rotation every orbit; the impacting photons have to approach the nucleus, as shown on **Figure 8(b)**, perpendicularly to the electron orbit plane, providing, to the electron, a radial velocity **w**.

Moreover, we can infer that the charge of the electron, has to correspond to the Impact Point (I_p), so we may infer that each photon *front* is provided with a positive charge, while its *tail* with an equal negative one. In fact, the photon may be represented as an electric bipole.

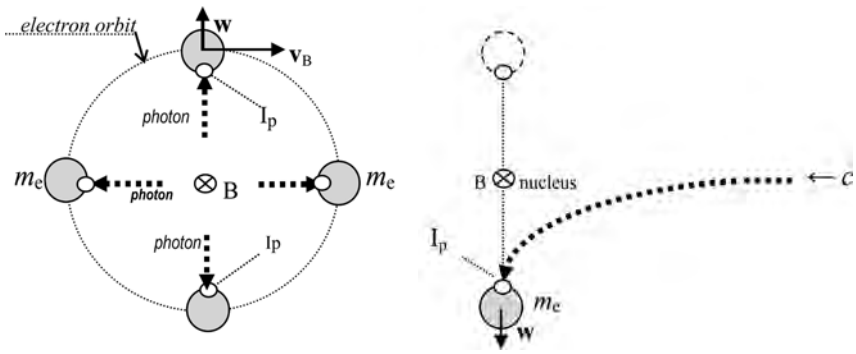

Figure 8. *Photon*-electron Impact point (I_p) and electron *radial* velocity w. (a) Electron orbit front view; (b) Side view.

2.2. Physical Characteristics of Photons

The total energy of a mass m is $E = mc^2$ also proved [12] by the evidence of nuclear reactions like $n + pd + \gamma$, hence this energy has to be valid for the (massive) light too, thus writing their energy as $E = \frac{1}{2}mc^2 + \frac{1}{2}mc^2$ we have to infer that photons are provided, out of their kinetic energy $K_c = \frac{1}{2}mc^2$ with an *internal* energy K_i equal to K_c and we point out that, toward the infinity, (where $U_\infty \to 0$ hence $c_\infty \to 0$), both K_c and K_i tend to 0; then, since for the light $E = h\nu$, the following relation

$$E = K_c + K_i = mc^2 = h\nu \tag{43}$$

has to represent the energy of *one* ray of light, (where photons are flowing), and

where

$$m = h\nu/c^2 \equiv \gamma\nu \tag{44}$$

is the mass of light, having frequency ν, passing along one ray in 1s, while the constant

$$\gamma = h/c^2 = m/\nu = mT = 7.372495\times10^{-51} \text{ kg s} \tag{45}$$

represents the mass of one photon crossing an observer during the transit time T, while the Planck's constant

$$h = \gamma c^2 \tag{46}$$

turns out to be the energy of one photon (mass of light of one ray passing during T).

Now, since m is the mass of light passing along one ray in 1s, the term $n_r mc^2$, with n_r the number of rays emitted by a source S, becomes the energy emitted by S in 1 s; this unitary (unit of time) energy shall be equal to the supplied power P during 1 s, yielding

$$n_r mc^2 = P \tag{47}$$

therefore

$$m_{\text{tot}} = n_r m = P/c^2 \tag{48}$$

is the total mass lost per second by a source of light; e.g. for a 1 W lamp, we get

$$m_{\text{tot}} = P/c^2 \cong 1.1\times10^{-17} \text{ kg s}^{-1} \tag{49}$$

while the number n_r of rays is

$$n_r \left(= m_{\text{tot}}/\gamma\nu\right) = P/c^2\gamma\nu = P/h\nu \tag{50}$$

in our case, $n_r \cong 3 \times 10^{18}$ rays, and we point out that, as for a given power P, the higher is the frequency, the lower is the number of rays, as shown by (50) written as $n_r\nu = P/h$. Then, the number of photons n_γ emitted in 1 s becomes

$$n_\gamma = \left(n_r\nu\right) = P\nu/h\nu = P/h \tag{51}$$

which, for $P = 1$ W, gives $n_\gamma = h^{-1}$ (=1.5 × 10^{33} photons/s), thus the **inverse of Planck's constant** turns out to be the number of photons emitted in 1s by a source of unitary power, and this great number of photons allows the light to be treated as a wave.

Now, during inelastic impacts photons-electron, (like on absorption or photoelectric effetcs), both kinetic and internal energy of the light are involved, so the momentum transferred to the electron is

$$\mathbf{p} = 2m\mathbf{c} = 2\gamma\nu\mathbf{c} = 2\gamma\mathbf{c}/T \tag{52}$$

whose validity is confirmed, see Table 2 of chapter 2.4, by the equality $w_{137} = v_{137}$ (with v_{137} the electron orbital speed along the H atom orbit # 137 and where w_{137} is the value of the electron radial speed along such orbit, as a condition for the H atom ionization.

Regarding elastic impacts, the momentum transferred to the electron, is

$$\mathbf{p}' = m'\mathbf{c} = \gamma v'\mathbf{c} = \gamma \mathbf{c}/T' \tag{53}$$

either for *incident* or for *reflectedphotons*, with T' the total impact time for this interaction; through the (53), and also through *our* Doppler effect equation, see (17), we got the Compton equation (which cannot be obtained by the Relativity via their Doppler effect equations).

2.3. H Atom Parameters and Meaning of Quantum Numbers

Figure 9(a) represents, on our bases, the H atom *basic* configuration; on the intermediate conf. (**b**) the electron is represented circling along the same orbit as its charge, while on conf. (**c**) the electron reduced mass $m_r = m_e/(1+m_e/m_p) = m_e/(1+\varepsilon_m)$, with $\varepsilon_m = m_e/m_p$, circling around the proton mass m_p fixed as origin, is represented either along the effective orbit r_0' or along r_0; referring to conf. (**a**) we define:

m_e: electron mass;

m_p: proton mass;

$v_e = |\mathbf{v}_e|$ electron ground-state (orbital) speed,

$v_p = |\mathbf{v}_p|$ proton ground-state speed,

r_B the ground-state orbit of the electron charge,

r_e the electron radius,

$\varepsilon_r \equiv r_e/r_B$

$r_B' = (r_B + r_e) = r_B(1+\varepsilon_r)$, ground-state orbit of the electron barycentre,

r_p the proton ground-state orbit.

Now, the constancy of momentum referred to conf. Figure 9(a) gives

$$m_e v_e = m_p v_p \Rightarrow v_p = m_e v_e/m_p \equiv \varepsilon_m v_e \tag{54}$$

then, equating on (**a**) the frequency of m_e and m_p, we get

$$v_e/r_B' = v_p/r_p \Rightarrow r_p(v_p/v_e)r_B' = \varepsilon_m r_B' = \varepsilon_m r_B(1+\varepsilon_r) \tag{55}$$

The conf. (**a**), moving m_e (without its charge) from the orbit r_B' to r_B (the electric forces acting on m_e are not involved), turns to conf. (**b**) where the equality between the frequency of m_e and the one of its charge, gives

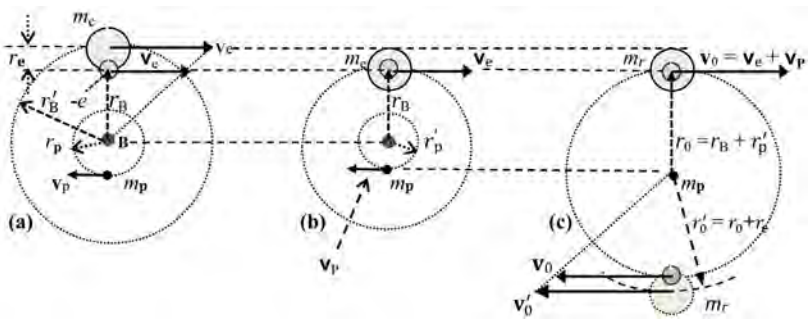

Figure 9. H atom equivalent configurations, on our bases. (a) Observed from the electron-proton common centre of gravity B; (b) Ditto, with the electron barycentre now coincident with its proper charge; (c) Observed from the proton fixed as origin, orbited by the electron reduced mass m_r represented either circling along r_0 or its effective orbit r_0'.

$$v_e/r'_B = \nu_e/r_B \Rightarrow \nu_e = v_e/(1+\varepsilon_r) \tag{56}$$

then the constancy of momentum referred to conf. (**b**), $m_e\nu_e = m_p\nu_p$, yields

$$\nu_p = m_e\nu_e/m_p = \varepsilon_m\nu_e \Rightarrow \nu_p/\nu_e = \varepsilon_m \tag{57}$$

then, equating on (**b**) the frequency of m_e and m_p, we get

$$\nu_e/r_B = \nu_p/r'_p \Rightarrow r'_p = (\nu_p/\nu_e)r_B = \varepsilon_m r_B \tag{58}$$

and finally, see conf. (**c**), we find

$$r_0 = r_B + r'_P = r_B + r_B\varepsilon_m = r_B(1+\varepsilon_m) = r'_B(1+\varepsilon_m)/(1+\varepsilon_r) \tag{59}$$

where m_r is circling with speed $v_0 = v_e + v_p = v_e(1 + \varepsilon_m)$; then

$$r'_0 = r_0 + r_e = r_0 + \varepsilon_r r_B = r_0\left[1+\varepsilon_r/(1+\varepsilon_m)\right] = r_0(1+\varepsilon_m+\varepsilon_r)/(1+\varepsilon_m) \tag{60}$$

Now, it is known that, on H atom, the admitted frequencies have to satisfy the relation

$$\nu_n = \nu_0/n^2 \quad (n = 1,2,3,\cdots) \tag{61}$$

with ν_n the *photons* admitted frequency along the *n-th* circular orbit and since, as claimed on Section 1.4, ν (=n/t) is the number of *photons* (of the same ray) crossing an observer during the time t, the integer n represents the number of *photons* absorbed by the electron during the photon-electron impact time t and *this number, for all the H atom circular orbits, is an integer starting with* 1 *along the electron ground-state orbit.*

The massiveness of light implies a finite impact time during which the electron is circling, and supposing, for now, that, for n = 1, the photon frequency ν_0 should be equal to the electron frequency along the ground-state orbit, that is ν_{e0} = $v_0/2\pi r_0$, where r_0, see conf. (**c**) is the electron ground-state orbit, with v_0 its orbital speed, we could write

$$\nu_0/\nu_{e0} = 1 \quad \text{(first assumption);} \tag{62}$$

to verify this ratio or to find the correct value, we may start from the experimental value of the ^{1}H ground-state ionization energy W_0 (electron extraction work) corresponding to

$$W_0 = -U_{r0}/2 = e^2/8\pi\varepsilon_0 r_0 = \tfrac{1}{2}m_r v_0^2 \cong 13.8954 \text{ eV} \tag{63}$$

with $U_{r0} = -e^2/4\pi\varepsilon_0 r_0$ the potential of the dipole electron-proton, yielding

$$r_0 = e^2/W_0 8\pi\varepsilon_0 \cong 5.29461\times10^{-11} \text{ m} \tag{64}$$

(rough value of the Bohr radius), thus the orbital speed of the electron along r_0 becomes

$$v_0 = \sqrt{e^2/4\pi\varepsilon_0 r_0 m_r} \cong 2.18770\times10^6 \text{ m/s} \tag{65}$$

Then, if W_0 is supplied by one ray of light (with energy $E = h\nu_0$) it must be

$$\tfrac{1}{2}m_r v_0^2 = h\nu_0 \Rightarrow \nu_0 = m_r v_0^2/2h \cong 3.28808\times10^{15} \text{ s}^{-1} \tag{66}$$

with ν_0 the admitted frequency along r_0; hence, the ratio ν_0/ν_{e0} becomes

$$v_0/v_{e0} = (T_{e0}/T_0) = v_0 2\pi r_0/v_0 = 0.499998 \quad (67)$$

meaning that during one electron orbit it should transit *half* of a photon, so we may infer that along r_0 it should be

$$2T_{e0}/T_0 = 2\nu_0/\nu_{e0} = 1 \quad \text{exact} \quad (68)$$

meaning that, along r_0 the impact time T_0 lasts for two electron *circular* orbits.

Now, see conf. (**c**) equating along r_0 the electron centrifugal force to the Coulomb force we have

$$m_r v_0^2/r_0 = \frac{e^2}{4\pi\varepsilon_0 r_0^2} \Rightarrow m_r v_0^2 = e^2/4\pi\varepsilon_0 r_0 = -U_{r0} \quad (69)$$

which, for a circular orbit, and since, see (66), $m_r v^2 = 2h\nu$, gives

$$\nu_n = e^2/4\pi\varepsilon_0 r_n 2h \quad (70)$$

then

$$r_n = e^2/8\pi\varepsilon_0 h\nu_n = e^2 n^2/8\pi\varepsilon_0 h\nu_0 = r_0 n^2 \quad (71)$$

while as for the orbital speed of the electron m_r along any circular orbit r_n the (65) gives

$$v_n^2 = e^2/4\pi\varepsilon_0 r_n m_r = e^2/4\pi\varepsilon_0 r_0 n^2 m_r = v_0^2/n^2 \Rightarrow v_n = v_0/n \quad (72)$$

and finally the electron frequency along a circular orbit becomes

$$\nu_{en} = v_n/2\pi r_n = v_0/n2\pi r_0 n^2 = \nu_{e0}/n^3 . \quad (73)$$

Now, along r_0, the (70) yields

$$\nu_0 = e^2/4\pi\varepsilon_0 r_0 2h = e^2 c/2\varepsilon_0 hc4\pi r_0 = \alpha c/4\pi r_0 \quad (74)$$

with $\alpha = e^2/2\varepsilon_0 hc$ the fine structure constant and given $2\nu_0/\nu_{e0} = 1$ (exact) we have

$$\delta_1 \equiv 2\nu_0/\nu_{e0} = (2\alpha c/4\pi r_0)/(v_0/2\pi r_0) = ac/v_0 = 1 \quad (75)$$

yielding

$$v_0 = \alpha c = e^2/2h\varepsilon_0 = 2187691.2 \text{ m/s} \quad (76)$$

and then the (66) becomes

$$v_0 = m_r v_0^2/2h = m_r \alpha^2 c^2/2h = R_H c \quad (77)$$

where $R_H = m_r \alpha^2 c/2h = 1/\lambda_0$ is the Rydberg constant.

Now, from (61) and (73), because of the ratio $\delta_1 \equiv 2\nu_0/\nu_{e0} = 1$, we also get

$$\delta_n \equiv 2\nu_n/\nu_{en} = (2\nu_0/n^2)/(\nu_{e0}/n^3) = n \quad (\text{with } n = 1, 2, 3, \cdots) \quad (78)$$

which written as $nT_n = 2T_{en}$ shows that the impact time nT_n of *n photons* (with frequency ν_n) equals the time the electron needs for two orbits along any circular orbit r_n.

Now the correct value of r_0, from (71), becomes

$$r_0 = \frac{e^2}{8\pi\varepsilon_0 h\nu_0} = \frac{e^2}{8\pi\varepsilon_0 hR_H c} = \frac{\alpha}{4\pi R_H} = 5.294654\times10^{-11} \text{ m} \quad (79)$$

which should represent the electron ground state orbit if the electron should circle, together with its charge, around r_0: indeed the ground-state effective orbit of the electron barycentre observed from m_p is r_0'. Then, writing the (59) as $r_B = r_0/(1+\varepsilon_m)$ we get

$$r_B = \frac{r_0}{1+\frac{m_e}{m_p}} = \alpha/4\pi R_H(1+\varepsilon_m) = \frac{\alpha}{4\pi R_\infty} = 5.291772\times10^{-11}\ \text{m} \tag{80}$$

corresponding to the Bohr radius which, on our results, is the orbit of the electron charge referred to B(centre of mass of the system electron-proton)see **Figure 9(a)**.

Now, still referring to conf. (**c**), the effective electron orbit (*i.e.* its barycenter) is r_0' where its effective speed is

$$\begin{aligned} v_0' &= \frac{v_0 r_0'}{r_0} = \frac{v_0(r_0+r_e)}{r_B(1+\varepsilon_m)} = v_0\left[r_B(1+\varepsilon_m)+\varepsilon_r r_B\right]/r_B(1+\varepsilon_m) \\ &= \frac{v_0(1+\varepsilon_m+\varepsilon_r)}{1+\varepsilon_m} = \alpha c\left(1+\frac{\varepsilon_r}{1+\varepsilon_m}\right) \end{aligned} \tag{81}$$

and since the distance between the electron charge and the proton charge is r_0 (either considering the electron circling along r_0' or r_0), it turns out that along r_0' the photon admitted frequency is $\nu_0' = \nu_0$, and therefore we get

$$\delta_1' = \frac{2\nu_0}{\nu_{e0}'} = 2\nu_0/(v_0'/2\pi r_0') = 2\nu_0\Big/\frac{v_0 r_0'}{r_0}\Big/2\pi r_0' = 2\nu_0 2\pi r_0/v_0 = 1 \tag{82}$$

meaning *one* photon every two electron ground-state orbit, and since $r_0' = (r_0 + r_e)$ is also a circular orbit, the *effective* electron orbit r_n' has following parameters:

$$r_n' = r_0' n^2;\ v_n' = v_0'/n;\ \nu_{en}' = \nu_{e0}'/n^3;\ \nu_n' = \nu_n \tag{83}$$

thus for each circular orbit we get

$$\delta_n' = \frac{2\nu_n}{\nu_{en}'} = \left(2\nu_0/n^2\right)/\left(\nu_{e0}'/n^3\right) = 2n\nu_0/\nu_{e0}' = n \tag{84}$$

the same as along r_n.

2.4. Electron Radial Speed, Ionization Condition, Electron Radius

To apply properly the Conservation of momentum (CoM) to the impact photon-electron, the atom nucleus has to be considered fixed as origin in the common centre of gravity nucleus-electrons. On H atom, referring to **Figure 9(c)**, an inelastic impact photon-electron, since photon and **w**, see **Figure 8**, have same direction, the (52), gives

$$w = 2mc/m_r = 2\gamma\nu c/m_r = 2\gamma\nu c^2/cm_r = 2h\nu/cm_r \tag{85}$$

where the frequency ν, see (70), depends on the effective distance r between the proton and the electron charge, while the term w, see also **Figure 10**, is the electron *radial* speed originated by the impact of **one** *photon* during the impact time $T(=1/\nu)$; for n photons of the same ray the (85) gives

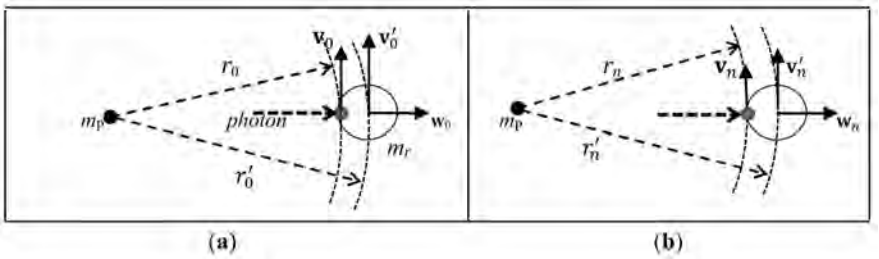

Figure 10. H atom: orbital and radial electron speed, see also **Figure 9(c)**. (a) Along r_0 we have: $\upsilon_0 = \alpha c; w_0 = \alpha^2 c$; then, along r'_0 we will find $\upsilon'_0 = c/137$; (b) Along the ionization orbit: $w_{n^2} = \upsilon'_n = c/137^2$.

$$w_n = nw = 2nh\nu/cm_r \tag{86}$$

while the generic condition

$$w = \upsilon \quad \text{(ionization condition)} \tag{87}$$

where υ is the electron speed along the ionization orbit, represents the sufficient condition for an electron to escape from its atom, (with zero final velocity of the electron, like on Absorption effect and, of course, for H atom).

Now, writing the (66) as $\nu_0 = m_r\upsilon_0^2/2h$, the (85) leads to

$$w_0 = \frac{2hm_r\upsilon_0^2}{2hcm_r} = \upsilon_0^2/c = \alpha^2 c = 15964.35 \text{ m/s} \cong c/137^2 \tag{88}$$

thus the ionization condition along r_0, for one photon only, becomes

$$\frac{w_0}{\upsilon_0} = \frac{\upsilon_0}{c} = \alpha \cong 1/137 \ll 1 \tag{89}$$

hence the ionization, requiring $w/\upsilon = 1$, could happen for n = 137, but the number of admitted photons, along r_0, is n = 1. Now, along the progressive orbit # n, the admitted photons frequency is $\nu_n = \nu_0/n^2$, and since n is the number of admitted photons along each electron circular d-orbit, we may infer that each progressive orbit is composed of n electron d-orbits, yielding n^2 admitted photons along each of these orbits.

Referring now to the electron effective ground-state orbit r'_0, regarding the orbit $r'_n \equiv r'_0 n^2$, where $\upsilon'_n = \upsilon'/n$, the (86), for n^2 photons, gives

$$w_{n^2}\left(= nw_{\#n}\right) = \frac{n^2 2h\nu'_n}{cm_r} = \frac{n^2 2h\nu'_0}{cm_r n^2} = \frac{2h\nu'_0}{cm_r} \tag{90}$$

constant along every circular orbit, and where ν'_0 from (66) becomes

$$\nu'_0 = m_r\upsilon'^2_0/2h \tag{91}$$

which represents the photon *virtual* frequency, intending the admitted frequency if the electron charge would be coincident with the electron barycenter along its effective orbit r'_0; indeed, the photons admitted frequency is related to the effective distance r_0, where the effective photon frequency is therefore ν_0. In fact, we introduce ν'_0 to determine the value of υ'_0 (ground-state electron effective orbital speed).

Therefore the ionization condition along r_n' becomes

$$w_{n^2} = v_n' = v_0'/n \tag{92}$$

yielding

$$2hv_0'/cm_r = v_0'/n \Rightarrow n = v_0' cm_r/2hv_0' \tag{93}$$

then

$$n = v_0' cm_r\, 2h/2hm_r v_0'^2 \Rightarrow n = \frac{c}{v_0'} \cong \frac{c}{v_0} = \frac{c}{\alpha c} \cong 137 \tag{94}$$

but n **has to be in integer**, so we can infer $n = c/v_0' = 137$ and therefore we get

$$v_0' = c/137 \tag{95}$$

representing the electron speed along its effective ground-state orbit, while

$$v_{137}' = v_0'/137 = c/137^2 \tag{96}$$

represents the electron speed along its ionization orbit, see also Table 2.

Then, since $v_0' = \alpha c\left(1 + \frac{\varepsilon_r}{1+\varepsilon_m}\right)$ we obtain

$$\frac{c}{137} = \frac{\alpha c\left(1+\varepsilon_m+\varepsilon_r\right)}{1+\varepsilon_m} \tag{97}$$

then

$$1+\varepsilon_m+\varepsilon_r = \frac{\left(1+\varepsilon_m\right)}{137\alpha} \Rightarrow \varepsilon_r = \left(1+\varepsilon_m\right)\left(\frac{1}{137\alpha}-1\right) = 0.0002629141 \tag{98}$$

and since, for definition, $r_e = \varepsilon_r r_B$, we get

$$r_e = \varepsilon_r r_B = \frac{\varepsilon_r \alpha}{4\pi R_\infty} = \left(1+\varepsilon_m\right)\left(\frac{1}{137\alpha}-1\right)\alpha/4\pi R_\infty = \left(\frac{1}{137\alpha}-1\right)\alpha/4\pi R_H \tag{99}$$

and since $4\pi R_H = \alpha/r_0$ we also get

$$r_e = \left(\frac{1}{137\alpha}-1\right)r_0 = 1.391281\times10^{-14}\,\text{m} \quad \text{(electron radius)} \tag{100}$$

Table 2. Parameters of H atom circular orbits up to the ionization, our results.

Progressive number of each circular d-orbit n-th	Total number of admitted photons along each orbit n^2	Photons effective frequency along orbit r_n $\nu_n = \nu_0/n^2$	Photons virtual Frequency along each orbit r_n' $\nu_n' = \nu_0'/n^2$	Electron radial speed due to n^2 photons $w_{n^2} = 2hv_0'/cm_r$	Electron orbital speed $v_0' = c/137$ $v_n' = v_0'/n$
-	-	($\times10^{10}$ Hz)	($\times10^{10}$ Hz)	m/s	m/s
1st	1	328,805.1	328,977.9	15,972.74	2,188,266
2nd	4	82,201.3	82,244.4	15,972.74	1,094,133
…	…	…	…	…	…
137th	137^2	17.52	17.53	**15,972.74**	**15,972.74**

2.5. Absorption/Emission Effect; Claimed Fall of Circling Electrons

Referring to Figure 11 representing the Absorption of *photons* into a circling electron, let us assume the nucleus mass $m_N >> m_e$ so to consider the nucleus fixed in the atom centre of gravity B.

Now, the expression of the total energy of the system photon-electron is given by

$$T = E + U_r + K_e + K_r \tag{101}$$

where $E\,(=mc^2)$ is the energy of the incident light, $U_r\,(=-e^2/4\pi\varepsilon_0 r)$ is the *potential* due to electrostatic attraction acting on the electron, $K_e\,(=\tfrac{1}{2}m_e v^2)$ is the electron *orbital* kinetic energy, and $K_r\,(=\tfrac{1}{2}m_e w^2)$ its *radial* kinetic energy related to its radial speed w due to the impact photon-electron.

Regarding the Absorption/Emission effect (elements on gaseous state), see Figure 11, along circular orbits it is $K_r = 0$ and moreover, at the end of absorption, along the orbit r_2, (where the photons have been absorbed), it is $E_2 = 0$; hence *between two circular orbits* r_1 and r_2, the (101) gives

$$E_1 + U_{r1} + K_{e1} = U_{r2} + K_{e2}. \tag{102}$$

Now, from (69) $U_r = -m_e v^2$ and since $K_e = \tfrac{1}{2}m_e v^2$, we get $(U_r + K_e) = -\tfrac{1}{2}m_e v^2$ thus from (102) we get $E_1 - \tfrac{1}{2}m_e v_1^2 = -\tfrac{1}{2}m_e v_2^2$; so, as $E_1 = h\nu$, and since $m_e v^2 = e^2/4\pi\varepsilon_0 r$ we find

$$h\nu = \tfrac{1}{2}m_e v_1^2 - \tfrac{1}{2}m_e v_2^2 = \frac{e^2}{8\pi\varepsilon_0}\left(\frac{1}{r_1} - \frac{1}{r_2}\right) \tag{103}$$

Then, according to (71) we have $r_1 = r_0 n^2$ and $r_2 = r_0 k^2$ (with $k > n$ as $r_2 > r_1$), thus

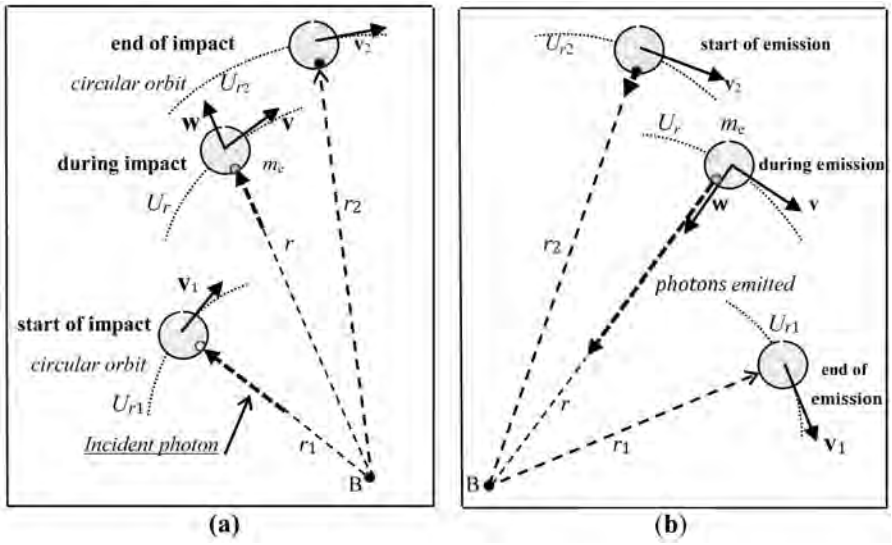

Figure 11. Absorption/Emission effect: (a) Incident photons are absorbed by the electron which moves toward wider orbits; (b) Emission: the electron moves toward inner orbits emitting photons.

$$\nu = \left(\frac{e^2}{8\pi\varepsilon_0 h r_0}\right)\left(\frac{1}{n^2} - \frac{1}{k^2}\right) \tag{104}$$

and plugging the (74) written as $\nu_0 = e^2/8\pi\varepsilon_0 h r_0$, we find

$$\nu = \nu_0\left(\frac{1}{n^2} - \frac{1}{k^2}\right) \tag{105}$$

which is the *photons* frequency between two circular orbits, where n represents the progressive specific number of each circular orbit and where k turns out to have, for each of them, the values $k = n + 1, n + 2, \cdots, n_i$ which are, one by one, the number of the *remaining* external circular orbits, and where n_i is the ionization orbit; on H atom, $n_i = 137$.

Claimed fall of a circling electron into its nucleus: an electrical current emits an electro-magnetic radiation and *therefore* it is claimed that the circulating electrical charge of an electron should also emit an e.m. radiation yielding the electron, in a short time, to fall into the nucleus; but on our results, a free electron, moving, for instance, along a copper wire under an electrical potential difference, when entering into an atom influence, (at that moment the electron charge will return to face the atom nucleus), will release the necessary *photons* to reach the atom energy level corresponding to the energy previously received (during the absorption effect). Indeed, along circular orbits, it is $w = 0$, therefore the absorption/emission of *photons* cannot happen along circular orbit, that is why the circling electrons are absorbing/emitting *photons* only *between* circular orbits, and therefore, the e.m. radiation is due to the emitted *photons* during their re-entry toward inner orbits; at this regard, *the photons emission is necessary for the electrons not to fall into their nucleus*.

2.6. Photoelectric Effect: Number of Involved Photons

Between the electron ground-state orbit r_0 and its extraction orbit $r \to \infty$ (intending on microscopic scale), the (101), valid for *every* interaction light-matter, gives

$$E + U_{r0} + K_{e0} + K_{r0} = E' + U_{r\to\infty} + K_{e\infty} + K_{ae} \tag{106}$$

where E' is the energy of re-emitted light, $K_{ae} = \frac{1}{2} m_e w_{ae}^2$ the electron kinetic energy after its extraction (intending on macroscopic scale), w_{ae} its related radial speed, while the other terms have been defined referring to (101).

On ground-state, as also shown between Equations (102) and (103), it is

$$U_{r0} + K_{e0} = -m_e v_0^2 + \frac{1}{2} m_e v_0^2 = -\frac{1}{2} m_e v_0^2 = -W_f \tag{107}$$

with v_0 the electron speed along r_0 and W_f the work function (electron extraction work); now, at the start of impact it is $w = 0$ giving $K_{r0}\left(=\frac{1}{2} m_e w^2\right) = 0$ while for $r \to \infty$, the electron orbital speed $v_\infty \to 0$,so

$$\left(U_{r\to\infty} + K_{e0}\right) = -\frac{1}{2} m_e v_\infty^2 \to 0 \tag{108}$$

hence the (106) gives

$$E - W_f = E' + K_{ae} \Rightarrow E = E' + W_f + K_{ae} \tag{109}$$

where $W_f + K_{ae}$ is the total kinetic energy transferred from light to electron, that is the sum of the sufficient energy to remove the electron plus the one to give it the energy after extraction.

On Photoelectric Effect (PhE), the light scatters off an electron ($K_{ae} \geq 0$), but it is not re-emitted, hence $E' = 0$, so the (109), with ν_f ($= W_f/h$) the specific threshold frequency, becomes

$$E = W_f + K_{ae} \Rightarrow h\nu = h\nu_f + \tfrac{1}{2} m_e w_{ae}^2 \tag{110}$$

showing that for $\nu = \nu_f$ there is ionization with $w_{ae} = 0$.

At frequency ν_f the electron radial speed w_f due to the impact of one *photon*, see Equation (85), is $w_f = 2h\nu_f / m_e c = 2W_f / m_e c$, and writing the (66) as

$$\upsilon_0 = \left(2h\nu_f / m_e\right)^{1/2} = \left(2W_f / m_e\right)^{1/2} \tag{111}$$

we get

$$\frac{w_f}{\upsilon_0} = \frac{\left(\dfrac{2W_f}{m_e c}\right)}{\left(\dfrac{2W_f}{m_e}\right)^{\frac{1}{2}}} = \left(\frac{2W_f}{m_e}\right)^{\frac{1}{2}} \Big/ c = \frac{\upsilon_0}{c} \Rightarrow w_f = \frac{\upsilon_0^2}{c} \tag{112}$$

which is equal to (88), and since the values of W_f are in the range $\cong$ 2 - 6 eV, the Equation (112) gives $w_f/\upsilon_0 \cong 0.0028$ - 0.0048 meaning that the ionization (which for elements on solid state where electrons are circling along fixed orbits requires $w = \upsilon_0$), at frequency ν_f needs n_f *photons*: indeed, the electron radial speed due to n_f *photons* with frequency ν_f, see (86), is

$$w_{nf} = n_f w_f = n_f 2W_f / m_e c \tag{113}$$

so the ionization condition becomes $w_{nf} = \upsilon_0$ leading to
$n_f 2W_f / m_e c = \left(2W_f / m_e\right)^{1/2}$ giving

$$n_f = c\Big/\sqrt{2W_f / m_e} = c\sqrt{m_e / 2W_f} = \upsilon_0 / w_f = c/\upsilon_0 \tag{114}$$

that is, on PhE, the number of photons at frequency ν_f *necessary* for ionization ($w_{ae} = 0$). Now, if n_f photons, at frequency ν_f, are sufficient for ionization, then the frequency

$$n_f \nu_f \equiv \nu_1 \tag{115}$$

is sufficient for ionization ($w_{ae} = 0$) with one *photon* only, so ν_1 is the threshold between PhE and Compton effect which requires one *photon* only, as shown on next chapter.

To find the number n_1 related to the frequency ν_1 let us equate the (66) written as $\upsilon_0 = \sqrt{2h\nu_1 / m_e}$, to the electron radial speed due to n_1 photons,
$w_{n1} = 2nh\nu_1 / cm_e$ yielding $\left(2h\nu_1 / m_e\right) = \left(2n_1 h\nu_1 / cm_e\right)^2$ and then

$$n_1^2 = \frac{m_e c^2}{2h\nu_1} = \frac{m_e c^2}{2hn_f \nu_f} = \frac{m_e c^2}{2n_f W_f} \Rightarrow n_1 = c\sqrt{m_e / 2n_f W_f} \tag{116}$$

and plugging $W_f = c^2 m_e / 2n_f^2$ as given by (114), we find

$$n_1 = \sqrt{n_f} \quad . \tag{117}$$

For instance as for caesium (Cs), having W_f 1.95 eV, since $n_f = c\left(m_e/2W_f\right)^{1/2} \cong 361.9$ we may infer $n_f = 361$ leading to $n_1 = 19$, while as for Be or Co, having $W_f \cong 5$ eV we may infer $n_f = 225$ leading to $n_1 = 15$.

2.7. Compton Effect and Its Equation via Doppler Effect

Here, see Figure 12, the incident photon (length λ, frequency ν), while ejecting a circling electron is also reflected (λ', ν) so the recoiling electron, emitting a *photon* λ' *tow*ard the Observer A, represents a source in motion from A along the direction **w**, implying an *undoubted* Doppler effect.

Now, on the basis that the incident *photon* starts to be reflected at the same time when it starts to hit the electron, and since $T' = 1/\nu'$ is the emission time of the reflected *photon*, it turns out that T' is also the whole interaction time (and this means that there is not a complete absorption of the incident photon followed by an emission). Now, with T' the whole impact time photon-electron, the momentum transferred from the *incident* light to the electron, as per (53), is

$$p' = m'c = \gamma\nu'c = \gamma c/T' \tag{118}$$

and the same value is then transferred from the reflected photon to the electron, so the Conservation of Momentum (CoM) along the direction normal to **w**, becomes

$$\gamma c/T' \sin\theta = \gamma c/T \sin\theta' \tag{119}$$

giving $\theta = \theta'$. Then, the length of the reflected photon, for the Observer A, see (17), is

$$\lambda' = \lambda + \Delta\lambda \tag{120}$$

where $\Delta\lambda = w_A T'$, where $w_A = w\cos\theta$ is the component of the electron speed along the direction of the Observer A, and $T' = 1/\nu'$ is, for A, the photon transit time, so we get

$$\lambda' - \lambda \equiv \Delta\lambda = wT'\cos\theta \tag{121}$$

Now the CoM along **w**, being $\theta = \theta'$, gives

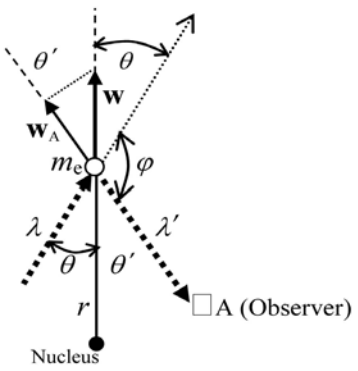

Figure 12. Compton effect (CE). φ: angle between the direction of the incident *photon* and the scattered one (λ'); θ: angle between the direction of the incident *photon* and the recoiled electron.

$$\frac{\gamma c\cos\theta}{T'}+\frac{\gamma c\cos\theta}{T'}=m_e w\Rightarrow wT'=\left(2\gamma c\cos\theta\right)/m_e \tag{122}$$

so the (121) becomes

$$\lambda'-\lambda\left(\equiv\Delta\lambda\right)=\frac{2\gamma c\cos^2\theta}{m_e}=\frac{2h\cos^2\theta}{cm_e} \tag{123}$$

Now, $2\theta+\varphi=\pi$, $\Rightarrow\theta=\left(\pi-\varphi\right)/2$, hence $\cos\theta=\sin\varphi/2$ and therefore

$$\Delta\lambda=2h\sin^2\left(\frac{\varphi}{2}\right)\Big/cm_e \tag{124}$$

and since $2\sin^2\left(\frac{\varphi}{2}\right)=\left(1-\cos\varphi\right)$, *we get the Compton equation*:

$$\Delta\lambda=\lambda'-\lambda=h\left(1-\cos\varphi\right)/cm_e \tag{125}$$

which cannot be obtained via the Doppler effect relativistic equations regarding the light.

We point out that the (122) written as $w=\left(2\gamma v' c\cos\theta\right)/m_e$, for $\cos\theta=1$ equals the (85), implying the impact of **one** *photon* only.

Now, the (123), for $\cos\theta=1$ gives $\lambda'=\frac{c}{\nu}+\frac{2\gamma c}{m_e}$ we can write as:

$$T'=\frac{1}{\nu}+\frac{2\gamma}{m_e}=\left(m_e+2\gamma\nu\right)/\nu m_e \tag{126}$$

which plugged into (122) gives

$$w=\left(\frac{2\gamma c}{m_e}\right)\Big/\left(m_e+2\gamma\nu\right)/\nu m_e=\frac{2\gamma\nu c}{2\gamma\nu+m_e}=\frac{c}{1+m_e/2\gamma\nu} \tag{127}$$

yielding $w\to c$ for $\nu\to\infty$.

3. Conclusions

This paper is mainly based on three conditions: $c = u$ (with u the *total* escape speed); a certain structure of the light (massive photons having variable length); the electron charge like a point-particle facing the atom nucleus during the electron orbit.

On these bases, we gave a *classical* reason to the apparent constancy of c, then we showed that the *time dilation* turns out to be an effect of the variation of the *total* gravitational potential U (inducing a variation of c) and we also showed that the high gravitational red shifts are also due to the same reason; we also showed that the quantum numbers are nothing else than the numbers of photons admitted on free atoms along an integer number of electron orbits; then we gave a reason why the circling electrons cannot fall into their nucleus, and we also showed that the ionization of free atoms happens when the electron radial speed (due to the impact photons-electron) equals the electron orbital speed.

Conflicts of Interest

The authors declare no conflicts of interest regarding the publication of this paper.

References

[1] Kragh, H. (1999) *Cosmology and Controversy*, 212.

[2] Gogberashvili, M., *et al.* (2014) Cosmological Parameter. ArXiv 1210.4618.

[3] Immerman, N. (2001) Nat'l Solar Observatory: The Universe. University of Massachusetts.

[4] Gott III, J.R., *et al. The Astrophysics Journal*, **624**, 8.

[5] Van Dokkum, P. (2010) *Nature*, **468**, 940-942. https://doi.org/10.1038/nature09578

[6] Schutz, B.F. (2003) Gravity from the Ground up. Cambridge University Press, 361.

[7] Blatt Frank, J. (1992) Modern Physics, Mossbauer Effect, McGraw Hill.

[8] Pound, R.V. and Rebka Jr., G.A. (1960) *Physical Rev*iew *Letters*, **4**, 337. https://doi.org/10.1103/PhysRevLett.4.337

[9] Pound, R.V. and Snider, J.L. (1964) *Physical Rev*iew *Letters*, **13**, 539. https://doi.org/10.1103/PhysRevLett.13.539

[10] Pound, R.V. and Snider, J.L. (1965) *Physical Review*, **140**, 788. https://doi.org/10.1103/PhysRev.140.B788

[11] (Yearly) NASA Extragalactic Database: (*i.e.* Galaxy M86 Has $z \cong 0.001$ with $s \cong 16$ Mpc; M99 Has $z \cong +0.008$ with $s \cong 15$ Mpc; NGC0063 Has $z \cong 0.004$ with $s \cong 20$ Mpc; VCC0815 Has $z \cong 0.0025$ with $s \cong 20$ Mpc).

[12] Halliday-Resnick (1981) *Fundamentals of Physics*, Chapter 47-2.

Journal of Modern Physics, 2018, 9, 2073-2089
http://www.scirp.org/journal/jmp
ISSN Online: 2153-120X
ISSN Print: 2153-1196

Preparation and Some Properties of Metal Organic Chemical Vapour Deposited Al-Doped ZnO Thin Films Using Single Solid Precursors

Olumide Oluwole Akinwunmi[1*], Johnson Ayodele O. Ogundeji[1], Adetokunbo Temitope Famojuro[2], Olakunle A. Akinwumi[1], Olusoji O. Ilori[3], Olatomide G. Fadodun[4], Ezekiel Oladele Bolarinwa Ajayi[1]

[1]Department of Physics and Engineering Physics, Obafemi Awolowo University, Ile-Ife, Nigeria
[2]Department of Chemistry, Obafemi Awolowo University, Ile-Ife, Nigeria
[3]Department of Electrical and Electronic, Obafemi Awolowo University, Ile-Ife, Nigeria
[4]Centre for Energy Research and development, Obafemi Awolowo University, Ile-Ife, Nigeria
Email: *oakinwunmi@oauife.edu.ng, *ooakinwunmi@gmail.com

How to cite this paper: Akinwunmi, O.O., Ogundeji, J.A.O., Famojuro, A.T., Akinwumi, O.A., Ilori, O.O., Fadodun, O.G. and Ajayi, E.O.B. (2018) Preparation and Some Properties of Metal Organic Chemical Vapour Deposited Al-Doped ZnO Thin Films Using Single Solid Precursors. *Journal of Modern Physics*, **9**, 2073-2089.
https://doi.org/10.4236/jmp.2018.911130

Received: July 13, 2018
Accepted: September 25, 2018
Published: September 28, 2018

Abstract

Zinc Oxide (ZnO) and Aluminium doped ZnO (AZO) thin films were deposited on soda lime glass by Metal Organic Chemical Vapour deposition technique (MOCVD), using prepared compound mixtures of Zinc Acetate di-hydrate ($Zn(CH_3COO)_2{\cdot}2H_2O$; ZAD) and Aluminium Acetyl-Acetonate ($Al(C_5H_70_2)_3$; AAA) precursors at a temperature of 420˚C. Effects of the varying mole percent concentrations of AAA precursor additives on the Al dopant concentrations in ZnO were systematically studied. The observations were made via investigations carried out on the morphological, optical, electrical and compositional properties of the deposited thin films. The thin films morphology was found to be strongly dependent on the varying concentration of AAA in the precursor mixtures. The average optical transmittance of the thin films in the uv-visible region was over 85% except 5 mol.% Al. While the energy band gaps were found to be in range of 3.27 - 3.36 eV. There is a blue-shift of the energy band edge observed between 0 and 5 mol.% AAA, which may be due to Burstein-Moss' band gap widening effect and an opposing band gap renormalization effect at 10 mol.% AAA along with an extra band gap stabilization effect (Roth's effect) at 15 mol.% AAA in rather quasi-sinusoidal or anomalous behaviour. The optical transmittance and electrical conductivity of ZnO were enhanced with addition of Al dopants. The RBS confirm the presence of Al, Zn and O, and evidence that Al dopants were successfully incorporated into the ZnO.

Keywords

ZnO Thin Film, ZnO:Al, MOCVD, Optical Properties, AAA, ZAD, Electrical Properties, FESEM, UV-Vis, Optoelectronic Properties

1. Introduction

Within the present decade, the rate of development of optoelectronic materials applications has rapidly increased, with current research in transparent conducting oxides (TCO's) being directed towards choice materials capable of combining economical and environmentally sustainable superior performance. TCO's are generally classified as materials with combined high average optical transparency > 80%, high electrical conductivity, and low resistivity of $\leq 1\times10^{-3}\Omega\text{cm}$. The currently ubiquitous optoelectronic devices such as thin film solar cells, light emitting diodes (LEDs), transparent thin film transistors, piezoelectric transducers, gas sensors, flat and touch panel displays [1] [2] [3] laud TCO materials as the focal point for the interests of numerous research groups seeking to explore, enhance, optimize, stabilize and economize superior TCO materials performance in the nearest future. AZO thin films have superior advantages when compared with known TCO (In_2O_3:Sn ITO) in that ZnO is abundant in the earth crust when compared to Indium (In), eco-friendly, has high thermal, chemical and radiation stability in hydrogen plasmas and other harsh environments [4]. Moreover, there is a general ongoing trend in the TCO industry to move towards alternative solutions for more advanced applications [5]. In the recent time, AZO thin films were been deposited on flexible substrates and are attracting both research and technology's attention [6] [7].

TCOs' are majorly compound semiconductors, generally classified as either n-type or p-type in line with their electrical properties. Their classifications are further subdivided into binary, ternary, quaternary compound and doped types. Doping ZnO with Group III elements (Al, In and Ga) drastically enhances the electrical conductivity [8] [9] [10] [11]. TCO's have been fabricated by various methods, ranging from physical methods to chemical methods [5] [12] [13]. Metal organic chemical vapour deposition (MOCVD), which is a variant of Chemical method is an attractive technique for the fabrication of TCO's. This is due to its large-area to volume and conformal deposition capability even with less sophisticated apparatus, as well as close to ambient temperature deposition in contrast to PVD techniques. This paper is a report of MOCVD AZO thin films deposited on soda lime glass substrate, using single solid source precursors and the trends observed in its properties with varying Al dopant concentration. The prepared precursors were characterized using Fourier Transform Infrared (FTIR) spectroscopy while the thin films' properties were characterized using Field Emission Scanning Electron Microscopy (FE-SEM), Ultraviolet-Visible (UV-Vis) Spectroscopy, Four Point Probe technique and Rutherford Backscat-

tering Spectroscopy (RBS).

2. Experimental Details

ZnO and AZO thin films were prepared by MOCVD technique. A schematic of the experimental set-up is shown in Figure 1(a). 0.03 M starting solution was prepared from analytic grade ZAD (Fisher Scientific, UK; 99.999%) and dissolved in methanol (BDH Analytical Chemicals, UK; 95.9999% dilute). Varying concentrations of AAA (BDH Analytical Chemicals, UK; 99.999%) previously dissolved in methanol at 0.03 M was added to the prepared ZAD solution in

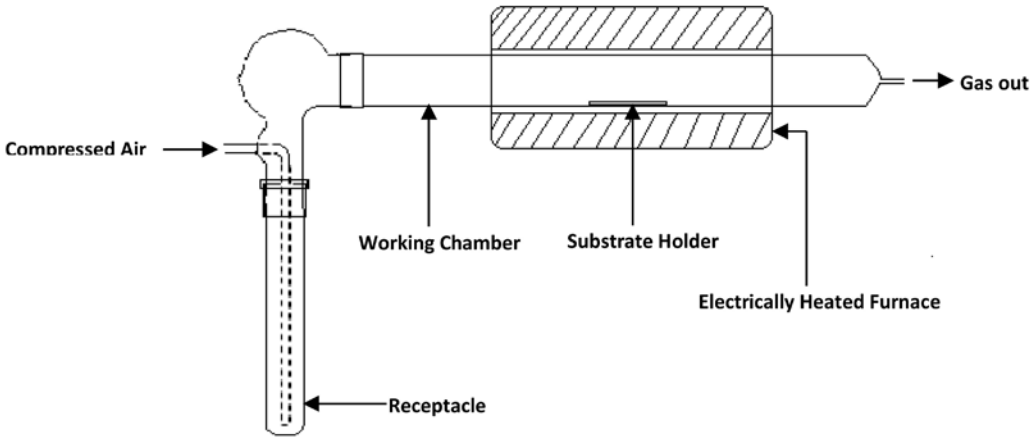

(a)

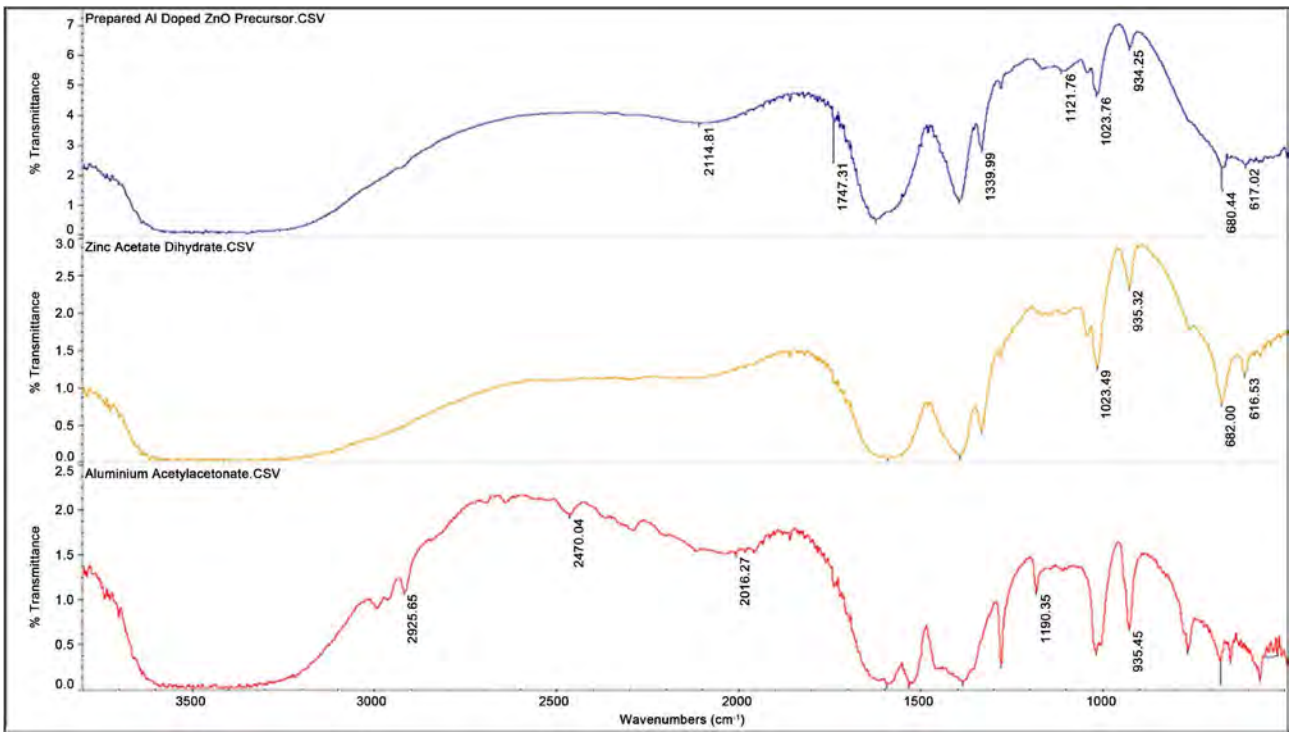

(b)

Figure 1. (a) A schematic of the experimental set-up; (b) FTIR spectra of the final single solid source precursor used and the starting solid materials ZAD and AAA.

other to doped the initial solution such that the mole ratios of the precursors would be 95:5, 90:10 and 85:15 mol.% respectively. The prepared solutions were oven dried to constant weight at 60˚C for 48 hours. The resulting caked solids were pulverized just before the pyrolysis. The thin films were deposited onto cleaned soda lime glass substrates at 420˚C for 2 hours using nitrogen as carrier gas with flow rate 2.5 dm^3/min (**Figure 1**). The FTIR Spectrum of the individual and prepared precursor were taken using a Nicolat iS5 Spectrometer. The FE-SEM micrographs of the AZO thin films were obtained using a Zeiss plus 55 FE-SEM. Transmittance spectra were measured with Shimadzu UV-Vis 1800 double beam spectrophotometer in the wavelength range 280 - 800 nm. The current-voltage (I-V) characteristics were studied within voltage sweep 0 - 0.5 V, and carried out under normal conditions at room temperature using the four point probe technique, a Jandel four point probe tool (model TY242MP), and a Keithly 2636A dual channel source/measurement equipment unit all sealed in a dark room.

RBS Spectrum of the thin films were taken using a National Electrostatic Corporation's (NEC) 1.7 MV Tandem Accelerator with 2.202 MeV He^{++} (mass = 4) nuclides as the ion beam. The beam incidence angle was 0.00˚; the RBS detector was placed at a 168˚ scattering angle and an exit angle of 12˚. The depth profile of the thin films and their elemental compositions were obtained from the RBS spectrum using the SIMNRA and RUMP simulation software.

3. Results and Discussion

A pyrolytic process is known to occur close to a heated glass substrate when aerosol droplets in a jet or cloud arrive at the substrate, so that a highly adherent thin films of ZnO and AZO were formed on the substrate.

3.1. Precursor Mixture Composition

FTIR spectrum of the final single solid source precursor used and the starting solid materials AAA and ZAD were shown in **Figure 1(b)**. As observed in the figure, AAA had undergone unintentional hydration. This can be interpreted in terms of the hydration of the complex in water. The distribution constants of metal acetylacetonates, between water and n-C_7H_{35} determined as a function of temperature have been reported to be most thermodynamically favourable than that of other trivalent acetylacetonates such as Co, Cr, Rh. The higher hydration of AAA supports the idea that the hydration took place through the octahedral faces in the laboratory atmosphere before the precursor preparation [14]. Hence, the FTIR spectra show a strong intensity of the broad-peaked O-H stiff bonds in a stretching mode at a higher vibrational frequency of between 3300 and 3500 cm^{-1}. The broad peak observed in the ZAD between the same frequencies represents the hydration present in its molecular formula. On the other hand, the final product precursor formed; contain the O-H broad peak contribution from the hydration of the AAA and ZAD precursor. The fingerprint region of each of the

precursors is approximately below 1500 cm^{-1}. Although, IR vibrations in this region are often complex and difficult to assign to a specific functional group of the molecule, the AAA, ZAD and final solid source product each have a distinct pattern in the region as can be observed by inspection. The ZAD spectrum is very similar to the solid source product than the AAA, since the number of possible vibrations for any given molecule is determined by the number of atoms present and hence the intensity of the peak observed. All the peaks in the fingerprint region of the solid source product align peak for peak with the ZAD with very minimal shifting or conjugation, except for the reductions in peak intensity of the solid source product precursor. SP^3 hybridized C-H bonds are observed in the AAA only between 2800 and 3000 cm^{-1}. The δ C-H bond peaks are observed in all the precursors between 1293 and 1464 cm^{-1}, as well as the ν C=O bond at 1596 cm^{-1}. While the ν C=O bond connected to Al in AAA is at 1532 cm^{-1}, its presence in the solid source product is observed as the left-skewed broad peak in the solid source product which is symmetrical in the ZAD. Also, the ν Al=O in AAA and ν Zn=O in ZAD spectra are observed at the same frequency, but diminished intensity in the solid source product between 1023 and 1026 cm^{-1} respectively, and suggesting a conjugation of the bonds between Al, Zn and O, as a result of the lowering of the stretching frequency resonance as observed at the peaks.

3.2. Surface Morphology

Field Emission Scanning Electron Microscopy (FE-SEM)

Figures 2(a)-(d) show the FE-SEM micrographs of as-deposited AZO thin films with ratio 0, 5, 10, 15 mol.% of Al dopant. The micrographs show a strong dependence of the AZO thin films morphology on increasing aluminium concentration. As observed, a uniform, continuous and pin hole free morphology is shown in **Figure 2(b)** at 5 mol.% Al dopant concentration implying the presence of low internal stress. The micrograph of as-deposited 10 mol.% AZO in **Figure 2(c)**, show a uniformly granular polycrystalline morphology having almost the same sizes, with well-defined grain boundaries and an inhomogeneous surface with polygon-like grains that may efficiently scatter incident photons. The as-deposited 15 mol.% AZO is polycrystalline with grains and obvious grain boundaries. This observation may be as a result of the an Al rich thin film, resulting in a degenerately doped layer of AZO and hence creating a highly distinct segregation of grains with possible accumulation of excess Al ions at the grain boundaries thus preventing further enlargement of the grains and grain boundaries. Al^{3+} as dopant substitute Zn^{2+} in AZO thereby increasing the nucleation site number [13]. In a degenerately doped ZnO, there is a tendency for heavy and localized nucleation of grains to occur, such as observed in **Figure 2(d)**.

3.3. Optical Properties

The effect of the increasing aluminium dopant concentrations on the optical

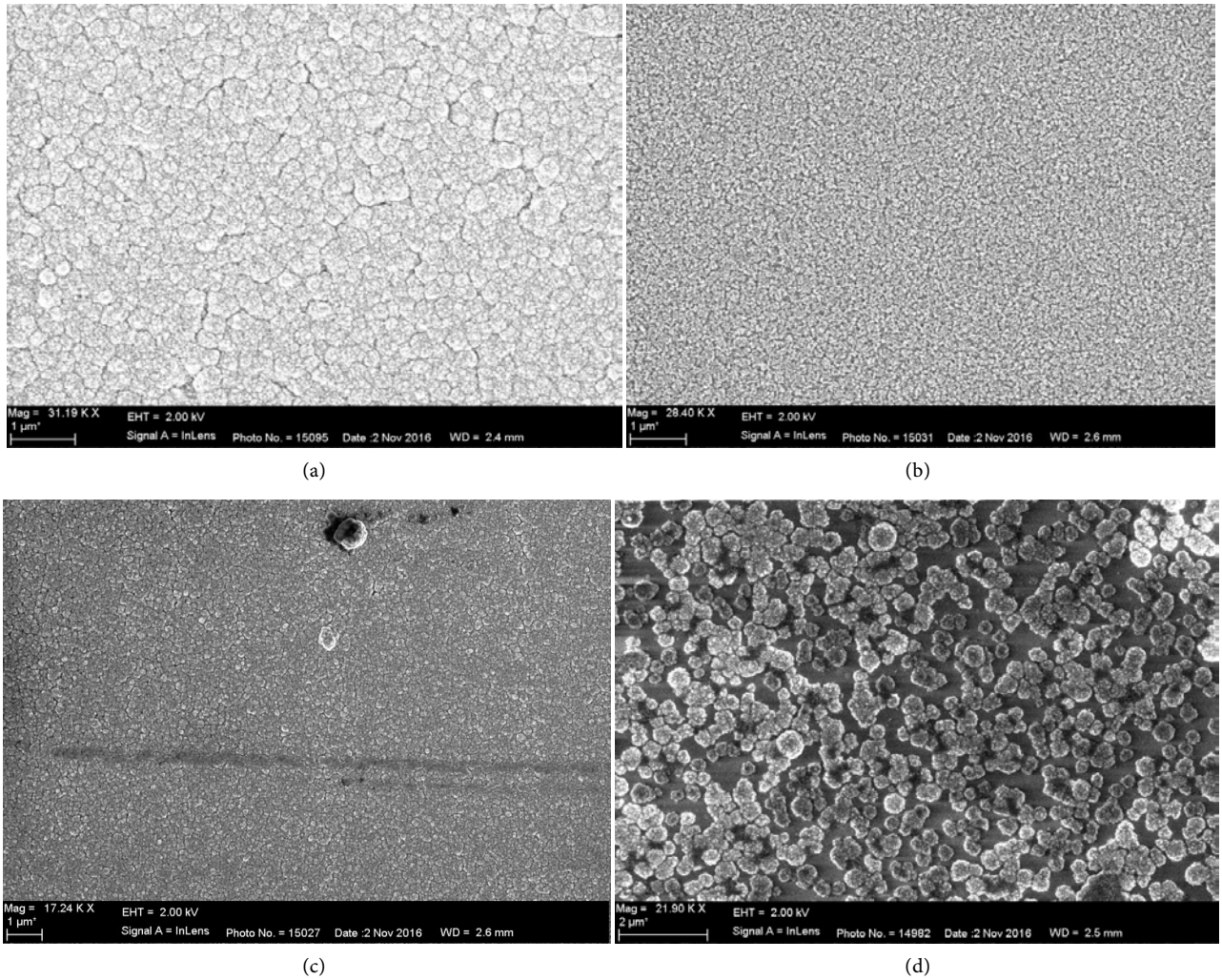

Figure 2. (a) FE-SEM image of AZO thin films (0 mol.% Al); (b) FE-SEM image of AZO thin films (5 mol.% Al); (c) FE-SEM image of AZO thin films (10 mol.% Al); (d) FE-SEM image of AZO thin films (15 mol.% Al).

transmittance of the AZO thin films are shown in **Figure 3(a)** & **Figure 3(b)**. The average transmittance in the near ultra-violet, visible and near infra-red region (380 to 800 nm) combined is over 85% except 5 mol.% Al. The heavily doped AZO thin films show increase in average transmittance up to 91% within the wavelenght region studied, while undoped ZnO thin films was found to be 86%. The 5 mol.% AZO thin film's low transmittance appears to be as a result of excessive scattering centres in the amorphous structure of the thin film. Compressed air and nitrogen gas were each used as carrier gas to deposit the thin films at 10 mol.% Al dopant concentration, and both gave an average transmittance of 92% within the same wavelength range. The transmittance of ZnO is greatly enhanced when the Al dopant concentration is greater than 10 mol.%. In general the transmittance of the deposited film improves from 5 mol.% Al dopant concentration in the presence of sufficient oxygen [10].

Other optical parameters of the AZO thin films such as the refractive index (**Figure 3(c)**) decreases with increase in transmittance. The observed opposite

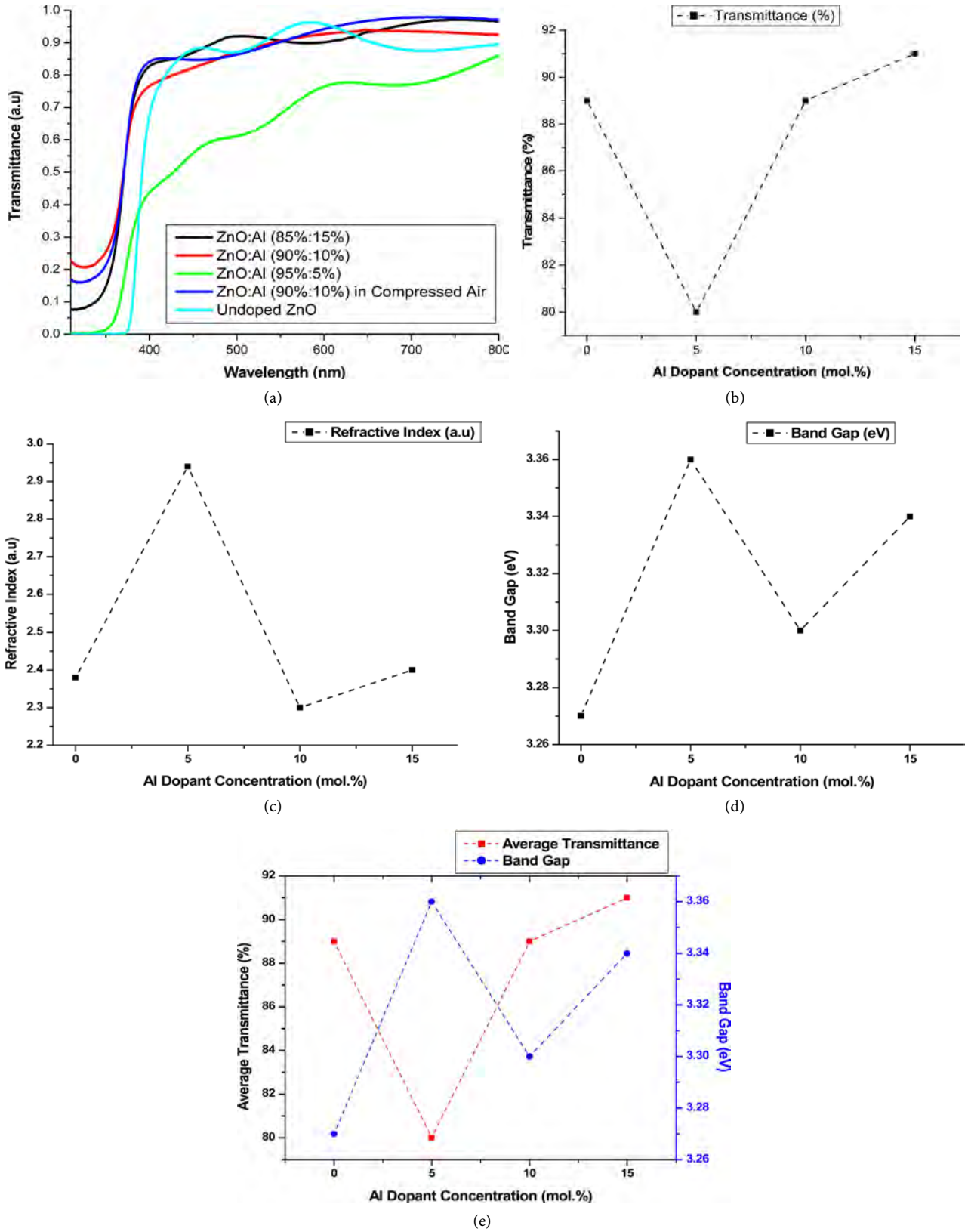

Figure 3. (a) Optical transmittance of the AZO thin films; (b) Average transmittance vs Al dopant concentration; (c) Refractive index ($n_{thin\ film}$) vs Al dopant concentration; (d) Energy band gap vs Al dopant concentration; (e) Average transmittance, band gap vs Al dopant concentration.

trend of the refractive index is known to be as a result of the change in the nature of the microstructure arising from the changes in grain sizes with increasing Al dopant concentration [15] [16]. In fact, the inhomogeneity of the grains resulted in the lower average transmittance in the 5 mol.% AZO thin film, creating uneven scattering centres and hence an abruptly increased refractive index. The band-gaps on the other hand, are observed to have all blue-shifted in ZnO with increasing Al dopant concentration as shown in **Figure 3(d)**. The blue-shift of the absorption edge may be due to the increase in carrier concentration as a result of the increase in the Al dopant concentration. The blue-shift is intricately related to the screening effect which occurs as low energy transitions are blocked, resulting in a Burstein-Moss band-gap widening effect [16] [17] [18]. The parabolic structure of the conduction band observed as an abrupt near zero tailing off of the absorption edge in undoped ZnO (**Figure 3(a)**) infers the theoretical absence of defects due to impurities in its structure. However, an exponential structure of the conduction band results as observed at the gradual tailing off of the absorption edges in the AZO thin films (**Figure 3(a)**), hence identifying deep band defect states due to Al dopants propagated as far as the absorption edges. Tail states created at the absorption edges are not terminated abruptly, but extend gradually from the near absorption band into the absorption band edges. The Tauc's equation was therefore used to evaluate the band gaps for the doped AZO thin films, since it gives a better estimate, taking into consideration the contributions of such deep band defect states as well as tail states near the absorption edges [19]. The energy band gap values of each AZO thin film was evaluated from $(\alpha h\nu)^2$ as a function of $(h\nu)$ in the Tauc's equation

$$\left(\alpha h\nu\right)^2 = A\left(h\nu - E_g\right) \tag{1}$$

where α is the absorption coefficient, $h\nu$ is the photon energy, A is a constant that depend on the material's properties, and E_g is the optical band gap energy respectively. The plot for undoped ZnO when extrapolated from the linear region of the square of the absorption coefficient tail to the point where $(\alpha h\nu)^2 = 0$, intercepted the abscissa at the energy band gap value 3.27 eV. However, in direct gap semiconductors such as ZnO, disorder due to impurity and temperature effects will cause the exponential band tails of the electronic states to extend into the semiconductors forbidden gap. This causes optical transitions to occur near the absorption edge such that the transitions manifest an exponentially varying absorption coefficient (α) as the electrons move from a parabolic band to an exponential band-tail state.

The sharp widening of the band gap of ZnO at Al dopant concentration of 5 mol.% may be due to Burstein-Moss effect. And the subsequent contraction 10 mol.% may be attributed to band-gap renormalization, followed by the phenomenon of an additional stabilization deposition temperature based effect known to occur in an inert gas atmosphere such as N_2(g) at 420˚C (Roth's effect) at 15 mol.%. This effect acts as an opposing force to the Burstein-Moss band gap widening effect and tries to restore or renormalize the band gap to its initial value

following a heavy dopant concentration [20]. These effects are typical of the optical band gap of nanocrystalline ZnO thin films. According to Srikant and Clarke, the Burstein-Moss effect is valid for materials having low effective mass of electrons and holes. That is, materials in which quantum confinement lead to an initial rise in the optical band gap [21]. This appears contradictory with the results of this study, in which the AZO thin films are not only degenerately n-type doped, but thicknesses are way more than that permissible in quantum confinement studies. Yet, an initial band gap widening offset partially by a band-gap renormalization was observed. However, recent studies through density-functional band-structure theory demonstrate that the band-gap renormalization is related to the non-parabolic nature of the host conduction band (ZnO), created as a result of the dopant impurities, and not because of a rigid shift of the band edges as studies have earlier assumed [22]. As a result, the carrier dependence of the Burstein-Moss' band-gap widening in this study is rather highly sensitive to the electronic states of the dopant ion (Al^{3+}) which in turn can be intrinsically involved in the complete reconstruction of the conduction band, thus lowering it. This effect is better observed in **Figure 3(e)**, the band-gap widening from 0 to 5 mol.% Al dopant concentration is as a result of the occupation of the AZO conduction band, inducing optical transitions at higher energies than the minimum-energy of the fundamental electronic gap (undoped ZnO). Meanwhile, and on the other hand, increase in free carrier screening will result in the decrease in the binding energy of the optical transitions associated with both free and bound excitons. So that, in the undoped ZnO and the AZO thin films, both the free and bound exciton transitions show a quasi-sinusoidal blue-shift and red-shift as the exciting wavelength of the UV-Visible radiation is decreased and intensity maintained with increasing dopant concentration [23]. The renormalization effect results in a red-shift of the optical transitions, and therefore a reduced free-carrier screening effect of photons resulting in increased average transmittance as a result of the reduction in the band-gap energy. The energies of the optical transitions are therefore the resultants of the blue-shift due to screening, and the red-shift due to the renormalization effect. The entire energy interplay weakens as the dopant concentration increases (up to15 mol.%), so that a stability effect (Roth's effect) converges both the average transmittance and the band-gap to a stable value. The energy positions are determinable by the aggregated effects of screening and band-gap renormalization resulting from the added free electrons. In this study the exact energy position was not determined but rather we try to establish the trend for the optical transition energies.

3.4. Electrical Properties

Linear current-voltage (I-V) characteristics are observed in the 5 and 10 mol.% AZO thin films as shown in **Figure 4(a)** and **Figure 4(b)**, while the non-linear I-V character of the 15 mol.% AZO thin film in **Figure 4(c)** predict that there might be more than one mechanism of electron transport at play. The values of the sheet resistances of the AZO thin films were calculated from equation

$$R_s = \rho / t \quad (2)$$

where R_s is the sheet resistance in ohm/square, ρ is the resistivity in ohm-cm and t is the thickness of the thin film.

A decrease in the sheet resistances of the AZO thin films is observed for thickness ranges from 487 to 634 nm. Therefore, a corresponding decrease in the resistivity is partly due to the presence of defects and majorly to Al dopants located as interstitial atoms and hence substitute Zn, and filling Oxygen vacancies [24]. This may be due to the donor states created as a result of the Al^{3+} ions impurity introduced in the ZnO lattice structure, producing in all cases an n-type semiconductor [4]. The degree of corresponding increase in the conductivity realizable, given the aforementioned processing conditions of the AZO thin films in the as-deposited state is directly influenced by point defects such as oxygen vacancies acting as doubly charged electron donor centres, and structural defects due to the substitution of Zn atoms amidst other defects. Together with the Al^{3+} ions impurity increasingly introduced, this defects impact greatly on the carrier mobility within the AZO thin films. In addition, an increase in oxygen vacancies will increase the number of free electrons, which in turn increases the conductivity abruptly [13]. Al dopant concentration and oxygen vacancies creation most possibly resulted in the abrupt increase of the conductivity from 0 mol.% to 5 mol.%. The interplay of increased Al^{3+} ion substitution of Zn atoms and oxygen vacancies more greatly modified the 10 mol.% Al dopant concentration as observed in the value of the sheet resistances shown in the legends in **Figures 4(a)-(c)** respectively. The conductivity of 15 mol.% AZO also increased, but was lower than that of 5 mol.% AZO given the same processing conditions and comparable film thicknesses. Apparently, the heavily doped 15 mol.% AZO thin film had the highest Al^{3+} ion impurity content, but as well the lowest number of oxygen vacancy which directly degrading the doping efficiency and compactness. At high Al dopant concentration, there is possibility that conduction by hopping mechanism will occur since the FE-SEM micrograph (**Figure 2(d)**) shows highly clustered and segregated grains across the AZO thin film [5] [13] [25].

TCO performance factor, energy band gaps, thickness and resistivity were shown in **Figures 4(d)-(g)**. The interpretation of these trends with the FE-SEM images reveals the microstructural evolution of the AZO thin films. In **Figure 4(d)** the sheet resistance and average transmittance are observed to decrease with increase in dopant concentration from 0 to 5 mol.%. However, a lower sheet resistance in combination with a higher average transmittance is desirable for TCO material applications. On the other hand, while the average transmittance of the AZO thin films increased from 5 mol.% to 10 mol.% dopant concentration, the sheet resistance effectively decreased as well; an advantageous trend.

It is therefore pertinent to note that both parameters are correlated by an important figure of merit [26] [27], which measures TCO performance (Φ_{TC}) as follows:

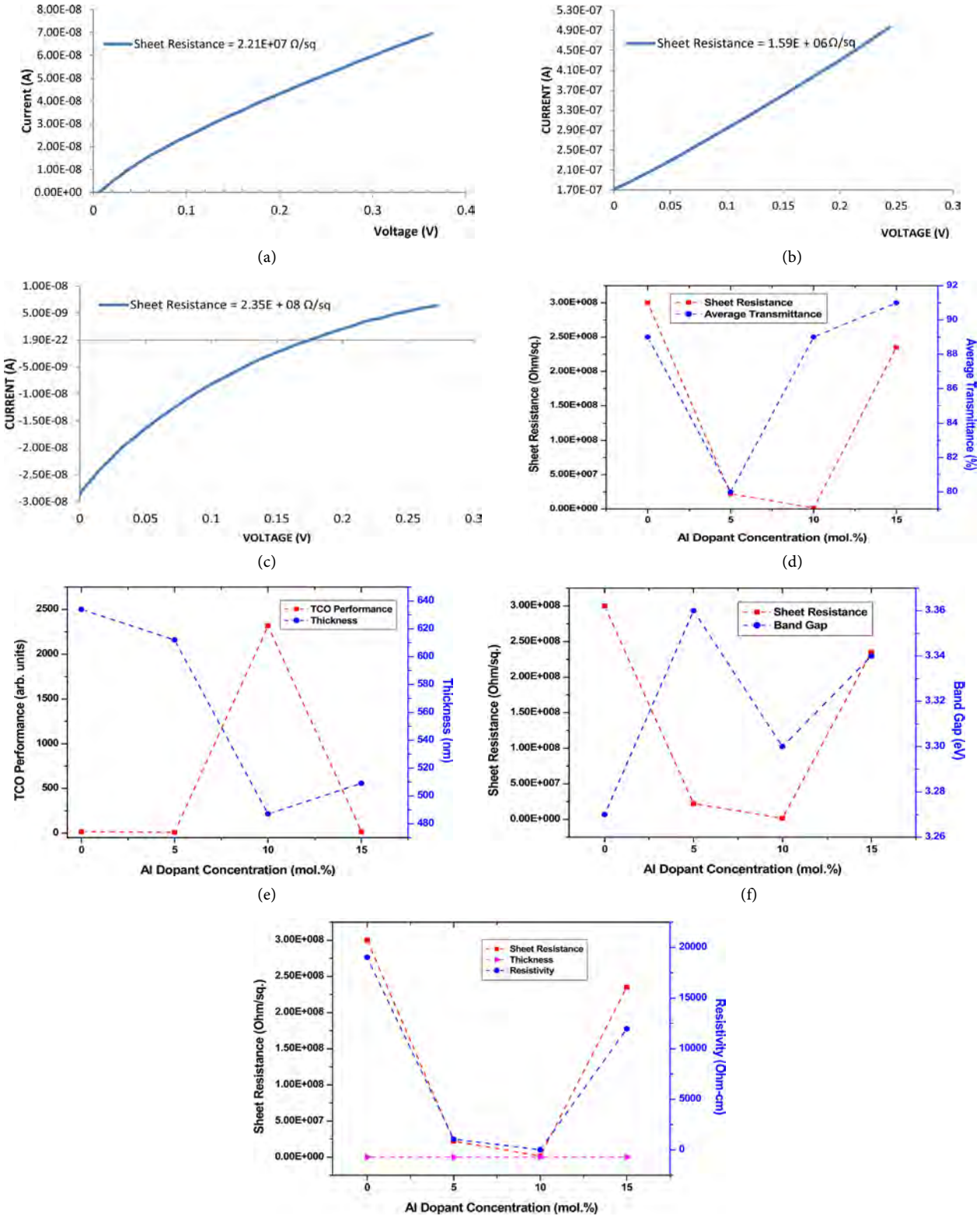

Figure 4. (a) Current vs voltage (ZnO:Al; 95:5); (b) Current vs voltage (ZnO:Al; 90:10); (c) Current vs voltage (ZnO:Al; 85:15); (d) Sheet resistance, average transmittance vs Al dopant concentration; (e) TCO performance (Φ_{TC}), thickness vs Al dopant concentration; (f) Sheet resistance, band gap vs Al dopant concentration; (g) Sheet resistance, resistivity and thickness vs Al dopant concentration.

$$\Phi_{TC} = \frac{T^{10}}{R_s} \tag{3}$$

where T (%) is the optical transmittance at a specified wavelenght λ = 550 nm, and R_s (Ω/sq) is the sheet resistance. Figure 4(e) shows that Φ_{TC} values of the thin films decrease from 0 mol.% to 5 mol.% with a slight decrease of the thin film thickness from 634 to 612 nm, but increase sharply beyond this range. The value of Φ_{TC} increased abruptly to a high level at 10 mol.% due to the low sheet resistance and the high transmission of the AZO layer combined with a decreased thickness of 487 nm. Φ_{TC} decreased sharply below the 10 mol.% value to a value comparable to the 0 mol.% value at 15 mol.%. This is due to a high sheet resistance, though with the same transmission as the 10 mol.% AZO thin film, but at a higher thickness of 509 nm. While Figure 4(f) shows an opposite trend with Figure 4(d) in the sheet resistance values with the band gap, Figure 4(g) shows a one to one correlation between the sheet resistance and resistivity giving an almost linear correlation in the values of the thickness as compared with the large magnitude of the sheet resistances.

3.5. Composition and Depth Profile of AZO Thin Films

RBS measurements were carried out in order to determine the composition of the undoped ZnO and AZO thin films deposited on soda lime glass substrates. Additional information regarding the depth profiles of the blank substrate, the undoped ZnO and the AZO thin films are given in Figures 5(a)-(c) respectively. The depth profile of all the deposited thin films confirmed the presence of Zn, O and Al along with an estimated ratio of the film thickness.

Table 1 shows the RBS absolute data of the elemental concentrations of each constituent atom in the as-deposited AZO thin films with undoped ZnO as reference. The spectroscopically determined Al dopant concentration in atom percent measured in the as-deposited AZO thin films layers are observed to be strongly correlated with the Al dopant concentration experimentally calculated by weight in the prepared precursor as shown in the Zn/Al ratios (Table 1) and were found to be close in value within approximate decimals for Al dopant concentrations in 10 and 15 mol% AZO thin films. Major constituent of the soda lime glass substrate used in this study is silicon (Si) and oxygen (O), with O having a concentration of 83.66 at.% as observed in the RBS depth profile of the blank soda lime glass slide in Figure 5(a).

The depth profiles of 0 and 15 mol.% AZO thin films were shown Figure 5(b) and Figure 5(c). This revealed almost constant elemental concentration of the O specie in all the as-deposited AZO thin film layers as contrasted with the reduced O concentration of 70.05 at.% in the substrate layer. A reduction in the O specie concentration from 83.66 to 70.5 at.% in the blank soda lime glass slide in all the AZO thin films substrates confirm an underlying process of the diffusion of O species from the substrates layers into the undoped ZnO and AZO thin films layers. This may be due to the deposition temperature and the elements to

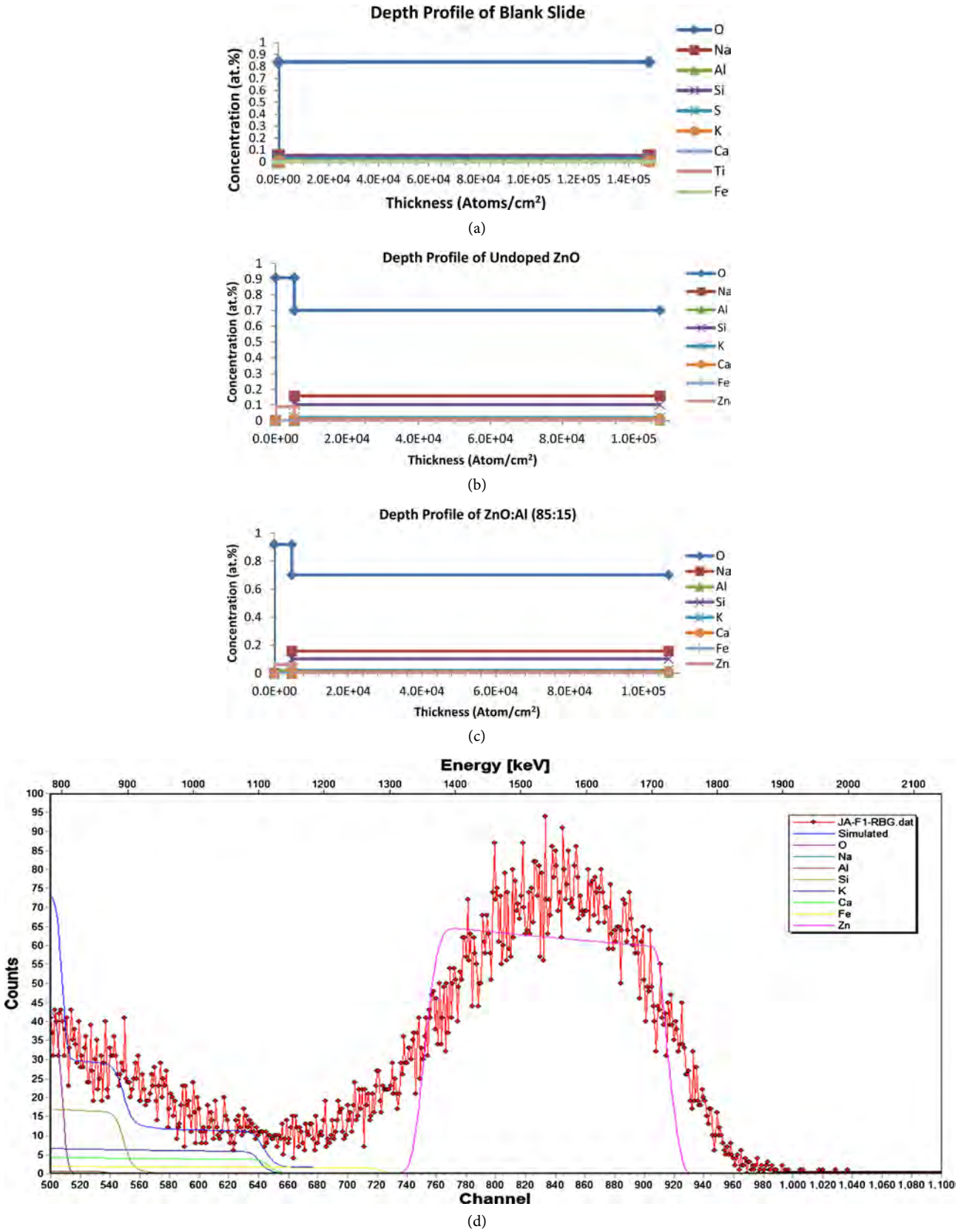

Figure 5. (a) Depth profile of blank slide substrate; (b) Depth profile of ZnO; (c) Depth profile of ZnO:Al (85:15); (d) RBS spectrum of AZO thin films on soda-lime glass substrate.

Table 1. RBS data of the elemental concentrations of each constituent atom in AZO thin films.

Experimentally Measured Ratio of Precursor Mixtures in mol.% (Zn Acetate:Al(Acac)$_3$)	Experimentally Calculated Zn/Al Ratio in Precursor Mixtures	RBS Elemental Concentration of Zn (at.%) in the Thin Films	RBS Elemental Concentration of O (at.%) in the Thin Films	RBS Elemental Concentration of Al (at.%) in the Thin Film	Zn/Al Ratio RBS Elemental Concentration in the Thin Films	RBS Determined Thin Film Thickness (10^{15} Atoms/cm^2)
100:0 (Undoped ZnO)	-	0.091136	0.908864	-	-	5230.50 (634 nm)
95:5	9.50	0.085263	0.902635	0.012102	7.05	5167.21 (612 nm)
90:10	4.50	0.073136	0.911772	0.015092	4.85	4488.07 (487 nm)
85:15	2.83	0.062243	0.918100	0.019657	3.17	4738.62 (509 nm)

which the O are bonded in the substrate. In addition, O impurities emanating from the substrate, and promoted by a high substrate temperature regime (420˚C) result in an out-diffusion effect, which compensate the donor character of the Al dopants in the AZO thin films [28]. This is evidence in observed highest sheet resistance obtained in the undoped ZnO layer with the highest O concentration in **Figure 5(b)**, and the lowest sheet resistance with a comparably low O concentration in the 10 mol.% AZO. The O contribution from the precursor mixtures to the stoichiometry of undoped ZnO and the AZO thin films is therefore greatly masked by the diffused O from the substrate layer. A direct deduction of the O contribution to the undoped ZnO and the AZO thin films from that of the soda lime glass substrate gives the stoichiometry expected from the precursor mixture. The relationship between the Zn and Al atomic content incorporated in the AZO thin films, as a function of Zn in the undoped ZnO were shown in **Table 1**. It is observed that the spectroscopically determined Zn/Al ratio in all the AZO thin films decreased by an approximate constant factor of 2, as the spectroscopically determined Al dopant concentration increased correspondingly with the experimentally calculated Al dopant concentration in the single solid precursors mixtures. This indicates that the Al dopants were successfully incorporated into the ZnO as each Al^{3+} cation substitutes Zn^{2+} cation in the lattice, and is attributed to the fact that the Al^{3+} is a most favorable Zn^{2+} substitute, because the ionic sizes of Al and Zn are closely matched; with Al^{3+} having the smaller ionic radius to easily substitute Zn^{2+}. According to normal doping rules, Al^{3+} can occupy Zn^{2+} sites only up to its solubility limit of 0.3 at.% in ZnO. Else, beyond the solubility limit, new phases of Al_2O_3 arise so that the substitution of Al is no longer as effective [29]. The study therefore shows Al^{3+} solubility factor of 15 below the solubility limit, implying the possibility of further incorporation of Al^{3+} in the ZnO lattice given the advantages of the favorable process conditions used. The RBS spectrum in **Figure 5(d)** shows the degree of the AZO thin film layer uniformity for the 15 mol.% Al dopant concentration and its corresponding simulated spectrum against the substrate background. Of particular interest also in this study from the figure is that the boundary layer between the substrate layer and thin film layer interface is not well defined. The thickness of the boundary layer is a function of the diffusion coefficient of the individual

impurity specie contained in the substrate. The effect is further compounded by the prevailing substrate temperature regime thereby defining the diffusion length and hence the depth of the boundary layer. This thin film-substrate interface effect is of immense importance in studying the efficiency of electron transport between thin film interfaces of ZnO based optoelectronic devices.

4. Conclusions

In this work, AZO thin films were deposited using MOCVD technique using single solid precursor. The factorial decrease in the Zn/Al ratio and the corresponding increase in the Al dopant concentrations of the AZO thin films play an important role in the properties of the AZO thin films, *i.e.* in the sheet resistance, morphology, transmittance and energy band gap after the thin films growth.

We have used a range of characterization techniques to study an ensemble of AZO thin films which allowed us to show that ZnO thin films can be effectively doped under improvable but yet economic processing conditions at relatively low temperature (420˚C). Particularly, 10 mol.% AAA AZO thin film exhibited a much promising lower resistivity of 19.88 Ω-cm with a corresponding average transmittance of 89% and 91% at λ = 550 nm. This value of resistivity establishes a remarkable improvement by a factor of 957 over that of the undoped ZnO and an improvement by a factor of 53 over that of 5 mol.% AAA. Thus, our results that the doping methodology adopted for deposition of AZO thin films in this work are suitable for potential applications in high performance optoelectronics devices. These results also establish a route to achieve adequately controllable doping efficiency of ZnO via the incorporation of Al dopants within its solubility limit.

Conflicts of Interest

The authors declare no conflicts of interest regarding the publication of this paper.

References

[1] Minami, T. (2005) *Semiconductor Science and Technology*, **20**, S35-S44. https://doi.org/10.1088/0268-1242/20/4/004

[2] Liu, H., Avrutin, V., Izyumskaya, N., Özgür, Ü. and Morkoç, H. (2010) *Superlattices and Microstructures*, **48**, 458-484. https://doi.org/10.1016/j.spmi.2010.08.011

[3] Ellmer, K. (2010) *Nature Photonics*, **6**, 809-817. https://doi.org/10.1038/nphoton.2012.282

[4] Xue, S.-W. (2012) *Physics Procedia*, **25**, 345-349. https://doi.org/10.1016/j.phpro.2012.03.307

[5] El hamali, S.O., Cranton, W.M., Kalfagiannis, N., Hou, X., Ranson, R. and Koutsogeorgis, D.C. (2016) *Optics and Lasers in Engineering*, **80**, 45-51.

[6] Lin, Y.C., Chen, M.Z., Kuo, C.C. and Yen, W.T. (2009) E *Colloids and Surfaces A*: *Physicochemical and Engineering Aspects*, **337**, 52-56.

https://doi.org/10.1016/j.colsurfa.2008.11.049

[7] Wang, X.-J., Lei, Q.-S., Xu, W., Zhou, W.-L. and Yu, J. (2009) *Materials Letters*, **63**, 1371-1373. https://doi.org/10.1016/j.matlet.2008.12.027

[8] Babu, B.J., Maldonado, A., Velumani, S. and Asomoza, R. (2010) *Materials Science and Engineering B*, **174**, 31-37. https://doi.org/10.1016/j.mseb.2010.03.010

[9] Chen, W.-J., Liu, W.-L., Hsieh, S.-H. and Hsu, Y.-G. (2012) *Procedia Engineering*, **36**, 54-61. https://doi.org/10.1016/j.proeng.2012.03.010

[10] Hou, Q., Meng, F. and Sun, J. (2013) *Nanoscale Research Letters*, **8**, 144-151. https://doi.org/10.1186/1556-276X-8-144

[11] Ammaih, Y., Lfakir, A., Hartiti, B., Ridah, A., Thevenin, P. and Siadat, M. (2014) *Optical and Quantum Electronics*, **46**, 229-234. https://doi.org/10.1007/s11082-013-9757-2

[12] Palimar, S., Banger, K.V. and Shivakumar, G.K. (2012) *Journal of Applied Sciences*, **12**, 1775-1777. https://doi.org/10.3923/jas.2012.1775.1777

[13] Kaur, G., Mitra, A. and Yadav, K.L. (2015) *Progress in Natural Science*: *Materials International*, **25**, 12-21.

[14] Hopkins, P.D. and Douglas, B.E. (1964) *Inorganic Chemistry*, **3**, 357-360. https://doi.org/10.1021/ic50013a011

[15] Park, K.C., Ma, D.Y. and Kim, K.H. (1997) *Thin Solid Films*, **305**, 201-209. https://doi.org/10.1016/S0040-6090(97)00215-0

[16] Fragala, M.E., Malandrino, G., Giangregorio, M.M., Losurdo, M., Bruno, G., Lettieri, S., Amato, L.S. and Maddalena, P. (2009) *Chemical Vapor Deposition*, **15**, 327-333.

[17] Burstein, E. (1954) *Physics Review B*, **93**, 632-633. https://doi.org/10.1103/PhysRev.93.632

[18] Roth, A.P., Webb, J.B. and Williams, D.F. (1982) *Physics Review B*, **25**, 7836-7839. https://doi.org/10.1103/PhysRevB.25.7836

[19] Tauc, J., Grigorovici, R. and Vancu, A. (1966) *Physica Status Solidi* (*b*), **15**, 627-637. https://doi.org/10.1002/pssb.19660150224

[20] Roth, A.P., Webb, J.B. and Williams, D.F. (1981) *Solid State Communications*, **39**, 1269-1271. https://doi.org/10.1016/0038-1098(81)90224-6

[21] Srikant, V. and Clarke, D.R. (1997) *Journal of Materials Research*, **12**, 1425-1428. https://doi.org/10.1557/JMR.1997.0193

[22] Walsh, A., Juarez, L.F., Da Silva and Wei, S.-H. (2008) *Physical Review B*, **78**, Article ID: 075211. https://doi.org/10.1103/PhysRevB.78.075211

[23] Reynolds, D.C., Look, D.C. and Jogai, B. (2000) *Journal of Applied Physics*, **88**, 5760-5763. https://doi.org/10.1063/1.1320026

[24] Li, L.N., Zhao, Y., Chen, X.L., Sun, J. and Zhang, X.D. (2012) *Physics Procedia*, **32**, 687-695. https://doi.org/10.1016/j.phpro.2012.03.619

[25] Huang, R., Robl, W., Ceric, H., Detzel, T. and Dehm, G. (2010) *IEEE Transactions on Device and Materials Reliability*, **10**, 47-53. https://doi.org/10.1109/TDMR.2009.2032768

[26] Haacke, G. (1976) *Journal of Applied Physics*, **47**, 4086-4089. https://doi.org/10.1063/1.323240

[27] Moholkar, A.V., Pawar, S.M., Rajpure, K.Y., Bhosale, C.H. and Kim, J.H. (2009) *Applied Surface Science*, **255**, 9358-9364. https://doi.org/10.1016/j.apsusc.2009.07.035

[28] Gomez, H., Maldonado, A., Casatanedo-perez, R., Torres-Delgado, G., de La, M. and Olvera, L. (2007) *Materials Characterization*, **58**, 708-714. https://doi.org/10.1016/j.matchar.2006.11.012

[29] Jayaraman, V.K., Álvarez, A.M., Bizarro, M., Koudriavtsev, Y. and de la Luz Olvera Amador, M. (2017) *Thin Solid Films*, **642**, 14-19. https://doi.org/10.1016/j.tsf.2017.09.012

Journal of Modern Physics, 2018, 9, 2090-2099
http://www.scirp.org/journal/jmp
ISSN Online: 2153-120X
ISSN Print: 2153-1196

Edge Modes and Teleportation in a Topologically Insulating Quantum Wire

Majd Ghrear, Brie Mackovic, Gordon W. Semenoff*

Department of Physics and Astronomy, University of British Columbia, Vancouver, Canada
Email: *gordonws@phas.ubc.ca

How to cite this paper: Ghrear, M., Mackovic, B. and Semenoff, G.W. (2018) Edge Modes and Teleportation in a Topologically Insulating Quantum Wire. *Journal of Modern Physics*, **9**, 2090-2099.
https://doi.org/10.4236/jmp.2018.911131

Received: August 12, 2018
Accepted: September 25, 2018
Published: September 28, 2018

Abstract

We find a simple model of an insulating state of a quantum wire which has a single isolated edge mode. We argue that, when brought to proximity, the edge modes on independent wires naturally form Bell entangled states which could be used for elementary quantum processes such as teleportation. We give an example of an algorithm which teleports the spin state of an electron from one quantum wire to another.

Keywords

Symmetry Protected Topological Order, Teleportation

1. Introduction

An important step in the evolution of quantum circuit technology would be the ability to reliably create Einstein-Podolsky-Rosen (EPR) entangled electron pairs at controllable locations in an electronic system. This would raise the possibility of making elementary quantum devices using the many existing technologies available for the fabrication and manipulation of electronic materials [1] [2] [3]. An obstacle to the use of electrons for EPR pairs is their susceptibility to decoherence which results from their interactions with their environment and with each other. Some effort has gone into inventing systems which minimize this decoherence by, for example, dynamically isolating the electron state in a band gap, minimizing its degeneracy and screening its charge. Kitaev's famous proposal of "Majorana fermions" is a good example [4] which achieves all of these and where possibilities of interesting non-local phenomena have been explored [5]-[19]. Braiding of Majorana fermion histories is one of the prime candidates for quantum computation [20]-[26]. However, a single Majorana state as a qubit has the drawback that it is a superposi-

tion of two states which differ in fermion number parity, $(-1)^F$, and the states where the Majorana level is occupied and unoccupied cannot be mixed with physical quantum gates. For a system with a few qubits, it can be useful to have more degeneracy.

In this paper, we shall seek an alternative using ordinary electrons which have both charge and spin. We isolate the states dynamically by considering modes at the center of a band gap. We shall propose a dynamical mechanism for combating decoherence. We will design a system where the EPR state is dynamically favoured in that it is the ground state of a subsystem, so that, even if it decoheres by jumping to an excited state, its natural dynamical evolution would let it decay to the ground state and thereby restore the coherence. As well as minimizing decoherence, this approach yields a tool for processing the system. Beyond applying quantum gates and performing quantum measurements, we can allow the system to go through a possibly dissipative relaxation from an excited state to its ground state. We will then use this additional tool in an essential way, to design an algorithm where the EPR state is used as a resource to teleport the spin wave-function of an electron between quantum wires. Although the material and the gates needed for the process are hypothetical, we conform to certain rules which are aimed at utility. We restrict ourselves to one and two-qubit gates which act on electron spins only, and, in particular, they are local operations and they respect electric charge and fermion number parity superselection rules.

2. The Model

We will make use of the fact that, in a system of noninteracting fermions, where there are single-particle levels with both positive and negative energies, and when there is a unitary transformation which maps positive energy levels onto negative energy levels (particle-hole symmetry), so that positive and negative single-particle states are paired, and when the number of energy levels must be odd, there is necessarily an unpaired zero energy state. Then, it is a simple exercise to design a system where that zero energy state is isolated in a band gap and it is an edge state. Our model is a system of spin-$\frac{1}{2}$ fermions bound to the atomic sites of a one-dimensional array of atoms. The lattice sites are considered immobile and the fermions are described using the tight-binding approximation. The array has an odd number of sites, labeled $n = 1, 2, \cdots, 2L+1$, and $\alpha_{n,\sigma}^{\dagger}$ and $\alpha_{n,\sigma}$ are the creation and annihilation operators for a fermion occupying site n with spin $\sigma = \uparrow, \downarrow$. They obey the anti-commutator algebra

$$\left\{\alpha_{n,\sigma}, \alpha_{n',\sigma'}^{\dagger}\right\} = \delta_{nn'}\delta_{\sigma\sigma'} \tag{1}$$

$$\left\{\alpha_{n,\sigma}, \alpha_{n',\sigma'}\right\} = 0 = \left\{\alpha_{n,\sigma}^{\dagger}, \alpha_{n',\sigma'}^{\dagger}\right\} \tag{2}$$

The Hamiltonian describes spin-independent tunnelling between nearest neighbours

$$H = \sum_{\sigma=\uparrow,\downarrow}\sum_{m=1}^{L}\left(t^{*}\alpha_{2m,\sigma}^{\dagger}\alpha_{2m+1,\sigma} + t\alpha_{2m+1,\sigma}^{\dagger}\alpha_{2m,\sigma}\right) + \sum_{\sigma=\uparrow,\downarrow}\sum_{m=1}^{L}\left(t'^{*}\alpha_{2m,\sigma}^{\dagger}\alpha_{2m-1,\sigma} + t'\alpha_{2m-1,\sigma}^{\dagger}\alpha_{2m,\sigma}\right) \tag{3}$$

We shall assume that the strengths of the tunnelling amplitude t for moving to the right from an even site and t' for moving to the left from an even site are different. These alternating "long" and "short" bonds, depicted in Figure 1, are similar to those in a polyacetylene molecule [27]. We shall assume that the phases of the creation and annihilation operators are adjusted so that t and t' are real and positive. It is important that the total number of sites, $2L+1$, is odd. The Schrödinger equation

$$i\hbar\frac{\mathrm{d}}{\mathrm{d}\tau}\alpha_{2m,\sigma}(\tau) = t\alpha_{2m+1,\sigma}(\tau) + t'\alpha_{2m-1,\sigma}(\tau) \tag{4}$$

$$i\hbar\frac{\mathrm{d}}{\mathrm{d}\tau}\alpha_{2m+1,\sigma}(\tau) = t'\alpha_{2m+2,\sigma}(\tau) + t\alpha_{2m,\sigma}(\tau) \tag{5}$$

with boundary conditions $\alpha_{0,\sigma} = 0 = \alpha_{2L+2,\sigma}$ is solved by the stationary states,

$$\alpha_{2m,\sigma}(\tau) = \frac{\mathrm{e}^{-i\varepsilon\tau/\hbar}}{\sqrt{L+1}}\sin\left(\frac{\pi k}{L+1}m\right), k = 1,2,\cdots,L$$

$$\alpha_{2m+1,\sigma}(\tau) = \frac{\mathrm{e}^{-i\varepsilon\tau/\hbar}}{\varepsilon\sqrt{L+1}}\left[t'\sin\left(\frac{\pi k(m+1)}{L+1}\right) + t\sin\left(\frac{\pi km}{L+1}\right)\right]$$

with positive (conduction) and negative (valence) energy bands and band gap $2|t-t'|$,

$$\varepsilon(k) = \pm\sqrt{(t-t')^{2} + 4tt'\cos^{2}\left[\frac{\pi k}{2L+2}\right]} \tag{6}$$

The spectrum is symmetric. For each k there is a positive and negative energy $\varepsilon(k)$. In addition, there is a single mid-gap zero mode, with $\varepsilon = 0$, and wave-function

$$\alpha_{2n,\sigma}^{0}(\tau) = 0, \alpha_{2n+1,\sigma}^{0}(\tau) = \sqrt{\frac{1-(t'/t)^{2}}{1-(t'/t)^{2L+2}}}\left(-\frac{t'}{t}\right)^{n} \tag{7}$$

which is concentrated near $n=0$ if $t'<t$ and near $n=L$ if $t'>t$. The probability density $\sum_{\sigma}\left|\alpha_{n,\sigma}^{0}\right|^{2}$ with $2L+1=59$ and $t'/t=2/3$ is depicted in Figure 2. The existence of the energy gap and the mid-gap zero mode concentrated at one end of the wire will be important to us. The number of sites is not important as long as this number is odd, in fact the wire could be very short if that is convenient.

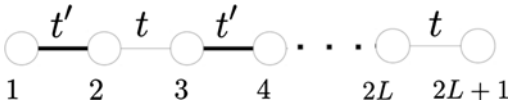

Figure 1. The odd-sited one-dimensional lattice with alternating long t and short t' bonds.

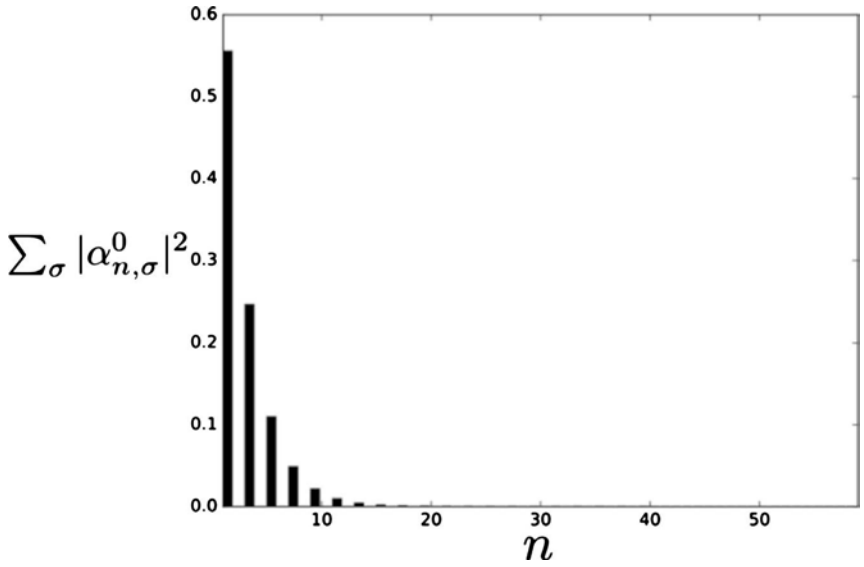

Figure 2. The probability density of the zero mode, $\sum_\sigma \left|\alpha^0_{n,\sigma}\right|^2$ with $2L+1=59$ and $t'/t=2/3$.

The existence of the zero mode is not an accident. As we have discussed, the spectrum is symmetric about $\varepsilon=0$. If $\alpha_{n,\sigma}$ is a solution of the Schrödinger equation with energy ε, then $(-1)^n\alpha_{n,\sigma}$ is also a solution with energy $-\varepsilon$. The non-zero energy states thus come in positive-negative pairs. Moreover, there must be an odd number of states, so there must necessarily be an un-paired zero mode. This feature is "topological" in the sense that it would be preserved by any modification of the Schrödinger equation which respected the particle-hole symmetry and the odd number of states.

In the following discussion, we shall consider the many-electron state which has all of the negative energy modes occupied and all of the positive energy modes empty. We assume that the energy gap is sufficiently large compared to the energy scales of phenomena of interest that the states with $|\varepsilon|\geq|t-t'|$ decouple and play no role. The active mode is the zero mode with wave-function (7) concentrated at one of the edges of the wire. Electrons occupying the zero mode are annihilated and created by $\left(a_\sigma, a^\dagger_\sigma\right)$ with the algebra

$$\left\{a_\sigma, a^\dagger_{\sigma'}\right\}=\delta_{\sigma\sigma'}, \left\{a_\sigma, a_{\sigma'}\right\}=0=\left\{a^\dagger_\sigma, a^\dagger_{\sigma'}\right\} \tag{8}$$

The space of states where the spin up or down zero modes are populated or unpopulated form a two qubit system with a four-dimensional Hilbert space, spanned by

$$\left\{|0\rangle, a^\dagger_\uparrow|0\rangle, a^\dagger_\downarrow|0\rangle, a^\dagger_\uparrow a^\dagger_\downarrow|0\rangle\right\}$$

where $|0\rangle$ is the state with the zero modes (and all other zero mode electron states which we shall discuss in the following) empty, $a_\uparrow|0\rangle=0$ and $a_\downarrow|0\rangle=0$. The ground state of the charge neutral system is two-fold degenerate in the span of $\left\{a^\dagger_\uparrow|0\rangle, a^\dagger_\downarrow|0\rangle\right\}$. It has charge zero and spin $\frac{1}{2}$. The "particle" and "hole"

states $a_{\uparrow}^{\dagger}a_{\downarrow}^{\dagger}|0\rangle$ and $|0\rangle$ have charges +1 and −1, respectively, and they are spin singlets. These unusual spin-charge relations, which have long been associated with fractionally charged solitons in polyacetylene [27] [28], in this case, are a simple consequence that the lattice has an odd number of sites.

Consider the scenario where edges containing zero modes of two wires are brought into proximity, depicted in **Figure 3**. We will describe the zero mode states of one wire as above, and the other similarly, with $\left(a_{\sigma}, a_{\sigma}^{\dagger}\right)$ replaced by $\left(b_{\sigma}, b_{\sigma}^{\dagger}\right)$. We model the interaction of the edge modes of the two wires by the Hubbard Hamiltonian

$$H_{\text{int}} = \frac{e^2}{2}\left(\sum_{\sigma} a_{\sigma}^{\dagger}a_{\sigma} - 1\right)^2 + \frac{e^2}{2}\left(\sum_{\sigma} b_{\sigma}^{\dagger}b_{\sigma} - 1\right)^2 + H_{\lambda} \tag{9}$$

$$H_{\lambda} = \sum_{\sigma=\uparrow,\downarrow} \lambda\left(a_{\sigma}^{\dagger}b_{\sigma} + b_{\sigma}^{\dagger}a_{\sigma}\right) \tag{10}$$

where λ is real and positive and $e^2 \gg \lambda$. The first two terms in H_{int} model the Coulomb energy which discourages nonzero charge at a site (the −1 is the charge of the ion at each lattice site). The first two terms in H_{int} have a degenerate, zero energy ground state with basis states $\left\{a_{\uparrow}^{\dagger}b_{\uparrow}^{\dagger}|0\rangle, a_{\uparrow}^{\dagger}b_{\downarrow}^{\dagger}|0\rangle, a_{\downarrow}^{\dagger}b_{\uparrow}^{\dagger}|0\rangle, a_{\downarrow}^{\dagger}b_{\downarrow}^{\dagger}|0\rangle\right\}$. The third term in (9), H_{λ} in (10), allows the electrons to hop between the edge states of the two wires. This weaker interaction splits the degeneracy of the ground state of the first two terms so that the lowest energy state is the spin singlet,

$$|g\rangle = \frac{1}{\sqrt{2}}\left[a_{\uparrow}^{\dagger}b_{\downarrow}^{\dagger} + b_{\uparrow}^{\dagger}a_{\downarrow}^{\dagger}\right]|0\rangle \tag{11}$$

and the excited state is a spin triplet. The energy of the ground state, $|g\rangle$, in second order perturbation theory, is $E_0 = -4\lambda^2/e^2$ and the spin triplet has energy $E_1 = 0 + \mathcal{O}\left(\lambda^4/e^6\right)$. We shall assume that $\lambda^2/e^2 \ll |t - t'|$ so that these states remain well within the energy gap. We assume that the hopping Hamiltonian H_{λ} can be turned on and off at will.

Then, on top of this, we shall assume that there is an additional, controllable, dissipative interaction which stimulates transitions between the energy levels of H_{int}. We need this dissipation so that the quantum state relaxes to the ground

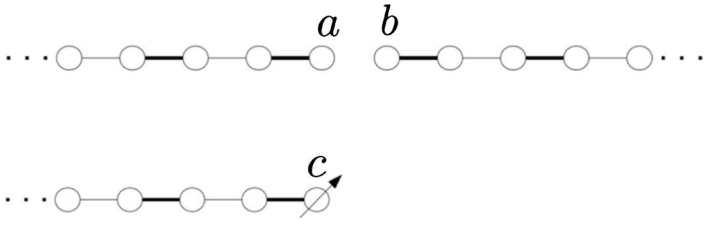

Figure 3. The *a*, *b* and *c* systems as edge states. *c* is occupied by an electron in a particular spin state and *a* and *b* are brought into proximity. The spin wave-function of the electron occupying *c* is to be teleported to a single electron occupying *b*. The *c*-electron does not interact with *a* or *b*. *a* and *b* interact via H_{int} in (9) which favours a state with *a* and *b* both singly occupied and together forming a spin singlet. Alice applies one and two qubit gates to *a* and *c* and Bob can apply gates to *b*.

state, $|g\rangle$, of H_{int} discussed above. We will also need the assumption that, although it dissipates energy, the dissipative process conserves the electric charge and the spin of the *a*-*b* system.

3. Teleportation

The state $|g\rangle$ in (11) is an entangled state of the *a*-*b* system. We will use it as a resource for quantum teleportation [29]. We shall assume that Alice has access to the *a*-system and Bob has access to the *b*-system. Now, we assume that Alice is in possession of another electron which is in a particular spin state, expressed as a superposition of its spin up and spin down states. It is dynamically independent of the *a*-*b* system, so that the total wave-function is the product state

$$\psi = \frac{g_1 c_\uparrow^\dagger + g_2 c_\downarrow^\dagger}{\sqrt{2}}\left[a_\uparrow^\dagger b_\downarrow^\dagger + b_\uparrow^\dagger a_\downarrow^\dagger\right]|0\rangle \tag{12}$$

where $|g_1|^2 + |g_2|^2 = 1$. Alice has access to the composite *a*-*c* system. Her goal is to teleport the spin wave-function of the *c*-electron to Bob. Alice should now turn off H_λ and do a measurement in a Bell basis of the *c*-*a* system. Equivalently, she can perform the following three steps: Alice applies the two-qubit CNOT gate to the *a*-*c* system. This gate leaves the terms with $c_\uparrow^\dagger$ unchanged and it interchanges $a_\uparrow^\dagger$ and $a_\downarrow^\dagger$ in the terms with $c_\downarrow^\dagger$. The state vector becomes

$$\psi = \left(\frac{g_1}{\sqrt{2}} c_\uparrow^\dagger\left(a_\uparrow^\dagger b_\downarrow^\dagger + b_\uparrow^\dagger a_\downarrow^\dagger\right) + \frac{g_2}{\sqrt{2}} c_\downarrow^\dagger\left(a_\downarrow^\dagger b_\downarrow^\dagger + b_\uparrow^\dagger a_\uparrow^\dagger\right)\right)|0\rangle. \tag{13}$$

Then, Alice applies the one-qubit Hadamard gate to the *c*-spins. This gate replaces $c_\uparrow^\dagger$ by $\frac{c_\uparrow^\dagger + c_\downarrow^\dagger}{\sqrt{2}}$ and $c_\downarrow^\dagger$ by $\frac{c_\uparrow^\dagger - c_\downarrow^\dagger}{\sqrt{2}}$ to put the state vectors in the form

$$\psi = \left(\frac{g_1}{\sqrt{2}}\frac{c_\uparrow^\dagger + c_\downarrow^\dagger}{\sqrt{2}}\left(a_\uparrow^\dagger b_\downarrow^\dagger + b_\uparrow^\dagger a_\downarrow^\dagger\right) + \frac{g_2}{\sqrt{2}}\frac{c_\uparrow^\dagger - c_\downarrow^\dagger}{\sqrt{2}}\left(a_\downarrow^\dagger b_\downarrow^\dagger + b_\uparrow^\dagger a_\uparrow^\dagger\right)\right)|0\rangle.$$

Next, Alice measures the total spin, *J*, and the *z*-component of the spin, J_z, of her system. The results for J, J_z and the resulting state-vectors are

$$J = 1, J_z = 1: \quad c_\uparrow^\dagger a_\uparrow^\dagger\left(g_1 b_\downarrow^\dagger - g_2 b_\uparrow^\dagger\right)|0\rangle \tag{14}$$

$$J = 1, J_z = 0: \quad \frac{c_\uparrow^\dagger a_\downarrow^\dagger + c_\downarrow^\dagger a_\uparrow^\dagger}{\sqrt{2}}\left(g_1\frac{b_\uparrow^\dagger - b_\downarrow^\dagger}{\sqrt{2}} - g_2\frac{b_\uparrow^\dagger + b_\downarrow^\dagger}{\sqrt{2}}\right)|0\rangle \tag{15}$$

$$J = 1, J_z = -1: \quad c_\downarrow^\dagger a_\downarrow^\dagger\left(g_1 b_\uparrow^\dagger + g_2 b_\downarrow^\dagger\right)|0\rangle \tag{16}$$

$$J = 0, J_z = 0: \quad \frac{c_\uparrow^\dagger a_\downarrow^\dagger - c_\downarrow^\dagger a_\uparrow^\dagger}{\sqrt{2}}\left(g_1\frac{b_\uparrow^\dagger + b_\downarrow^\dagger}{\sqrt{2}} + g_2\frac{b_\uparrow^\dagger - b_\downarrow^\dagger}{\sqrt{2}}\right)|0\rangle \tag{17}$$

Alice then uses a classical communication channel to communicate the two bits of data, J, J_z, to Bob. This tells Bob which gates to apply to recover the original wave-function:

J	J_z	Bob gate
1	1	iY
1	0	H then iY
1	−1	I
0	0	H

where H is the Hadamard gate and $iY\left(b_\uparrow, b_\downarrow\right) = \left(b_\downarrow, -b_\uparrow\right)$. As a result, Bob has placed the *b*-electron into the same spin state that the *c*-electron originally occupied. The spin state has been teleported.

Alternative to an electronic system, one might envisage engineering such a system with spin $\frac{1}{2}$ fermion atoms occupying an optical lattice. In that case, the atoms would have only a weak repulsion, the parameter e^2 would be small and the interaction between the zero modes on wires in proximity would be dominated by H_λ. In that case, the ground state of H_λ is

$$\frac{1}{2}\left(a_\uparrow^\dagger - b_\uparrow^\dagger\right)\left(a_\downarrow^\dagger - b_\downarrow^\dagger\right)|0\rangle$$

which is a spin singlet, like (11), but it contains components where the edge modes are doubly occupied. Alice then begins with the state

$$\frac{1}{2}\left(g_1 c_\uparrow^\dagger + g_2 c_\downarrow^\dagger\right)\left(a_\uparrow^\dagger - b_\uparrow^\dagger\right)\left(a_\downarrow^\dagger - b_\downarrow^\dagger\right)|0\rangle \tag{18}$$

She should first do a measurement to see whether her *c*-*a* system is in a state of integer or half-odd-integer spin. If it is integer spin, the measurement projects onto the state in (12) and she can proceed with the teleportation protocol as before. If the result is half-odd-integer, the state thereafter is

$$\psi' = \frac{1}{\sqrt{2}}\left(g_1 c_\uparrow^\dagger + g_2 c_\downarrow^\dagger\right)\left[a_\uparrow^\dagger a_\downarrow^\dagger + b_\uparrow^\dagger b_\downarrow^\dagger\right]|0\rangle \tag{19}$$

We have not devised a simple algorithm for teleporting the spin wave-function to Bob when this is the state. The most efficient way to proceed is to simply start again, to turn on H_λ and dissipation and to allow the *a*-*b* subsystem to relax to its ground state,

$$\frac{1}{\sqrt{2}}\left(g_1 c_\uparrow^\dagger + g_2 c_\downarrow^\dagger\right)\left[a_\uparrow^\dagger a_\downarrow^\dagger + b_\uparrow^\dagger b_\downarrow^\dagger\right]|0\rangle \to \frac{1}{2}\left(g_1 c_\uparrow^\dagger + g_2 c_\downarrow^\dagger\right)\left(a_\uparrow^\dagger - b_\uparrow^\dagger\right)\left(a_\downarrow^\dagger - b_\downarrow^\dagger\right)|0\rangle$$

This evolution conserves spin and charge, there is only energy dissipation. It restores the state (18). Then, Alice once again measures the total spin. If it is integer, she turns off H_λ and proceeds with the teleportation protocol. If it is half-odd-integer, she repeats the restart. Each time, the probability of obtaining integer spin is $\frac{1}{2}$ so that the probability of failure after n tries is $\frac{1}{2^n}$ which converges to zero. By this process, Alice succeeds in teleporting the spin wave-function, from the test electron to which Alice has access, to the edge electron on Bob's quantum wire.

The most important role of H_λ and dissipation in the above discussion can be seen as the production of a charge neutral spinless state of the *a*-*b* system. In

fact, we could be more general and assume that the resource *a*-*b* system is in a mixed state composed of all of its states which are charge neutral and have spin zero, that is, that the state is described by any density matrix in the vector space spanned by $\left\{a_\uparrow^\dagger a_\downarrow^\dagger|0\rangle, b_\uparrow^\dagger b_\downarrow^\dagger|0\rangle, \frac{1}{\sqrt{2}}\left(a_\uparrow^\dagger b_\downarrow^\dagger + b_\uparrow^\dagger a_\downarrow^\dagger\right)|0\rangle\right\}$ which has a non-zero diagonal component in the direction $\frac{1}{\sqrt{2}}\left(a_\uparrow^\dagger b_\downarrow^\dagger + b_\uparrow^\dagger a_\downarrow^\dagger\right)|0\rangle$. Again, when Alice measures the total spin of her subsystem, she either obtains integer spin, with the pure state (12) whence she can complete the teleportation, or a mixed state made in the space spanned by

$$\left(g_1 c_\uparrow^\dagger + g_2 c_\downarrow^\dagger\right)a_\uparrow^\dagger a_\downarrow^\dagger|0\rangle, \left(g_1 c_\uparrow^\dagger + g_2 c_\downarrow^\dagger\right)b_\uparrow^\dagger b_\downarrow^\dagger|0\rangle$$

whence she should redo the process.

4. Conclusions

We have studied a one-dimensional model of a finite length quantum wire in a topologically insulating state. We have shown that an ordinary electronic zero mode with spin, although it has a significant amount of degeneracy, can still be used as a resource for quantum teleportation. What is teleported is the spin wave-function of an auxiliary electron.

The zero modes associated with solitons in polyacetylene [28] [30] were originally discussed in the context where the associated mid-gap states lead to exotic quantum numbers such as fractional fermion number [27] [31]. The disentanglement of the states of paired zero modes in order to find localized fractional charges dates to that time [32]. The polyacetylene model, with alternating strong and weak bonds has since become one of the primary examples of a one-dimensional topological insulator [33]. It would be interesting to study this scenario with proximity induced superconductivity to understand the fate of the Majorana mode which one might expect to emerge there. The polyacetylene molecule could be a candidate for the insulator that we are discussing, if its chain can contain an odd number of sites. An alternative would be to implement such a system using cold atoms in an optical lattice [9] [34].

This work was supported in part by NSERC.

Conflicts of Interest

The authors declare no conflicts of interest regarding the publication of this paper.

References

[1] Milburn, G.J. (1997) Schrödinger's Machines. W. H. Freeman & Co., San Francisco.

[2] Dowling, J.P. and Milburn, G.J. (2003) *Transactions of the Royal Society A*, **361**, 3655.

[3] Deutsch, D. (2003) Physics, Philosophy, and Quantum Technology. In: Shapiro, J. and Hirota, O., Eds., *Proceedings of Sixth International Conference on Quantum*

Communication, Measurement and Computing, Rinton Press, Princeton, NJ.

[4] Kitaev, A.Y. (2001) *Physics-Uspekhi*, **44**, 131. https://doi.org/10.1070/1063-7869/44/10S/S29

[5] Semenoff, G.W. and Sodano, P. (2006) arXiv:cond-mat/0601261.

[6] Semenoff, G.W. and Sodano, P. (2006) *Electronic Journal of Theoretical Physics*, **3**, 157.

[7] Fu, L. and Kane, C.L. (2008) *Physical Review Letters*, **100**, Article ID: 096407.

[8] Ruostekoski, J., Dunne, G.V. and Javanainen, J. (2002) *Physical Review Letters*, **88**, Article ID: 180401. https://doi.org/10.1103/PhysRevLett.88.180401

[9] Ruostekoski, J., Javanainen, J. and Dunne, G.V. (2008) *Physical Review A*, **77**, Article ID: 013603.

[10] Bolech, C.J. and Demler, E. (2007) *Physical Review Letters*, **98**, Article ID: 237002. https://doi.org/10.1103/PhysRevLett.98.237002

[11] Tewari, S., Zhang, C., Das Sarma, S., Nayak, C. and Lee, D.-H. (2008) *Physical Review Letters*, **100**, Article ID: 027001.

[12] Bolech, C.J. and Demler, E. (2008) *Physica B*, **403**, 994. https://doi.org/10.1016/j.physb.2007.10.075

[13] Fu, L. (2010) *Physical Review Letters*, **104**, Article ID: 056402. https://doi.org/10.1103/PhysRevLett.104.056402

[14] Bermudez, A., Amico, L. and Martin-Delgado, M.A. (2010) *New Journal of Physics*, **12**, Article ID: 055014.

[15] Chamon, C., Jackiw, R., Nishida, Y., Pi, S.-Y. and Santos, L. (2010) *Physical Review B*, **81**, Article ID: 224515. https://doi.org/10.1103/PhysRevB.81.224515

[16] Wu, B.H. and Cao, J.C. (2012) *Physical Review B*, **85**, Article ID: 085415. https://doi.org/10.1103/PhysRevB.85.085415

[17] Sau, J.D., Swingle, B. and Tewari, S. (2015) *Physical Review B*, **92**, Article ID: 020511. https://doi.org/10.1103/PhysRevB.92.020511

[18] Mizushima, T., Tsutsumi, Y., Kawakami, T., Sato, M., Ichioka, M. and Machida, K. (2016) *Journal of the Physical Society of Japan*, **85**, Article ID: 022001.

[19] Ren, C., Yang, J., Xiang, J., Wang, S. and Tian, H. (2017) *Journal of the Physical Society of Japan*, **86**, Article ID: 124715. https://doi.org/10.7566/JPSJ.86.124715

[20] Kitaev, A.Y. (2003) *Annals of Physics*, **303**, 2-30. https://doi.org/10.1016/S0003-4916(02)00018-0

[21] Bravyi, S., Terhal, B.M. and Leemhuis, B. (2010) *New Journal of Physics*, **12**, Article ID: 083039.

[22] Vijay, S. and Fu, L. (2016) *Physica Scripta*, **T168**, Article ID: 014002.

[23] Landau, L.A., Plugge, S., Sela, E., Altland, A., Albrecht, S.M. and Egger, R. (2016) *Physical Review Letters*, **116**, Article ID: 050501. https://doi.org/10.1103/PhysRevLett.116.050501

[24] Plugge, S., Landau, L.A., Sela, E., Altland, A., Flensberg, K. and Egger, R. (2016) *Physical Review B*, **94**, Article ID: 174514.

[25] Li, Y. (2016) *Physical Review Letters*, **117**, Article ID: 120403. https://doi.org/10.1103/PhysRevLett.117.120403

[26] Litinski, D. and von Oppen, F. (2018) *Physical Review B*, **97**, Article ID: 205404.

[27] Niemi, A.J. and Semenoff, G.W. (1986) *Physics Reports*, **135**, 99-193. https://doi.org/10.1016/0370-1573(86)90167-5

[28] Su, W.P., Schrieffer, J.R. and Heeger, A.J. (1979) *Physical Review Letters*, **42**, 1698. https://doi.org/10.1103/PhysRevLett.42.1698

[29] Bennett, C.H., Brassard, G., Crepeau, C., Jozsa, R., Peres, A. and Wootters, W.K. (1993) *Physical Review Letters*, **70**, 1895. https://doi.org/10.1103/PhysRevLett.70.1895

[30] Su, W.P., Schrieffer, J.R. and Heeger, A.J. (1980) *Physical Review B*, **22**, 2099. https://doi.org/10.1103/PhysRevB.22.2099

[31] Jackiw, R. and Schrieffer, J.R. (1981) *Nuclear Physics B*, **190**, 253-265. https://doi.org/10.1016/0550-3213(81)90557-5

[32] Jackiw, R., Kerman, A.K., Klebanov, I. and Semenoff, G.W. (1983) *Nuclear Physics B*, **225**, 233-246. https://doi.org/10.1016/0550-3213(83)90051-2

[33] Guo, H.-M. (2016) *Science China Physics, Mechanics and Astronomy*, **59**, Article ID: 637401. https://doi.org/10.1007/s11433-015-5773-5

[34] Pachos, J.K. and Knight, P.L. (2003) *Physical Review Letters*, **91** Article ID: 107902. https://doi.org/10.1103/PhysRevLett.91.107902

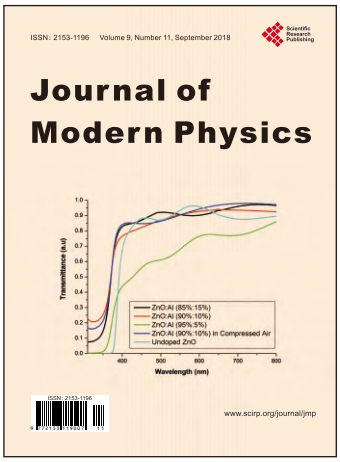

Call for Papers

Journal of Modern Physics

ISSN: 2153-1196 (Print) ISSN: 2153-120X (Online)
http://www.scirp.org/journal/jmp

Journal of Modern Physics **(JMP)** is an international journal dedicated to the latest advancement of modern physics. The goal of this journal is to provide a platform for scientists and academicians all over the world to promote, share, and discuss various new issues and developments in different areas of modern physics.

Editor-in-Chief

Prof. Yang-Hui He City University, UK

Executive Editor-in-Chief

Prof. Marko Markov Research International, Buffalo Office, USA

Subject Coverage

Journal of Modern Physics publishes original papers including but not limited to the following fields:

Biophysics and Medical Physics
Complex Systems Physics
Computational Physics
Condensed Matter Physics
Cosmology and Early Universe
Earth and Planetary Sciences
General Relativity
High Energy Astrophysics
High Energy/Accelerator Physics
Instrumentation and Measurement
Interdisciplinary Physics
Materials Sciences and Technology
Mathematical Physics
Mechanical Response of Solids and Structures
New Materials: Micro and Nano-Mechanics and Homogeneization
Non-Equilibrium Thermodynamics and Statistical Mechanics
Nuclear Science and Engineering
Optics
Physics of Nanostructures
Plasma Physics
Quantum Mechanical Developments
Quantum Theory
Relativistic Astrophysics
String Theory
Superconducting Physics
Theoretical High Energy Physics
Thermology

We are also interested in: 1) Short Reports—2-5 page papers where an author can either present an idea with theoretical background but has not yet completed the research needed for a complete paper or preliminary data; 2) Book Reviews—Comments and critiques.

Notes for Intending Authors

Submitted papers should not have been previously published nor be currently under consideration for publication elsewhere. Paper submission will be handled electronically through the website. All papers are refereed through a peer review process. For more details about the submissions, please access the website.

Website and E-Mail

http://www.scirp.org/journal/jmp **E-mail: jmp@scirp.org**

What is SCIRP?

Scientific Research Publishing (SCIRP) is one of the largest Open Access journal publishers. It is currently publishing more than 200 open access, online, peer-reviewed journals covering a wide range of academic disciplines. SCIRP serves the worldwide academic communities and contributes to the progress and application of science with its publication.

What is Open Access?

All original research papers published by SCIRP are made freely and permanently accessible online immediately upon publication. To be able to provide open access journals, SCIRP defrays operation costs from authors and subscription charges only for its printed version. Open access publishing allows an immediate, worldwide, barrier-free, open access to the full text of research papers, which is in the best interests of the scientific community.

- High visibility for maximum global exposure with open access publishing model
- Rigorous peer review of research papers
- Prompt faster publication with less cost
- Guaranteed targeted, multidisciplinary audience

Scientific Research Publishing

Website: http://www.scirp.org

Subscription: sub@scirp.org

Advertisement: service@scirp.org